

AXON GUIDANCE AND SORTING IN THE  
ZEBRAFISH RETINOTECTAL SYSTEM

by

Melissa Elizabeth Hardy

A dissertation submitted to the faculty of  
The University of Utah  
in partial fulfillment of the requirements for the degree of

Doctor of Philosophy

Department of Neurobiology and Anatomy

University of Utah

August 2010

Copyright © Melissa Elizabeth Hardy 2010

All Rights Reserved



## ABSTRACT

The nervous system is comprised of an estimated 100 billion individual neurons, which are connected to one another to form a network that senses environmental stimuli and coordinates the organism's behavior. Because of the complexity of the nervous system, deciphering the developmental processes and adult wiring diagram has proved challenging. A number of axon guidance molecules have been identified; however, the means by which they guide billions of axons to their target cells *in vivo* remains poorly understood. Several axon guidance molecules have been found to be bifunctional, meaning they can elicit different growth cone responses depending on the presence or absence of other molecules, such as growth cone receptors, intracellular signal transduction molecules, or extracellular modulators. Axon sorting within axon tracts is perhaps a means by which axons are presorted to make a precise connection on their target cells. The zebrafish, *Danio rerio*, is an ideal model organism to study vertebrate axon guidance and axon sorting due to its external fertilization, optical transparency, amenability to forward genetics, and ease of making transgenic lines.

In order to study axon guidance within the zebrafish retinotectal system, I developed a new method of misexpressing genes. Local misexpression can be induced by using a modified soldering iron in transgenic zebrafish in which a gene of interest is driven by a heat shock promoter. This method allowed me to examine the mechanisms by which Slit1a and Slit2 guide axons from the retina to the optic tectum. I determined the expression pattern of Slits in the zebrafish and used antisense morpholino technology to knock down Slit1a. The

resultant axon guidance errors indicated that Slit1a acts to guide retinal axons through the optic tract. I then misexpressed Slit1a and Slit2 near the optic tract to observe their effect on axons. I found that both proteins appeared to attract retinal axons. Additionally, I saw that Slit2 seems to attract retinal axons earlier in the retinotectal pathway, at the optic chiasm. I also report on a new method, to whose development I contributed, for automated tracking of axons through electron microscopy datasets. Taken together, my results add new methods to the endeavor of mapping neural connectivity and development, and suggest a new role for Slits in axon guidance.

## TABLE OF CONTENTS

ABSTRACT .....	iii
ACKNOWLEDGEMENTS.....	vii
1: OVERVIEW .....	1
Introduction.....	2
Nervous system architecture and connectivity .....	3
Development of the nervous system .....	4
The canonical axon guidance molecules .....	6
Regulation of receptors can change the growth cone response .....	7
Intracellular molecules can modulate axon guidance signaling .....	8
Extracellular cofactors can change axon responses to guidance cues.....	10
Slit and Robo structure .....	12
Slit-Robo signaling in axon guidance .....	13
Axon sorting .....	16
Zebrafish retinotectal system as an experimental model.....	17
Research summary .....	20
References.....	24
2: FOCAL GENE MISEXPRESSION IN ZEBRAFISH EMBRYOS INDUCED BY LOCAL HEAT SHOCK USING A MODIFIED SOLDERING IRON .....	36
3: THE ROLE OF SLIT1A AND SLIT2 IN AXON GUIDANCE IN THE ZEBRAFISH RETINOTECTAL SYSTEM .....	44
Introduction.....	45
Experimental procedures .....	48
Results .....	53
Discussion.....	76
Acknowledgements .....	82
References.....	83
4: AXON TRACKING IN SERIAL BLOCK-FACE SCANNING ELECTRON MICROSCOPY .....	86
Introduction.....	87
References.....	90

5: DISCUSSION.....	100
Summary.....	101
Local heat shock as a method of misexpression.....	101
Slit function in the zebrafish retinotectal system.....	102
Axon sorting in the zebrafish retinotectal system.....	115
Conclusions.....	116
References.....	118

## ACKNOWLEDGEMENTS

I would like to thank my advisor, Chi-Bin Chien, for mentoring me during my graduate studies. Chi-Bin is not only one of the smartest people I know, he is also one of the kindest. I particularly have to thank him for setting up a collaboration that allowed me to move to San Francisco to be with my husband for nine months after I got married. I am also thankful for his ability to attract students and postdocs that are fun to be around, and for setting a friendly tone for the lab.

I am also thankful to the other members of my committee: Ed Levine, Erik Jorgensen, Rich Dorsky, and Maureen Condic. I value the critical feedback and support that they gave me during my graduate studies.

I am grateful to the National Institutes of Health for providing funding that supported me during my graduate work, through the NIH Developmental Biology Training Grant (5T32 HD07491). Susan Mango did an excellent job administering the grant and I am thankful for her comments and advice on my project and talks.

The members of the developmental biology and zebrafish communities gave excellent feedback and suggestions on my project over the years.

I would like to thank my labmates from the Chien Lab. In particular, Kristen Kwan became a dear friend. It was always a joy to have coffee or lunch with Kristen and talk about science or, more often, life. I also would like to thank Fabienne Poulain, Amy Lim, Arminda Suli, Andrew Pittman, Doug Campbell, Coni Stacher Hörndli, Mei-Yee Law, Nick Dambrauskas, and the other members of Chien Lab.

I made many good friends during my graduate studies. I would particularly like to thank George Eisenhoffer for many enjoyable conversations as we went through graduate school together.

My family has been a constant source of support. I would like to thank my parents for their emphasis on the value of education and my brothers and sister and their families for many fun times.

Finally, I want to thank my husband, Paul House, for his unwavering support and love. Thank you for everything.

## CHAPTER 1

### OVERVIEW

## Introduction

Neuroscience was pioneered by the great Spanish histologist Santiago Ramon y Cajal in the late 1800s and early 1900s. He deduced that the nervous system was comprised of billions of separate nerve cells, rather than a continuous network of fibers, as had been assumed by other leading neuroscientists of the time. In addition, he proposed that the transmission of nerve impulses is unidirectional from axonal terminations to dendrites, passing through a contact site, or synapse (Cajal, 1917). These insights are fundamental doctrines of neuroscience today. However, although we know the basic architecture of the nervous system, the sheer number of cells and synapses has thus far made it impossible to know in fine detail how the vertebrate brain is wired. New imaging and analysis methods currently in development may allow us to start solving this puzzle (Chapter 4).

Another important insight of Ramon y Cajal was the discovery of the growth cone, the structure that he hypothesized to guide the axon to its final target during development. This idea, remarkable given that he only had fixed tissue to work with, is another basic tenet of modern neuroscience. This eventually led to Roger Sperry's landmark 1963 paper, in which he proposed the chemoaffinity hypothesis, stating that "[t]he final course laid down by any given fiber reflects the history of a continuous series of decisions based on differential affinities between the various advance filaments that probe the surroundings ahead and the diverse elements that each encounters." In other words, growth cones are guided by chemical factors (Sperry, 1963). The discovery of these factors, however, would have to wait until recent decades for modern genetic and biochemical methods. A number of axon guidance molecules have been discovered; however, the details of how they act to guide all the neurons of the developing nervous system are still being investigated (Chapter 3).

This chapter will provide an overview of the architecture of the nervous system, methods used to study the development and connectivity of the nervous system, and mechanisms of axon guidance with an emphasis on Slit-Robo signaling. The rationale for undertaking the research described in the main body of the thesis will also be presented.

### **Nervous system architecture and connectivity**

The evolution of multicellularity required communication between cells and ultimately, a central organ to integrate sensory inputs and control the organism's responses. The nervous system evolved to fulfill this requirement. Greater complexity of behavior necessitated a more complex nervous system. The human brain is estimated to contain 86 billion individual cells, which are connected to make neural networks that process sensory input and regulate behavior (Williams and Herrup, 1988; Azevedo et al., 2009).

To date, the only completely mapped nervous system wiring diagram is that of the nematode *Caenorhabditis elegans*, which contains 302 neurons (White et al., 1986). Although the connectivity map alone is insufficient to explain all behavior, it has proved to be a valuable resource for forming and testing hypotheses about specific *C. elegans* behaviors (Chalfie et al., 1985; Gray et al., 2005; Mori and Ohshima, 1995). Mapping neural connections in vertebrates would similarly open new avenues of research. Although initially the work of mapping a wiring diagram is descriptive rather than hypothesis-driven, “comprehensive, high-quality data sets are essential for developing well thought-out hypotheses” (Lichtman and Sanes, 2008).

Several human diseases that include axon guidance defects have been identified: Corpus Callosum Dysgenesis, L1 Syndrome, Joubert Syndrome, Horizontal Gaze Palsy with Progressive Scoliosis, Kallmann Syndrome, Oculocutaneous Albinism, Congenital Fibrosis

of the Extraocular Muscles Type I, Duane Retraction Syndrome, Pontine Tegmental Cap Dysplasia, and TUBB3 Syndromes (Engle, 2010; Tischfield et al., 2010). It is thought that a number of other, more common, neurological disorders are also due to defects in axon guidance. However, testing for axon guidance defects in live humans is difficult, unless a large anatomical abnormality exists. For instance, Corpus Callosum Dysgenesis, in which the entire corpus callosum is missing or reduced, can be identified by computerized tomography (CT) or magnetic resonance imaging (MRI). However, Kallman Syndrome, in which, among other defects, olfactory neurons do not pathfind correctly, was not known to involve aberrant axon guidance until a detailed postmortem analysis was done (Schwanzel-Fukuda et al., 1989).

Intriguingly, mutations in axon guidance molecules have been identified as risk factors for dyslexia (Hannula-Jouppi et al., 2005) and autism (Degano et al., 2009; Vorstman et al., 2010; Anitha et al., 2008). Animal models also suggest an axon guidance component of epilepsy (Yaron and Zheng, 2007) and Fragile X Syndrome (Tucker et al., 2006; Li et al., 2009). A neural map of axonal connections in fine detail would allow scientists and physicians to test for an axon guidance defect in these common developmental diseases, as well as in degenerative disorders such as Parkinson's Disease, by comparing normal neural circuitry to that of affected individuals.

To understand the etiology of diseases involving axon guidance defects, we need to understand not only the wiring diagram in adults, but the mechanisms by which it develops.

### **Development of the nervous system**

Neurons develop by a well-defined sequence of events: fate specification, axon extension, axon guidance, and synaptogenesis. Axon guidance is the process by which a

growing axon finds its way to its target cell. Once there, it forms a synapse. Although this sounds simple, navigating through the developing embryo is not a trivial problem. The growth cone encounters a multitude of changing and conflicting extracellular cues as it extends over long distances. It must interpret these cues and mediate the necessary cytoskeletal response - extension, retraction, or turning - all along its trajectory. Roger Sperry summarized the process thus: "[t]he cells and fibers of the brain must carry some kind of individual identification tags, presumably cytochemical in nature, by which they are distinguished one from another almost, in many regions, to the level of the single neurons" (Sperry, 1963).

To date, four major families of “canonical” axon guidance ligands have been discovered: Netrins, Slits, Semaphorins, and Ephrins (Dickson, 2002). Each signals through transmembrane receptors to induce cytoskeletal changes that result in growth cone behaviors: extension, retraction, or turning. In addition, some morphogens, such as Wnt, and cell adhesion molecules, such as cadherins, are capable of directing axon guidance. Still, even given the most generous count of axon guidance molecules, there is a problem – how can dozens or hundreds of molecules precisely guide millions of axons?

Part of the answer is that guidance cues can elicit different responses in growth cones depending on context. The difference can be cell autonomous: for example, expression of different receptor or co-receptor types, modulation of receptor expression level, or changes in downstream intracellular factors. There could also be non-cell autonomous differences, such as the presence or absence of extracellular proteins that modulate the concentration or conformation of the ligand. Intracellular differences could lead to different responses by different axons within a tract, while extracellular differences could induce changes in growth cone response in different regions of the developing embryo.

## **The canonical axon guidance molecules**

The four families of canonical axon guidance molecules are the most well understood axon guidance factors and seem to be highly conserved across at least 600 million years of evolution (Cebrià and Newmark, 2005; Cebrià et al., 2007).

Netrin/Unc-6 was first identified in *C.elegans* as an axon guidance molecule (Hedgecock et al., 1990; Ishii et al., 1992). A subsequent biochemical purification scheme revealed that it was conserved in vertebrates and functioned to attract commissural axons to the ventral midline of the embryonic spinal cord (Kennedy et al., 1994; Serafini et al., 1994). The major known Netrin receptors are DCC/Unc-40 and Unc5. Netrin was first isolated as an attractant, and the attractive response is mediated through the DCC receptor. Growth cones that express Unc-5 receptors, on the other hand, are repelled by Netrin.

Semaphorins are secreted or transmembrane molecules that signal through receptor complexes that can include Plexin, Neuropilin, Met, L1, and OTK. They were first identified as repulsive cues in grasshopper and chick (Kolodkin et al., 1992; Luo et al., 1993), and were later found to function as axon guidance molecules in fly, mouse, and zebrafish.

Ephrins signal through Ephs, although because Ephrins are either transmembrane or GPI-anchored, there can be reverse signaling as well. Ephrins and Ephs generally have a repulsive interaction and are responsible for axon guidance and topographic mapping (Cheng et al., 1995; Drescher et al., 1995; Wilkinson, 2001).

Slits are the fourth major family of guidance ligands. They signal through Roundabout, or Robo, receptors and the interaction is usually repulsive. Because I focus on Slit-Robo signaling in this dissertation, an extensive background is presented later in this chapter.

Although the four canonical guidance families are thought to be either generally attractive (Netrin), or repulsive (Slit, Sema, Ephrin), a large body of literature indicates that guidance ligands may elicit the opposite response when certain conditions are met. Three factors that regulate different growth cone responses are receptors, intracellular factors such as Rho GTPases, and extracellular molecules such as heparan sulfate proteoglycans (HSPGs).

### **Regulation of receptors can change the growth cone response**

A simple way for the growth cone to change its response to an extracellular cue is to express different receptors that mediate different cytoskeletal responses. For instance, Netrin/Unc-6 is an attractive ligand for growth cones expressing DCC/Unc-40 and a repulsive ligand for growth cones that express Unc-5 in addition to Unc-40 (Leung-Hagesteijn et al., 1992; Keino-Masu et al., 1996; Guthrie, 1997; Hamelin et al., 1993; Hedgecock et al., 1990).

Semaphorins also can be attractive or repulsive depending on the receptor. For example, in zebrafish, Sema3D appears to be attractive to axons of the anterior commissure and repulsive to axons of the nucleus of the medial longitudinal fasciculus. The repellent response appears to be regulated by Neuropilin-1A, while the putative attractive response seems to be a function of both Neuropilin-1A and Neuropilin-2B acting in combination (Wolman et al., 2004). Growth cones in primary cultures of mouse cortical neurons are repelled by Sema3E when they express PlexinD1 alone, but are attracted by Sema3E when they express both PlexinD1 and Neuropilin-1 (Chauvet et al., 2007).

Although Robos are the only Slit receptors identified in vertebrates so far, there is evidence that Slit does have other receptors. Genetic analysis of arbor formation in zebrafish RGCs reveals that Slit1a inhibits arborization through both Robo2-dependent and Robo2-

independent mechanisms (Campbell et al., 2007). Moreover, another Slit receptor was recently discovered in *C. elegans*. EVA-1 likely acts with Robo/SAX-3 as a co-receptor for Slit. Neurons expressing both receptors are sensitive to Slit signaling, but neurons with only Robo/SAX-3 likely are insensitive to Slit (Fujisawa et al., 2007).

Another way to modulate the response to a signal is by regulating the surface concentration of receptors. Commissural axons in *Drosophila* achieve this by downregulating Robo receptors until they have crossed the Slit-expressing midline (Kidd et al., 1998). Comm protein binds to Robo and targets it for trafficking to the endosome for degradation prior to and during midline crossing (Myat et al., 2002; Keleman et al., 2005, 2002). In vertebrates, no Comm homolog has been found, but Robo3/Rig-1 seems to play a similar role by inactivating Robo1 or Robo2 on commissural spinal cord axons until they have crossed the midline (Long et al., 2004; Sabatier et al., 2004; Chen et al., 2008).

### **Intracellular molecules can modulate axon guidance signaling**

Axon guidance receptors initiate a cascade of intracellular events that lead to cytoskeletal rearrangement and thus control growth cone behavior. A number of intracellular factors have been shown to be important in modulating growth cone response to ligands, including cyclic nucleotides, calcium, and Rho GTPases.

Cyclic nucleotides are one family of molecules that can change growth cone response. Changing the level of cyclic AMP or cyclic GMP can switch attraction to repulsion or vice versa. This was initially demonstrated in cultures of *Xenopus* neurons by Mu-Ming Poo's laboratory. They induced growth cone turning by applying a gradient of BDNF on one side of the growth cone, which attracts the *Xenopus* neurons. However, when they added a competitive nonhydrolyzable analog of cAMP or an inhibitor of protein kinase A, the neurons were repelled by BDNF (Song et al., 1997). Further research demonstrated a

similar effect in the presence of netrin (Ming et al., 1997). Finally, they looked at Sema3D, which is normally repulsive. Adding a cGMP analog or activating cGMP with an agonist of endogenous cGMP converted the repulsive response to an attractive one (Song et al., 1998). Interestingly, depleting extracellular calcium abolished both attractive and repulsive responses to Netrin, but not to Semaphorin, suggesting a role for calcium in mediating the intracellular response to Netrin.

Rho GTPases are molecular switches that play a role in transducing most, if not all, guidance responses to ligands. Rho GTPases are known to regulate growth cone motility and act downstream of a number of axon guidance ligands, including Slits, Semaphorins, Ephrins, and Netrins (Wahl et al., 2000; Whitford and Ghosh, 2001; Wong et al., 2001; Li et al., 2002). Calcium gradient changes induced by ligand binding probably activate local changes in Rho GTPase concentration. Activating intracellular calcium is sufficient to change the direction of growth cone turning (Hong et al., 2000; Zheng, 2000). Stimulation of the growth cone by at least some ligands, such as BDNF, causes calcium to be released from intracellular stores and form a gradient with a higher concentration of calcium in the direction of turning. Calcium seems to activate the Rho GTPases Cdc42 and Rac, which in turn can change cytoskeletal dynamics to cause extension of the growth cone on the side of higher Cdc42 or Rac function (Jin et al., 2005), while RhoA probably mediates retraction on the side of higher RhoA function (Yuan et al., 2003).

Evidence for the *in vivo* relevance of these data comes from genetic studies in both fly and mouse. Disrupting Rac or Cdc42 function causes axon guidance errors in *Drosophila* (Luo et al., 1994; Kaufmann et al., 1998). Conditionally knocking out Rac in mouse cortical neurons results in normal axon extension but defects in midline commissure formation (Chen et al., 2007; Kassai et al., 2008). In *Drosophila*, Rac is required to mediate the repulsive

response elicited by Slit. The binding of Slit to Robo causes recruitment of Dock/Nck, Sos, and PAK to the intracellular domain of Robo, and Sos activates Rac (Fan et al., 2003; Yang and Bashaw, 2006). Rac, and therefore the repulsive response, is inhibited by the GTPase activating protein CrGAP/Vilse (Lundström et al., 2004; Hu et al., 2005).

The intracellular factors such as these that affect growth cone dynamics and thus axon guidance may either be different in different neurons, or they may change over time. For instance, Sema3F is repellent for a population of basal ganglia mouse neurons at E12.5, but attractive for the same neurons at E14.5 (Kolk et al., 2009a).

### **Extracellular cofactors can change axon responses to guidance cues**

In addition to intracellular factors, extracellular factors can also change how the growth cone reacts to axon guidance molecules. One class of extracellular molecules that is particularly important is the heparan sulfate proteoglycans (HSPGs). These are proteins that are secreted or expressed on the cell membrane and have side chains made of repeated disaccharides. HSPGs have many roles in development, including regulating the distribution of morphogens and mediating binding between FGF and FGFR (reviewed in Hacker et al., 2005). In addition, they seem to play an important role in axon guidance (Van Vactor et al., 2006).

Evidence that HSPGs could play an important role in axon guidance by Slit-Robo came from cell culture studies, in which rat Robo-1 was expressed on HEK293 cells and heparinase was subsequently added to the culture. The cultures were then exposed to Slit2 and stained for Slit2 expression on the cell surface. Heparinase largely abolished the Slit2 signal, indicating that HSPGs were necessary for Slit-Robo binding. Further coculture experiments with mouse olfactory explants revealed that heparan sulfate was also required for Slit-induced repulsion of olfactory neurons (Hu, 2001).

These results were soon shown to be relevant *in vivo* in both mouse and zebrafish. Exostosin-1 (EXT1) is one of the enzymes that catalyzes heparan sulfate side chain formation, and mice deficient for EXT1 in the brain have guidance errors in midline axon tracts (Inatani et al., 2003). Zebrafish mutant for two other EXT family members, *ext2* and *ext3*, have axon sorting errors in the optic tract (Lee et al., 2004). Double mutants show axon guidance errors similar to *robo2* mutants. Later steps in the HS synthesis pathway are also important for Slit-Robo signaling in *C. elegans*, as demonstrated by genetic interactions of mutants for one epimerase and two sulfotransferase genes with the *slt-1* and *sax-3* mutants (Bülow and Hobert, 2004). Finally, syndecan, an HSPG core protein, genetically interacts with the Slit-Robo pathway in both *Drosophila* and *C. elegans* to regulate axon guidance (Steigemann et al., 2004; Johnson et al., 2004; Rhiner et al., 2005).

In addition to HSPGs, chondroitin sulfate proteoglycans (CSPGs) can convert Sema5A from an attractant to a repellent in rat diencephalon explants (Kantor et al., 2004). CSPGs had been previously described as inhibitory to growth cones (Dou and Levine, 1994; Snow et al., 2001), but this was the first evidence that they can interact with other guidance cues to provide instruction.

Finally, evidence suggests that other extracellular factors, such as matrix metalloproteases (MMPs) and morphogens, may have an indirect effect on axon guidance by regulating expression of axon guidance ligands. In *Xenopus*, pharmacologically inhibiting MMPs results in RGC axon guidance defects at the optic chiasm and optic tract (Hehr et al., 2005). Pharmacologically inhibiting FGF signaling in *Xenopus* results in a reduction in *slit1* and *sema3a* expression and axon guidance errors in the optic tract. Knocking down *slit1* or *sema3a* phenocopied the FGF-inhibited phenotype (Atkinson-Leadbetter et al., 2010).

Axon guidance cues can be bifunctional when receptor type or level is altered, when certain intracellular molecules are expressed at different levels, or when extracellular factors interact with guidance molecules.

### **Slit and Robo structure**

In this dissertation, I focus on a particular canonical ligand-receptor pair, Slit-Robo. There are 3 Slit family members in mammals, 4 in zebrafish, and 1 in *Drosophila melanogaster* and *C. elegans*. Slit proteins have the following domains, from N-terminal to C-terminal: 4 leucine-rich repeats, 6 EGF repeats, a laminin G-like beta-sandwich domain, 1 or 3 EGF repeats, and a C-terminal cysteine knot (Hohenester et al., 2006; Itoh et al., 1998; Li et al., 1999; Brose et al., 1999). Mammalian Slit2 is proteolytically processed with a cleavage site after the fifth EGF domain; the N-terminal fragment retains the biological activity (Brose et al., 1999; Wang et al., 1999; Nguyen Ba-Charvet et al., 2001). The crystal structure of the *Drosophila* Slit-Robo complex has been solved, revealing that the second leucine-rich repeat of Slit binds all three *Drosophila* Robo proteins (Howitt et al., 2004).

The Roundabout (Robo) receptor is characterized by 5 Ig-like domains, 3 FN3 domains, a transmembrane domain, and a cytoplasmic domain with several short conserved elements. *Drosophila* has 3 Robo genes, mammals and zebrafish have 4 Robos, and *C. elegans* has 1 Robo (SAX-3) (Kidd et al., 1999; Yuan et al., 1999; Zallen et al., 1998). Deletion experiments show that Robo domains IG1 and IG2 are important for Slit binding and the crystal structure confirms that these are the Slit-binding regions of the Robo protein (Liu et al., 2004; Hohenester et al., 2006; Fukuhara et al., 2008; Morlot et al., 2007).

Interestingly, heparan sulfate seems to be a required component of the Slit-Robo complex. Adding heparin to an *in vitro* preparation increases the affinity of Robo for Slit by ten-fold (Hussain et al., 2006). Moreover, an RGC collapse assay using *Xenopus* RGC

cultures demonstrated that heparin was required for Slit-dependent growth cone collapse (Hussain et al., 2006). In addition, *boxer;dackel (extl3;ext2)* double zebrafish mutants, in which there is very little heparan sulfate present, show strong pathfinding defects similar to those seen in the *astray/Robo2* mutant (Lee et al., 2004).

### **Slit-Robo signaling in axon guidance**

*Roundabout (Robo)* was first identified in a genetic screen in *Drosophila* that recovered mutants affecting midline guidance in the ventral nerve cord (Seeger et al., 1993). Commissural neurons of the ventral nerve cord normally cross the midline exactly once and then project on the contralateral side of the midline. In contrast, commissural axons in *Robo* mutants recross the midline. *Robo* was identified to be an axon guidance receptor that is expressed at low levels by axons prior to crossing the midline, and at high levels after crossing the midline (Kidd et al., 1998). At the same time, *sax-3*, the *Robo* homolog in *C. elegans*, was identified and found to control ventral cord axon crossing, as in *Drosophila* (Zallen et al., 1998).

*Slit* was later identified as the ligand for *Robo* expressed at the midline of the fly ventral nerve cord (Kidd et al., 1999). *Slit* mutants had been previously identified as being defective in midline guidance, but because the phenotype was much more severe than that of *Robo* mutants it had not been immediately obvious that they functioned in the same pathway. *Slit* and *Robo* were shown to interact both genetically and biochemically (Brose et al., 1999; Kidd et al., 1999). *Slit* null mutants show a complete collapse of the ventral nerve axon scaffold, with all commissural axons growing in the midline, rather than crossing and recrossing like the *Robo* mutant axons (Rothberg et al., 1990). Further studies show that knocking down all three *Robos* phenocopies the *Slit* mutant (Rajagopalan et al., 2000; Simpson et al., 2000).

The *Slit-Robo* signaling pathway was subsequently found to function in vertebrates as well. A zebrafish mutant that had aberrant retinal ganglion cell axon guidance, *astray*, was found to lack a functional *robo2* gene (Fricke et al., 2001). The mouse double knockout for *Slit1* and *Slit2* has a similar axon guidance phenotype at the optic chiasm (Plump et al., 2002). In addition, the *Slit1;Slit2* knockout mouse has axon guidance defects in several other brain pathways, including the corticofugal, thalamocortical, and callosal tracts (Bagri et al., 2002). Both the mouse and zebrafish phenotypes were presumed to be due to loss of a repellent signal or the loss of growth cone ability to sense the repellent signal. Subsequent studies have demonstrated that Robo-Slit signaling controls pathfinding in a number of commissural and longitudinal axon tracts in vertebrates, including the cranial motor axon tract, lateral olfactory tract, vomeronasal tract, and longitudinal dopaminergic diencephalospinal tract (Knöll et al., 2003; Miyasaka et al., 2005; Fouquet et al., 2007; Nguyen-Ba-Charvet et al., 2008; López-Bendito et al., 2007; Kasthuber et al., 2009; Prince et al., 2009; Hammond et al., 2005). Additionally, a human mutation in *Robo3* has been identified and shown to cause horizontal gaze palsy with progressive scoliosis (HGPPS) (Jen et al., 2004; Chan et al., 2006). Defects in horizontal eye movement in these patients are most likely due to a deficiency in crossing fibers in the brain (Sicotte et al., 2006), while the cause of the accompanying scoliosis is still unknown.

Although axon guidance studies have generally identified the Slit-Robo interaction as repellent, Slit can also stimulate axon branching. This was first found using *in vitro* culture assays in which cells from rat dorsal root ganglia were dissociated and exposed to purified Slit2 (Wang et al., 1999). These results were confirmed *in vivo* in zebrafish trigeminal sensory axons (Miyashita et al., 2004; Yeo et al., 2001), as well as in sensory axons and cortical dendrites of *Slit* and *Robo* mouse knockouts (Ma and Tessier-Lavigne, 2007). These

studies suggest that Slit can have a positive effect on Robo-expressing axons, in addition to its known repellent role.

Slit-Robo signaling is not confined to axon guidance, but also mediates a number of cell migration pathways. In vertebrates, *Slit* regulates migration of several neuron populations by repelling them from inappropriate regions of the brain. For instance, progenitors of mouse olfactory bulb neurons migrate from the subventricular zone through the rostral migratory stream to the olfactory bulb. During this process, they are kept out of the septum and the choroid plexus by Slit1, which is expressed throughout adulthood (Nguyen-Ba-Charvet et al., 2004). *Slit/Robo* signaling also functions during neural crest migration in the trunk, where it keeps migrating cells confined to the ventral migratory pathway (Jia et al., 2005).

Intriguingly, in *Drosophila*, Slit can function as either a repellent or as an attractant to migrating cells. Slit functions as a repellent to migrating salivary glands and to neurons of the lobula cortex in the fly brain (Kolesnikov and Beckendorf, 2005; Tayler et al., 2004). Slit acts to guide muscle precursor cells in two ways: first, the cells are repelled by Slit expressed at the midline; however, as they reach their final destination, they seem to be attracted by Slit secreted by muscle attachment sites (Kramer et al., 2001). Although Slit could be acting as either an attractant or a stop signal, it is certainly not repellent at the muscle attachment sites. Both of these effects are mediated through Robo and Robo2.

Similarly, *Drosophila* tracheal branches are both attracted and repelled by Slit. They are repelled by midline Slit, and Robo is required for this response. They seem to be attracted by Slit in several target tissues; this response is mediated by Robo2 (Englund et al., 2002). When *slit* or *robo* is removed, a tracheal branch fails to enter the CNS, which the authors interpret to be due to loss of attraction. Moreover, when they misexpress Slit, they

see ectopic turning of the tracheal branches. The simplest explanation of these data is that Slit acts as an attractant for the tracheal branches. These papers raise the possibility that Slit/Robo signaling could function attractively in axon guidance as well.

### **Axon sorting**

Axon guidance cues from the environment are clearly important to axon targeting. In addition, there is evidence that axon-axon interactions are also important for proper pathfinding. Axon sorting, in which axons change their position within a tract, could be due to axon-axon interactions and/or other extracellular cues. Axon sorting is known to occur in both the optic nerve and tract and in the olfactory nerve; presumably this sorting within tracts prepares axons to find their synaptic partners. In both the optic tectum and the olfactory bulb, there is a topographic order of projection. Presorting within the tracts may be important to the final establishment of a topographic map.

This hypothesis is supported by a recent paper in which disrupting axon sorting of olfactory sensory neurons is correlated with defects in targeting. Previous work had established that axons became progressively sorted as they grew toward the glomeruli (Satoda et al., 1995). The authors observed that olfactory sensory neurons expressed Neuropilin-1 and Semaphorin-3A in a complementary pattern and that the repulsive interaction of the two molecules sorts the axons as they make their way to the glomeruli. Manipulating the levels of either molecule resulted not only in missorting of axons, but a shifting of their termination zones on the glomeruli (Imai et al., 2009).

Retinal ganglion cell axons are ordered within the optic nerve. They undergo a rearrangement in the optic chiasm and emerge in the optic tract with a new topographic order (Scholes, 1979; Leung et al., 2003). Zebrafish mutant for *ext2* or *extl3* show axon sorting defects within the optic tract; however they still project correctly on the optic tectum (Lee et

al., 2004). Disrupting dorsal-ventral topography within the mouse retina by misexpressing BMP2 causes missorting of axons within both the optic nerve and the optic tract, and results in mistargeting of ventral axons on the superior colliculus (Plas et al., 2008).

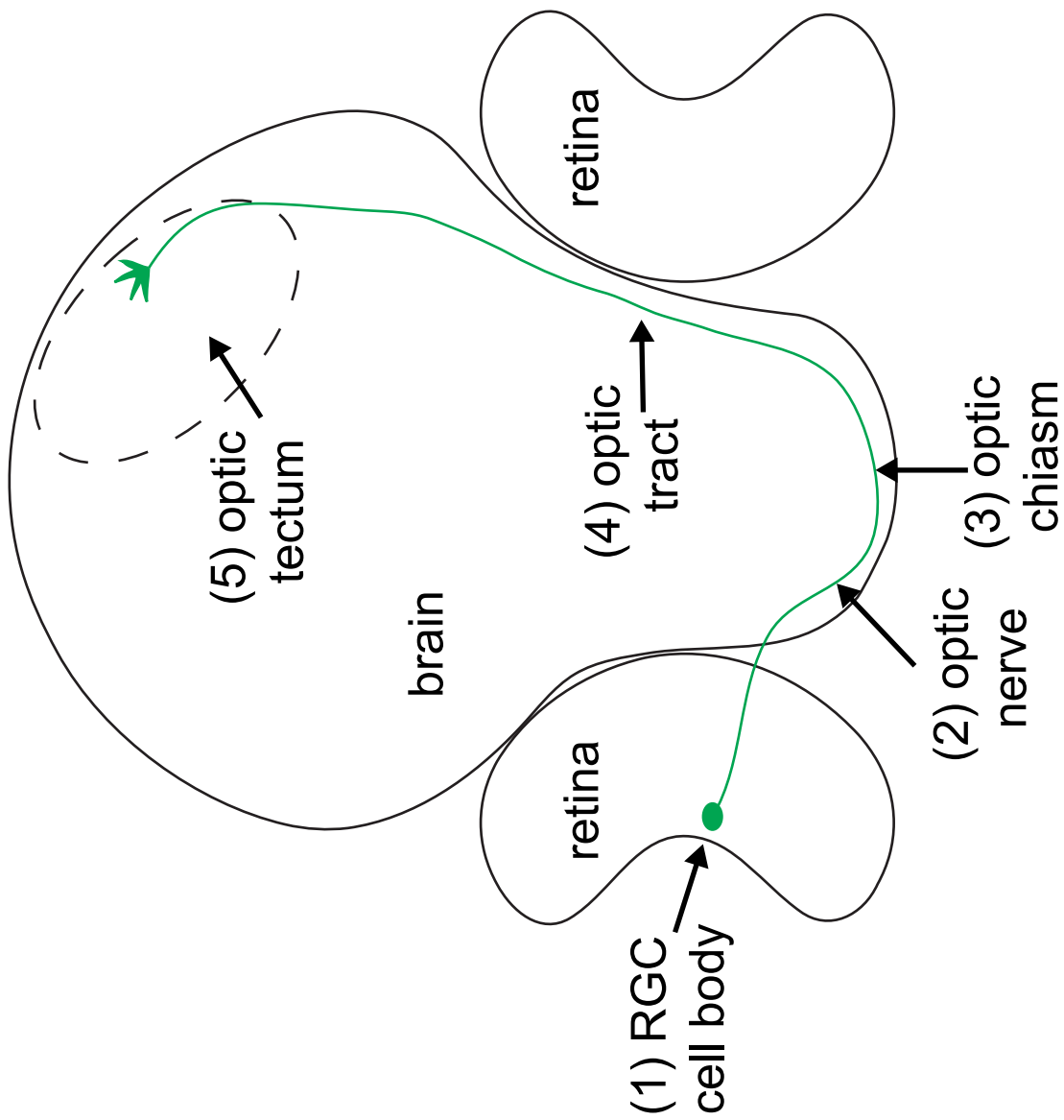
Axon guidance has been extensively studied; however axon sorting has not. It is likely that axon-axon interactions within axon tracts have an unappreciated role in establishing topography.

### **Zebrafish retinotectal system as an experimental model**

The zebrafish (*Danio rerio*) retinotectal system is an excellent system in which to study axon guidance and sorting. The zebrafish is amenable to performing forward genetics, and a number of mutants with defects in the retinotectal system have been identified (Baier et al., 1996; Trowe et al., 1996; Hutson et al., 2004). Moreover, external fertilization and optical transparency make the zebrafish embryo ideal for studying development, including axon guidance (Fetcho and Liu, 1998). Transgenic zebrafish are also relatively easy to make (Kwan et al., 2007). I took advantage of all of these properties while researching my dissertation.

Development of the zebrafish retinotectal system begins with the birth of retinal ganglion cells (RGCs) in the retina (Figure 1.1). The first RGCs are born at 28 hours postfertilization (hpf). Shortly after birth, they extend axons, which exit the eye through the optic nerve head and grow toward the ventral midline starting at 32 hpf. Before crossing the midline, the bundle of RGC axons is called the optic nerve. All RGC axons cross the midline beginning at 34 hpf; the structure of the axon fascicles at the point of crossing is called the optic chiasm. The axons then grow dorsally along the pial surface of the brain; the axons are referred to as the optic tract between the chiasm and the tectum. The first pioneer axons being growing in the tract at 36 hpf and reach the tectum at 48 hpf. Most of the axons

Figure 1.1: Schematic of retinotectal pathway. This cartoon shows a zebrafish brain in a coronal view, with dorsal up and a retina on the left and right sides. Retinal ganglion cells are born in the retina starting at 28 hpf (1). They project an axon into the brain. The optic nerve consists of RGC axons before crossing the midline (2). RGC axons cross the midline in the ventral diencephalon, at the optic chiasm (3). After crossing the midline, they grow dorsally along the pial surface of the brain. The postcrossing axons are called the optic tract (4). Some RGC axons innervate pretectal targets, but most terminate and form synapses in the optic tectum (5).



terminate in the optic tectum, where they form synapses with tectal cells. The remainder terminate in several pretectal nuclei.

Four Slits and four Robos are present in zebrafish. Three *slits*, *slit1a*, *slit2*, and *slit3* are expressed near the retinotectal pathway (Hutson and Chien, 2002; Hutson et al., 2003; Barresi et al., 2005). Figure 1.2 shows the distribution of *slit* mRNA near the optic chiasm. *robo2* is expressed in RGC axons and seems to be the only *robo* present in RGCs (Lee et al., 2001). The current model of Slit-Robo function is that Robo2 receptors expressed in RGC cause growth cones to be repelled by Slit2 and Slit3 anterior and posterior to the optic chiasm. Slit2 and Slit3 therefore channel RGC axons across the midline. When Robo2 is removed, in the *astray* mutant, growth cones are now insensitive to Slits and misproject anteriorly (Fricke et al., 2001; Hutson et al., 2002).

### **Research summary**

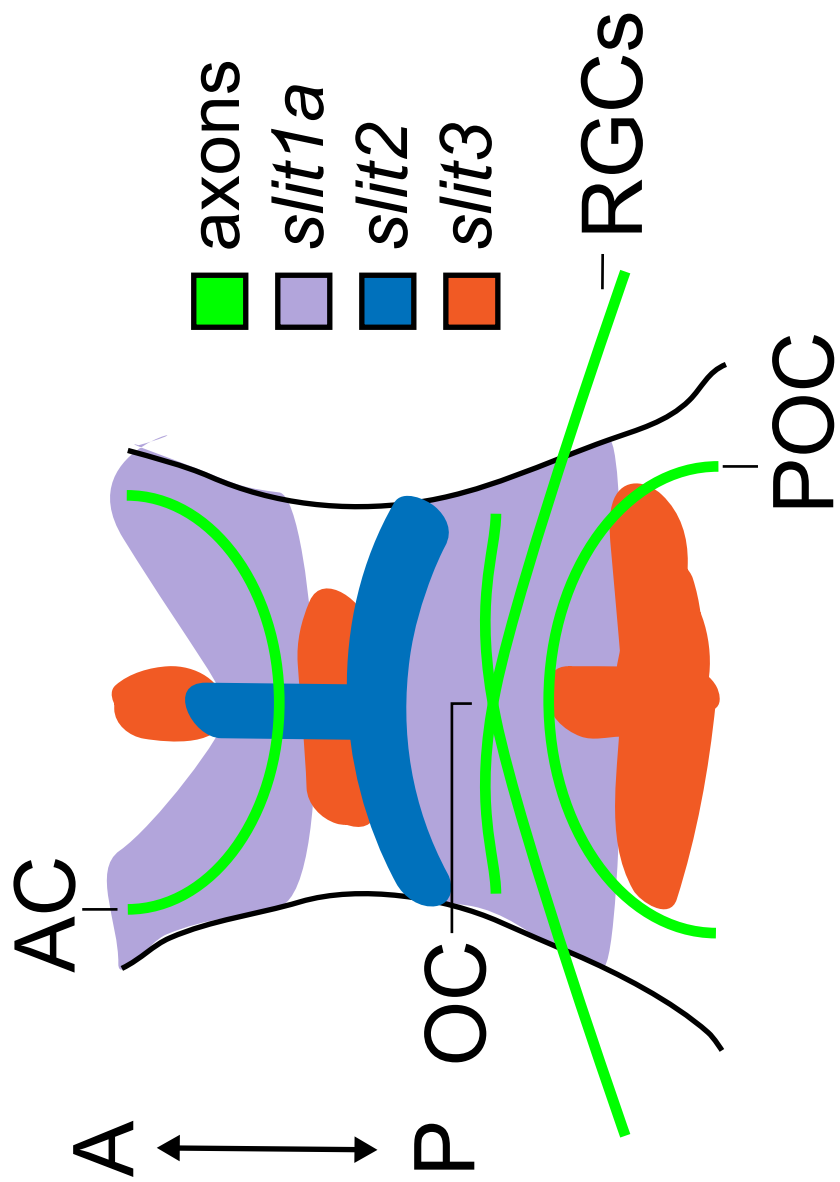
This dissertation will describe my work to develop a new method of gene misexpression in the zebrafish, my findings on how Slits work to regulate axon guidance in the zebrafish retinotectal system, and my work on a new method of studying axon sorting.

In Chapter 2, I describe using a modified soldering iron to induce local misexpression of genes. By making stable transgenic zebrafish with a gene of interest under the control of the heat shock promoter, I was able to make animals in which tissue could be induced to misexpress that gene in a temporally and spatially controlled manner.

I used this method in Chapter 3 to investigate how Slit1a and Slit2 act in the zebrafish retinotectal system. Expression analysis of Slit1a revealed that it was broadly expressed in the zebrafish brain in the same area through which axons from the retina pathfind, making it unlikely that it acts as a repellent cue for retinal ganglion cell axons in the optic tract.

Antisense morpholino experiments showed that knocking down Slit1a caused axon guidance

Figure 1.2: Schematic of *slit* expression at optic chiasm. Based on Hutson and Chien (2002) and Barresi et al. (2005). Cartoon shows a ventral view of the zebrafish brain with anterior up. RGC axons grow in an area of high *slit1a* expression and between zones of *slit2* and *slit3* expression. AC, anterior commissure. POC, postoptic commissure. RGCs, retinal ganglion cells. OC, optic chiasm.



errors in the optic tract similar to those seen in the *astray* mutant, which lacks functional Robo2. Gain-of-function experiments, using my soldering iron misexpression system, showed that misexpressing either Slit1a or Slit2 near RGC axons caused them to turn toward the source of ectopic Slit. This confirmed my hypothesis that Slit1a acts as an attractant to Robo2-expressing axons. However, the Slit2 results were unexpected and contrary to our model for Slit function at the optic chiasm. These data are evidence that Slits can act as attractants to axons, a novel finding.

In Chapter 4, I describe work I undertook to study retinal axon sorting in the optic tract. Axon sorting within a tract is difficult to study using current methods. I used a new method of three-dimensional electron microscopy to obtain a dataset of a wild-type optic tract. Although this dataset was of limited utility for describing axon sorting, I was able to provide the data to computer scientists and assist in developing a new computational method of automated three-dimensional tracking of axons.

To summarize, I have added a new method to the zebrafish misexpression toolbox, and contributed to a new method for automated axon reconstruction. Furthermore, I have provided the first evidence that Slits can act to attract axons *in vivo*.

## References

- Anitha, A., Nakamura, K., Yamada, K., Suda, S., Thanseem, I., Tsujii, M., Iwayama, Y., Hattori, E., Toyota, T., Miyachi, T., et al. (2008). Genetic analyses of roundabout (ROBO) axon guidance receptors in autism. *Am. J. Med. Genet. B Neuropsychiatr. Genet* *147B*, 1019-1027.
- Atkinson-Leadbetter, K., Bertolesi, G. E., Hehr, C. L., Webber, C. A., Cechmanek, P. B., and McFarlane, S. (2010). Dynamic expression of axon guidance cues required for optic tract development is controlled by fibroblast growth factor signaling. *J. Neurosci* *30*, 685-693.
- Azevedo, F. A., Carvalho, L. R., Grinberg, L. T., Farfel, J. M., Ferretti, R. E., Leite, R. E., Filho, W. J., Lent, R., and Herculano-Houzel, S. (2009). Equal numbers of neuronal and nonneuronal cells make the human brain an isometrically scaled-up primate brain. *The Journal of Comparative Neurology* *513*, 532-541.
- Bagri, A., Marín, O., Plump, A. S., Mak, J., Pleasure, S. J., Rubenstein, J. L. R., and Tessier-Lavigne, M. (2002). Slit proteins prevent midline crossing and determine the dorsoventral position of major axonal pathways in the mammalian forebrain. *Neuron* *33*, 233-248.
- Baier, H., Klostermann, S., Trowe, T., Karlstrom, R. O., Nüsslein-Volhard, C., and Bonhoeffer, F. (1996). Genetic dissection of the retinotectal projection. *Development* *123*, 415-425.
- Barresi, M. J. F., Hutson, L. D., Chien, C., and Karlstrom, R. O. (2005). Hedgehog regulated Slit expression determines commissure and glial cell position in the zebrafish forebrain. *Development* *132*, 3643-3656.
- Brose, K., Bland, K. S., Wang, K. H., Arnott, D., Henzel, W., Goodman, C. S., Tessier-Lavigne, M., and Kidd, T. (1999). Slit proteins bind Robo receptors and have an evolutionarily conserved role in repulsive axon guidance. *Cell* *96*, 795-806.
- Bülow, H. E., and Hobert, O. (2004). Differential sulfations and epimerization define heparan sulfate specificity in nervous system development. *Neuron* *41*, 723-736.
- Cajal, S. (1917). *Recollections of my Life* (E.H. Craigie & J. Cano Trans, MIT Press 1989.).
- Campbell, D. S., Stringham, S. A., Timm, A., Xiao, T., Law, M., Baier, H., Nonet, M. L., and Chien, C. (2007). Slit1a inhibits retinal ganglion cell arborization and synaptogenesis via Robo2-dependent and -independent pathways. *Neuron* *55*, 231-245.
- Cebrià, F., Guo, T., Jopek, J., and Newmark, P. A. (2007). Regeneration and maintenance of the planarian midline is regulated by a slit orthologue. *Dev. Biol* *307*, 394-406.

- Cebrià, F., and Newmark, P. A. (2005). Planarian homologs of netrin and netrin receptor are required for proper regeneration of the central nervous system and the maintenance of nervous system architecture. *Development* 132, 3691-3703.
- Chalfie, M., Sulston, J., and White, J. (1985). The neural circuit for touch sensitivity in *Caenorhabditis elegans*. *Journal of Neuroscience* 5, 956-964.
- Chan, W., Traboulsi, E. I., Arthur, B., Friedman, N., Andrews, C., and Engle, E. C. (2006). Horizontal gaze palsy with progressive scoliosis can result from compound heterozygous mutations in ROBO3. *J. Med. Genet* 43, e11.
- Chauvet, S., Cohen, S., Yoshida, Y., Fekrane, L., Livet, J., Gayet, O., Segu, L., Buhot, M., Jessell, T. M., and Henderson, C. E. (2007). Gating of Sema3E/PlexinD1 signaling by Neuropilin-1 switches axonal repulsion to attraction during brain development. *Neuron* 56, 807-822.
- Chen, L., Liao, G., Waclaw, R. R., Burns, K. A., Linquist, D., Campbell, K., Zheng, Y., and Kuan, C. (2007). Rac1 controls the formation of midline commissures and the competency of tangential migration in ventral telencephalic neurons. *J. Neurosci* 27, 3884-3893.
- Chen, Z., Gore, B. B., Long, H., Ma, L., and Tessier-Lavigne, M. (2008). Alternative splicing of the Robo3 axon guidance receptor governs the midline switch from attraction to repulsion. *Neuron* 58, 325-332.
- Cheng, H. J., Nakamoto, M., Bergemann, A. D., and Flanagan, J. G. (1995). Complementary gradients in expression and binding of ELF-1 and Mek4 in development of the topographic retinotectal projection map. *Cell* 82, 371-381.
- Degano, A. L., Pasterkamp, R. J., and Ronnett, G. V. (2009). MeCP2 deficiency disrupts axonal guidance, fasciculation, and targeting by altering Semaphorin 3F function. *Mol. Cell. Neurosci* 42, 243-254.
- Dickson, B. J. (2002). Molecular mechanisms of axon guidance. *Science* 298, 1959-1964.
- Dou, C. L., and Levine, J. M. (1994). Inhibition of neurite growth by the NG2 chondroitin sulfate proteoglycan. *J. Neurosci* 14, 7616-7628.
- Drescher, U., Kremoser, C., Handwerker, C., Löschinger, J., Noda, M., and Bonhoeffer, F. (1995). In vitro guidance of retinal ganglion cell axons by RAGS, a 25 kDa tectal protein related to ligands for Eph receptor tyrosine kinases. *Cell* 82, 359-370.
- Engle, E. C. (2010). Human genetic disorders of axon guidance. *Cold Spring Harb Perspect Biol* 2, a001784.
- Englund, C., Steneberg, P., Falileeva, L., Xylourgidis, N., and Samakovlis, C. (2002). Attractive and repulsive functions of Slit are mediated by different receptors in the

- Drosophila trachea*. *Development* 129, 4941-4951.
- Fan, X., Labrador, J. P., Hing, H., and Bashaw, G. J. (2003). Slit stimulation recruits Dock and Pak to the roundabout receptor and increases Rac activity to regulate axon repulsion at the CNS midline. *Neuron* 40, 113-127.
- Fetcho, J. R., and Liu, K. S. (1998). Zebrafish as a model system for studying neuronal circuits and behavior. *Ann. N. Y. Acad. Sci* 860, 333-345.
- Fouquet, C., Di Meglio, T., Ma, L., Kawasaki, T., Long, H., Hirata, T., Tessier-Lavigne, M., Chedotal, A., and Nguyen-Ba-Charvet, K. T. (2007). Robo1 and Robo2 control the development of the lateral olfactory tract. *J. Neurosci.* 27, 3037-3045.
- Fricke, C., Lee, J. S., Geiger-Rudolph, S., Bonhoeffer, F., and Chien, C. B. (2001). astray, a zebrafish roundabout homolog required for retinal axon guidance. *Science* 292, 507-510.
- Fujisawa, K., Wrana, J. L., and Culotti, J. G. (2007). The Slit Receptor EVA-1 Coactivates a SAX-3/Robo mediated guidance signal in *C. elegans*. *Science* 317, 1934-1938.
- Fukuhara, N., Howitt, J. A., Hussain, S., and Hohenester, E. (2008). Structural and Functional analysis of Slit and Heparin binding to immunoglobulin-like domains 1 and 2 of *Drosophila* Robo. *Journal of Biological Chemistry* 283, 16226-16234.
- Gray, J. M., Hill, J. J., and Bargmann, C. I. (2005). A circuit for navigation in *Caenorhabditis elegans*. *Proceedings of the National Academy of Sciences of the United States of America* 102, 3184-3191.
- Guthrie, S. (1997). Axon guidance: Netrin receptors are revealed. *Current Biology* 7, R6-R9.
- Hacker, U., Nybakken, K., and Perrimon, N. (2005). Heparan sulphate proteoglycans: the sweet side of development. *Nat Rev Mol Cell Biol* 6, 530-541.
- Hamelin, M., Zhou, Y., Su, M. W., Scott, I. M., and Culotti, J. G. (1993). Expression of the UNC-5 guidance receptor in the touch neurons of *C. elegans* steers their axons dorsally. *Nature* 364, 327-330.
- Hammond, R., Vivancos, V., Naeem, A., Chilton, J., Mambetisaeva, E., Mambetisaeva, E., Andrews, W., Sundaresan, V., and Guthrie, S. (2005). Slit-mediated repulsion is a key regulator of motor axon pathfinding in the hindbrain. *Development* 132, 4483-4495.
- Hannula-Jouppi, K., Kaminen-Ahola, N., Taipale, M., Eklund, R., Nopola-Hemmi, J., Kääriäinen, H., and Kere, J. (2005). The axon guidance receptor gene ROBO1 is a candidate gene for developmental dyslexia. *PLoS Genet* 1, e50.
- Hedgecock, E. M., Culotti, J. G., and Hall, D. H. (1990). The unc-5, unc-6, and unc-40 genes guide circumferential migrations of pioneer axons and mesodermal cells on the

- epidermis in *C. elegans*. *Neuron* 4, 61-85.
- Hehr, C. L., Hocking, J. C., and McFarlane, S. (2005). Matrix metalloproteinases are required for retinal ganglion cell axon guidance at select decision points. *Development* 132, 3371-3379.
- Hohenester, E., Hussain, S., and Howitt, J. A. (2006). Interaction of the guidance molecule Slit with cellular receptors. *Biochem. Soc. Trans* 34, 418-421.
- Hong, K., Nishiyama, M., Henley, J., Tessier-Lavigne, M., and Poo, M. (2000). Calcium signalling in the guidance of nerve growth by netrin-1. *Nature* 403, 93-98.
- Howitt, J. A., Clout, N. J., and Hohenester, E. (2004). Binding site for Robo receptors revealed by dissection of the leucine-rich repeat region of Slit. *EMBO J* 23, 4406-4412.
- Hu, H., Li, M., Labrador, J., McEwen, J., Lai, E. C., Goodman, C. S., and Bashaw, G. J. (2005). Cross GTPase-activating protein (CrossGAP)/Vilse links the Roundabout receptor to Rac to regulate midline repulsion. *Proc. Natl. Acad. Sci. U.S.A* 102, 4613-4618.
- Hu, H. (2001). Cell-surface heparan sulfate is involved in the repulsive guidance activities of Slit2 protein. *Nat Neurosci* 4, 695-701.
- Hussain, S., Piper, M., Fukuhara, N., Strohlic, L., Cho, G., Howitt, J. A., Ahmed, Y., Powell, A. K., Turnbull, J. E., Holt, C. E., et al. (2006). A molecular mechanism for the heparan sulfate dependence of Slit-Robo signaling. *Journal of Biological Chemistry* 281, 39693-39698.
- Hutson, L. D., Campbell, D. S., and Chien, C. (2004). Analyzing axon guidance in the zebrafish retinotectal system. *Methods Cell Biol* 76, 13-35.
- Hutson, L. D., and Chien, C. B. (2002). Pathfinding and error correction by retinal axons: the role of *astray/robo2*. *Neuron* 33, 205-217.
- Hutson, L. D., Jurynek, M. J., Yeo, S., Okamoto, H., and Chien, C. (2003). Two divergent *slit1* genes in zebrafish. *Dev. Dyn* 228, 358-369.
- Imai, T., Yamazaki, T., Kobayakawa, R., Kobayakawa, K., Abe, T., Suzuki, M., and Sakano, H. (2009). Pre-target axon sorting establishes the neural map topography. *Science* 325, 585-590.
- Inatani, M., Irie, F., Plump, A. S., Tessier-Lavigne, M., and Yamaguchi, Y. (2003). Mammalian brain morphogenesis and midline axon guidance require heparan sulfate. *Science* 302, 1044-1046.
- Ishii, N., Wadsworth, W. G., Stern, B. D., Culotti, J. G., and Hedgecock, E. M. (1992). UNC-6, a laminin-related protein, guides cell and pioneer axon migrations in *C. elegans*.

Neuron 9, 873-881.

- Itoh, A., Miyabayashi, T., Ohno, M., and Sakano, S. (1998). Cloning and expressions of three mammalian homologues of *Drosophila* slit suggest possible roles for Slit in the formation and maintenance of the nervous system. *Brain Res. Mol. Brain Res* 62, 175-186.
- Jen, J. C., Chan, W., Bosley, T. M., Wan, J., Carr, J. R., Rüb, U., Shattuck, D., Salamon, G., Kudo, L. C., Ou, J., et al. (2004). Mutations in a human ROBO gene disrupt hindbrain axon pathway crossing and morphogenesis. *Science* 304, 1509-1513.
- Jia, L., Cheng, L., and Raper, J. (2005). Slit/Robo signaling is necessary to confine early neural crest cells to the ventral migratory pathway in the trunk. *Dev. Biol* 282, 411-421.
- Jin, M., Guan, C., Jiang, Y., Chen, G., Zhao, C., Cui, K., Song, Y., Wu, C., Poo, M., and Yuan, X. (2005). Ca<sup>2+</sup>-Dependent regulation of Rho GTPases triggers turning of nerve growth cones. *J. Neurosci.* 25, 2338-2347.
- Johnson, K. G., Ghose, A., Epstein, E., Lincecum, J., O'Connor, M. B., and Van Vactor, D. (2004). Axonal heparan sulfate proteoglycans regulate the distribution and efficiency of the repellent Slit during midline axon guidance. *Current Biology* 14, 499-504.
- Kantor, D., Chivatakarn, O., Peer, K., Oster, S., Inatani, M., Hansen, M., Flanagan, J., Yamaguchi, Y., Sretavan, D., Giger, R., et al. (2004). Semaphorin 5A is a bifunctional axon guidance cue regulated by heparan and chondroitin sulfate proteoglycans. *Neuron* 44, 961-975.
- Kasai, H., Terashima, T., Fukaya, M., Nakao, K., Sakahara, M., Watanabe, M., and Aiba, A. (2008). Rac1 in cortical projection neurons is selectively required for midline crossing of commissural axonal formation. *Eur. J. Neurosci* 28, 257-267.
- Kastenhuber, E., Kern, U., Bonkowsky, J. L., Chien, C., Driever, W., and Schweitzer, J. (2009). Netrin-DCC, Robo-Slit, and heparan sulfate proteoglycans coordinate lateral positioning of longitudinal dopaminergic diencephalospinal axons. *J. Neurosci* 29, 8914-8926.
- Kaufmann, N., Wills, Z. P., and Van Vactor, D. (1998). *Drosophila* Rac1 controls motor axon guidance. *Development* 125, 453-461.
- Keino-Masu, K., Masu, M., Hinck, L., Leonardo, E., Chan, S., Culotti, J., and Tessier-Lavigne, M. (1996). Deleted in Colorectal Cancer (DCC) encodes a netrin receptor. *Cell* 87, 175-185.
- Keleman, K., Rajagopalan, S., Cleppien, D., Teis, D., Paiha, K., Huber, L. A., Technau, G. M., and Dickson, B. J. (2002). Comm sorts robo to control axon guidance at the *Drosophila* midline. *Cell* 110, 415-427.

- Keleman, K., Ribeiro, C., and Dickson, B. J. (2005). Comm function in commissural axon guidance: cell-autonomous sorting of Robo in vivo. *Nat. Neurosci* 8, 156-163.
- Kennedy, T. E., Serafini, T., de la Torre, J. R., and Tessier-Lavigne, M. (1994). Netrins are diffusible chemotropic factors for commissural axons in the embryonic spinal cord. *Cell* 78, 425-435.
- Kidd, T., Bland, K. S., and Goodman, C. S. (1999). Slit is the midline repellent for the robo receptor in *Drosophila*. *Cell* 96, 785-794.
- Kidd, T., Brose, K., Mitchell, K. J., Fetter, R. D., Tessier-Lavigne, M., Goodman, C. S., and Tear, G. (1998). Roundabout controls axon crossing of the CNS midline and defines a novel subfamily of evolutionarily conserved guidance receptors. *Cell* 92, 205-215.
- Knöll, B., Schmidt, H., Andrews, W., Guthrie, S., Pini, A., Sundaresan, V., and Drescher, U. (2003). On the topographic targeting of basal vomeronasal axons through Slit-mediated chemorepulsion. *Development* 130, 5073-5082.
- Kolesnikov, T., and Beckendorf, S. K. (2005). NETRIN and SLIT guide salivary gland migration. *Dev. Biol* 284, 102-111.
- Kolk, S. M., Gunput, R. F., Tran, T. S., van den Heuvel, D. M. A., Prasad, A. A., Hellemons, A. J. C. G. M., Adolfs, Y., Ginty, D. D., Kolodkin, A. L., Burbach, J. P. H., et al. (2009). Semaphorin 3F is a bifunctional guidance cue for dopaminergic axons and controls their fasciculation, channeling, rostral growth, and intracortical targeting. *J. Neurosci.* 29, 12542-12557.
- Kolodkin, A. L., Matthes, D. J., O'Connor, T. P., Patel, N. H., Admon, A., Bentley, D., and Goodman, C. S. (1992). Fasciclin IV: sequence, expression, and function during growth cone guidance in the grasshopper embryo. *Neuron* 9, 831-845.
- Kramer, S. G., Kidd, T., Simpson, J. H., and Goodman, C. S. (2001). Switching repulsion to attraction: changing responses to slit during transition in mesoderm migration. *Science* 292, 737-740.
- Kwan, K. M., Fujimoto, E., Grabher, C., Mangum, B. D., Hardy, M. E., Campbell, D. S., Parant, J. M., Yost, H. J., Kanki, J. P., and Chien, C. (2007). The Tol2kit: a multisite gateway-based construction kit for Tol2 transposon transgenesis constructs. *Dev. Dyn* 236, 3088-3099.
- Lee, J., von der Hardt, S., Rusch, M. A., Stringer, S. E., Stickney, H. L., Talbot, W. S., Geisler, R., Nüsslein-Volhard, C., Selleck, S. B., Chien, C., et al. (2004). Axon sorting in the optic tract requires HSPG synthesis by ext2 (dackel) and extl3 (boxer). *Neuron* 44, 947-960.
- Lee, J., Ray, R., and Chien, C. (2001). Cloning and expression of three zebrafish roundabout homologs suggest roles in axon guidance and cell migration. *Dev. Dyn.* 221, 216-230.

- Leung-Hagesteijn, C., Spence, A., Stern, B., Zhou, Y., Su, M., Hedgecock, E., and Culotti, J. (1992). UNC-5, a transmembrane protein with immunoglobulin and thrombospondin type 1 domains, guides cell and pioneer axon migrations in *C. elegans*. *Cell* *71*, 289-299.
- Leung, K., Taylor, J. S. H., and Chan, S. (2003). Enzymatic removal of chondroitin sulphates abolishes the age-related axon order in the optic tract of mouse embryos. *Eur J Neurosci* *17*, 1755-1767.
- Li, C., Bassell, G. J., and Sasaki, Y. (2009). Fragile X mental retardation protein is involved in protein synthesis-dependent collapse of growth cones induced by Semaphorin-3A. *Front Neural Circuits* *3*, 11.
- Li, H. S., Chen, J. H., Wu, W., Fagaly, T., Zhou, L., Yuan, W., Dupuis, S., Jiang, Z. H., Nash, W., Gick, C., et al. (1999). Vertebrate slit, a secreted ligand for the transmembrane protein roundabout, is a repellent for olfactory bulb axons. *Cell* *96*, 807-818.
- Li, X., Saint-Cyr-Proulx, E., Aktories, K., and Lamarche-Vane, N. (2002). Rac1 and Cdc42 but not RhoA or Rho kinase activities are required for neurite outgrowth induced by the Netrin-1 receptor DCC (Deleted in Colorectal Cancer) in N1E-115 neuroblastoma cells. *Journal of Biological Chemistry* *277*, 15207-15214.
- Lichtman, J. W., and Sanes, J. R. (2008). Ome sweet ome: what can the genome tell us about the connectome? *Curr. Opin. Neurobiol* *18*, 346-353.
- Liu, Z., Patel, K., Schmidt, H., Andrews, W., Pini, A., and Sundaresan, V. (2004). Extracellular Ig domains 1 and 2 of Robo are important for ligand (Slit) binding. *Mol. Cell. Neurosci* *26*, 232-240.
- Long, H., Sabatier, C., Ma, L., Plump, A., Yuan, W., Ornitz, D. M., Tamada, A., Murakami, F., Goodman, C. S., and Tessier-Lavigne, M. (2004). Conserved roles for Slit and Robo proteins in midline commissural axon guidance. *Neuron* *42*, 213-223.
- López-Bendito, G., Flames, N., Ma, L., Fouquet, C., Di Meglio, T., Chedotal, A., Tessier-Lavigne, M., and Marín, O. (2007). Robo1 and Robo2 cooperate to control the guidance of major axonal tracts in the mammalian forebrain. *J. Neurosci* *27*, 3395-3407.
- Lundström, A., Gallio, M., Englund, C., Steneberg, P., Hemphälä, J., Aspenström, P., Keleman, K., Falileeva, L., Dickson, B. J., and Samakovlis, C. (2004). Vilse, a conserved Rac/Cdc42 GAP mediating Robo repulsion in tracheal cells and axons. *Genes Dev* *18*, 2161-2171.
- Luo, L., Liao, Y. J., Jan, L. Y., and Jan, Y. N. (1994). Distinct morphogenetic functions of similar small GTPases: *Drosophila* Drac1 is involved in axonal outgrowth and myoblast fusion. *Genes Dev* *8*, 1787-1802.

- Luo, Y., Raible, D., and Raper, J. A. (1993). Collapsin: a protein in brain that induces the collapse and paralysis of neuronal growth cones. *Cell* *75*, 217-227.
- Ma, L., and Tessier-Lavigne, M. (2007). Dual branch-promoting and branch-repelling actions of Slit/Robo signaling on peripheral and central branches of developing sensory axons. *J. Neurosci* *27*, 6843-6851.
- Ming, G. L., Song, H. J., Berninger, B., Holt, C. E., Tessier-Lavigne, M., and Poo, M. M. (1997). cAMP-dependent growth cone guidance by netrin-1. *Neuron* *19*, 1225-1235.
- Miyasaka, N., Sato, Y., Yeo, S., Hutson, L. D., Chien, C., Okamoto, H., and Yoshihara, Y. (2005). Robo2 is required for establishment of a precise glomerular map in the zebrafish olfactory system. *Development* *132*, 1283-1293.
- Miyashita, T., Yeo, S., Hirate, Y., Segawa, H., Wada, H., Little, M. H., Yamada, T., Takahashi, N., and Okamoto, H. (2004). PlexinA4 is necessary as a downstream target of Islet2 to mediate Slit signaling for promotion of sensory axon branching. *Development* *131*, 3705-3715.
- Mori, I., and Ohshima, Y. (1995). Neural regulation of thermotaxis in *Caenorhabditis elegans*. *Nature* *376*, 344-348.
- Morlot, C., Thielens, N. M., Ravelli, R. B. G., Hemrika, W., Romijn, R. A., Gros, P., Cusack, S., and McCarthy, A. A. (2007). Structural insights into the Slit-Robo complex. *Proc. Natl. Acad. Sci. U.S.A* *104*, 14923-14928.
- Myat, A., Henry, P., McCabe, V., Flintoft, L., Rotin, D., and Tear, G. (2002). *Drosophila* Nedd4, a ubiquitin ligase, is recruited by Commissureless to control cell surface levels of the roundabout receptor. *Neuron* *35*, 447-459.
- Nguyen Ba-Charvet, K. T., Brose, K., Ma, L., Wang, K. H., Marillat, V., Sotelo, C., Tessier-Lavigne, M., and Chédotal, A. (2001). Diversity and specificity of actions of Slit2 proteolytic fragments in axon guidance. *J. Neurosci* *21*, 4281-4289.
- Nguyen-Ba-Charvet, K. T., Di Meglio, T., Fouquet, C., and Chédotal, A. (2008). Robos and slits control the pathfinding and targeting of mouse olfactory sensory axons. *J. Neurosci* *28*, 4244-4249.
- Nguyen-Ba-Charvet, K. T., Picard-Riera, N., Tessier-Lavigne, M., Baron-Van Evercooren, A., Sotelo, C., and Chédotal, A. (2004). Multiple roles for slits in the control of cell migration in the rostral migratory stream. *J. Neurosci* *24*, 1497-1506.
- Plas, D. T., Dhande, O. S., Lopez, J. E., Murali, D., Thaller, C., Henkemeyer, M., Furuta, Y., Overbeek, P., and Crair, M. C. (2008). Bone morphogenetic proteins, eye patterning, and retinocollicular map formation in the mouse. *J. Neurosci* *28*, 7057-7067.
- Plump, A. S., Erskine, L., Sabatier, C., Brose, K., Epstein, C. J., Goodman, C. S., Mason, C. A., and Tessier-Lavigne, M. (2002). Slit1 and Slit2 cooperate to prevent premature

- midline crossing of retinal axons in the mouse visual system. *Neuron* 33, 219-232.
- Prince, J. E. A., Cho, J. H., Dumontier, E., Andrews, W., Cutforth, T., Tessier-Lavigne, M., Parnavelas, J., and Cloutier, J. (2009). Robo-2 controls the segregation of a portion of basal vomeronasal sensory neuron axons to the posterior region of the accessory olfactory bulb. *J. Neurosci* 29, 14211-14222.
- Rajagopalan, S., Nicolas, E., Vivancos, V., Berger, J., and Dickson, B. J. (2000). Crossing the midline: roles and regulation of Robo receptors. *Neuron* 28, 767-777.
- Rhiner, C., Gysi, S., Fröhli, E., Hengartner, M. O., and Hajnal, A. (2005). Syndecan regulates cell migration and axon guidance in *C. elegans*. *Development* 132, 4621-4633.
- Rothberg, J. M., Jacobs, J. R., Goodman, C. S., and Artavanis-Tsakonas, S. (1990). slit: an extracellular protein necessary for development of midline glia and commissural axon pathways contains both EGF and LRR domains. *Genes Dev* 4, 2169-2187.
- Sabatier, C., Plump, A. S., Le Ma, Brose, K., Tamada, A., Murakami, F., Lee, E. Y. P., and Tessier-Lavigne, M. (2004). The divergent Robo family protein rig-1/Robo3 is a negative regulator of slit responsiveness required for midline crossing by commissural axons. *Cell* 117, 157-169.
- Satoda, M., Takagi, S., Ohta, K., Hirata, T., and Fujisawa, H. (1995). Differential expression of two cell surface proteins, neuropilin and plexin, in *Xenopus* olfactory axon subclasses. *J. Neurosci.* 15, 942-955.
- Scholes, J. H. (1979). Nerve fibre topography in the retinal projection to the tectum. *Nature* 278, 620-624.
- Schwanzel-Fukuda, M., Bick, D., and Pfaff, D. W. (1989). Luteinizing hormone-releasing hormone (LHRH)-expressing cells do not migrate normally in an inherited hypogonadal (Kallmann) syndrome. *Brain Res. Mol. Brain Res* 6, 311-326.
- Seeger, M., Tear, G., Ferres-Marco, D., and Goodman, C. S. (1993). Mutations affecting growth cone guidance in drosophila: Genes necessary for guidance toward or away from the midline. *Neuron* 10, 409-426.
- Serafini, T., Kennedy, T. E., Galko, M. J., Mirzayan, C., Jessell, T. M., and Tessier-Lavigne, M. (1994). The netrins define a family of axon outgrowth-promoting proteins homologous to *C. elegans* UNC-6. *Cell* 78, 409-424.
- Sicotte, N. L., Salamon, G., Shattuck, D. W., Hageman, N., Rüb, U., Salamon, N., Drain, A. E., Demer, J. L., Engle, E. C., Alger, J. R., et al. (2006). Diffusion tensor MRI shows abnormal brainstem crossing fibers associated with ROBO3 mutations. *Neurology* 67, 519-521.
- Simpson, J. H., Kidd, T., Bland, K. S., and Goodman, C. S. (2000). Short-range and long-range guidance by slit and its Robo receptors. Robo and Robo2 play distinct roles in

- midline guidance. *Neuron* 28, 753-766.
- Snow, D. M., Mullins, N., and Hynds, D. L. (2001). Nervous system-derived chondroitin sulfate proteoglycans regulate growth cone morphology and inhibit neurite outgrowth: a light, epifluorescence, and electron microscopy study. *Microsc. Res. Tech* 54, 273-286.
- Song, H., Ming, G., He, Z., Lehmann, M., McKerracher, L., Tessier-Lavigne, M., and Poo, M. (1998). Conversion of neuronal growth cone responses from repulsion to attraction by cyclic nucleotides. *Science* 281, 1515-1518.
- Song, H., Ming, G., and Poo, M. (1997). cAMP-induced switching in turning direction of nerve growth cones. *Nature* 388, 275-279.
- Sperry, R. W. (1963). Chemoaffinity in the orderly growth of nerve fiber patterns and connections. *Proceedings of the National Academy of Sciences of the United States of America* 50, 703-710.
- Steigemann, P., Molitor, A., Fellert, S., Jäckle, H., and Vorbrüggen, G. (2004). Heparan sulfate proteoglycan Syndecan promotes axonal and myotube guidance by Slit/Robo signaling. *Current Biology* 14, 225-230.
- Taylor, T. D., Robichaux, M. B., and Garrity, P. A. (2004). Compartmentalization of visual centers in the *Drosophila* brain requires Slit and Robo proteins. *Development* 131, 5935-5945.
- Tischfield, M. A., Baris, H. N., Wu, C., Rudolph, G., Van Maldergem, L., He, W., Chan, W., Andrews, C., Demer, J. L., Robertson, R. L., et al. (2010). Human TUBB3 mutations perturb microtubule dynamics, kinesin interactions, and axon guidance. *Cell* 140, 74-87.
- Trowe, T., Klostermann, S., Baier, H., Granato, M., Crawford, A. D., Grunewald, B., Hoffmann, H., Karlstrom, R. O., Meyer, S. U., Müller, B., et al. (1996). Mutations disrupting the ordering and topographic mapping of axons in the retinotectal projection of the zebrafish, *Danio rerio*. *Development* 123, 439-450.
- Tucker, B., Richards, R. I., and Lardelli, M. (2006). Contribution of mGluR and Fmr1 functional pathways to neurite morphogenesis, craniofacial development and fragile X syndrome. *Hum. Mol. Genet* 15, 3446-3458.
- Van Vactor, D., Wall, D. P., and Johnson, K. G. (2006). Heparan sulfate proteoglycans and the emergence of neuronal connectivity. *Current Opinion in Neurobiology* 16, 40-51.
- Vorstman, J. A. S., van Daalen, E., Jalali, G. R., Schmidt, E. R. E., Pasterkamp, R. J., de Jonge, M., Hennekam, E. A. M., Janson, E., Staal, W. G., van der Zwaag, B., et al. (2010). A double hit implicates DIAPH3 as an autism risk gene. *Mol Psychiatry*. Available at: <http://www.ncbi.nlm.nih.gov/pubmed/20308993> [Accessed March 31, 2010].

- Wahl, S., Barth, H., Ciossek, T., Aktories, K., and Mueller, B. K. (2000). Ephrin-A5 induces collapse of growth cones by activating Rho and Rho kinase. *J. Cell Biol.* *149*, 263-270.
- Wang, K. H., Brose, K., Arnott, D., Kidd, T., Goodman, C. S., Henzel, W., and Tessier-Lavigne, M. (1999). Biochemical purification of a mammalian slit protein as a positive regulator of sensory axon elongation and branching. *Cell* *96*, 771-784.
- White, J. G., Southgate, E., Thomson, J. N., and Brenner, S. (1986). The structure of the nervous system of the nematode *Caenorhabditis elegans*. *Philosophical Transactions of the Royal Society of London. B, Biological Sciences* *314*, 1-340.
- Whitford, K. L., and Ghosh, A. (2001). Plexin signaling via off-track and rho family GTPases. *Neuron* *32*, 1-3.
- Wilkinson, D. G. (2001). Multiple roles of eph receptors and ephrins in neural development. *Nat Rev Neurosci* *2*, 155-164.
- Williams, R. W., and Herrup, K. (1988). The control of neuron number. *Annu. Rev. Neurosci.* *11*, 423-453.
- Wolman, M. A., Liu, Y., Tawarayama, H., Shoji, W., and Halloran, M. C. (2004). Repulsion and attraction of axons by Semaphorin3D are mediated by different Neuropilins in vivo. *J. Neurosci.* *24*, 8428-8435.
- Wong, K., Ren, X. R., Huang, Y. Z., Xie, Y., Liu, G., Saito, H., Tang, H., Wen, L., Brady-Kalnay, S. M., Mei, L., et al. (2001). Signal transduction in neuronal migration: roles of GTPase activating proteins and the small GTPase Cdc42 in the Slit-Robo pathway. *Cell* *107*, 209-221.
- Yang, L., and Bashaw, G. J. (2006). Son of sevenless directly links the Robo receptor to rac activation to control axon repulsion at the midline. *Neuron* *52*, 595-607.
- Yaron, A., and Zheng, B. (2007). Navigating their way to the clinic: Emerging roles for axon guidance molecules in neurological disorders and injury. *Developmental Neurobiology* *67*, 1216-1231.
- Yeo, S. Y., Little, M. H., Yamada, T., Miyashita, T., Halloran, M. C., Kuwada, J. Y., Huh, T. L., and Okamoto, H. (2001). Overexpression of a slit homologue impairs convergent extension of the mesoderm and causes cyclopia in embryonic zebrafish. *Dev. Biol* *230*, 1-17.
- Yuan, W., Zhou, L., Chen, J. H., Wu, J. Y., Rao, Y., and Ornitz, D. M. (1999). The mouse SLIT family: secreted ligands for ROBO expressed in patterns that suggest a role in morphogenesis and axon guidance. *Dev. Biol* *212*, 290-306.
- Yuan, X., Jin, M., Xu, X., Song, Y., Wu, C., Poo, M., and Duan, S. (2003). Signalling and

- crosstalk of Rho GTPases in mediating axon guidance. *Nat. Cell Biol* 5, 38-45.
- Zallen, J. A., Yi, B. A., and Bargmann, C. I. (1998). The conserved immunoglobulin superfamily member SAX-3/Robo directs multiple aspects of axon guidance in *C. elegans*. *Cell* 92, 217-227.
- Zheng, J. Q. (2000). Turning of nerve growth cones induced by localized increases in intracellular calcium ions. *Nature* 403, 89-93.

CHAPTER 2

FOCAL GENE MISEXPRESSION IN ZEBRAFISH EMBRYOS  
INDUCED BY LOCAL HEAT SHOCK USING  
A MODIFIED SOLDERING IRON

MELISSA E. HARDY, LOUIS V. ROSS, CHI-BIN CHIEN

DEVELOPMENTAL DYNAMICS 236:3071-3076, 2007.

"

"

"

The following paper was published in *Developmental Dynamics* and is used with permission. When I began to study Slits in the zebrafish retinotectal system, it became clear that I would need to misexpress the Slits in a spatially and temporally restricted manner. Chi-Bin Chien proposed using a soldering iron to locally heat a region of a transgenic embryo, in which the heat shock promoter drove transgene expression. I undertook this project with assistance from Louis Ross, an undergraduate in the lab. Louis built the perfusion apparatus and sharpened the soldering tips. I tested the apparatus and soldering iron, and gave him suggestions to improve the equipment. I tested three different stable transgenic lines and was able to activate robust transgene expression in each. Developing this technique allowed me to control transgene expression both temporally and spatially, and allowed me to test Slit function in the retinotectal system, as described in Chapter 3.

# Focal Gene Misexpression in Zebrafish Embryos Induced by Local Heat Shock Using a Modified Soldering Iron

Melissa E. Hardy,<sup>1</sup> Louis V. Ross,<sup>1</sup> and Chi-Bin Chien<sup>1,2\*</sup>

Misexpression of genes in a temporally and spatially controlled fashion is an important tool for assessing gene function during development. Because few tissue-specific promoters have been identified in zebrafish, inducible systems such as the Cre/LoxP and Tet repressor systems are of limited utility. Here we describe a new method of misexpression: local heat shock using a modified soldering iron. Zebrafish carrying transgenes under the control of a heat shock promoter (*hsp70*) are focally heated with the soldering iron to induce gene expression in a small area of the embryo. We have validated this method in three stable transgenic lines and at three developmental timepoints. Local heat shock is a fast, easy, and inexpensive method for gene misexpression. *Developmental Dynamics* 236:3071–3076, 2007. © 2007 Wiley-Liss, Inc.

**Key words:** transgene; conditional expression; *hsp70*, GFP

Accepted 3 August 2007

## INTRODUCTION

The zebrafish is an excellent model for developmental biology due to its transparency, external fertilization, and large clutch size, which allow both embryological and genetic manipulation. Forward genetics has been very successful, yielding hundreds of mutants from various screens (reviewed in Amsterdam and Hopkins, 2006); reverse genetics is commonly approximated with antisense morpholinos (Nasevicius and Ekker, 2000); and zebrafish mutant for specific genes can be isolated using TILLing (Wienholds et al., 2003). However, while these loss-of-function methods allow powerful tests of required gene functions, gain-of-function experiments are

needed to test sufficiency. Moreover, some biological questions require expression or knockdown of a particular gene in a spatially and temporally controlled manner, especially when a gene has both an early and a late role in development. Ideally, one would like methods to misexpress or knock down a gene of interest at any desired time and place in the embryo in order to test gene function.

A number of methods have been used for gene misexpression in zebrafish, including electroporation, mRNA injection, mosaic expression from injected DNA constructs, and inducible systems, such as the Tet repressor and Cre/Lox systems; each has its own advantages and disadvan-

tages (Ungar et al., 1995; Teh et al., 2003; Liu and Halloran 2005; Huang et al., 2005; Langenau et al., 2005; Cerda et al., 2006; Hendricks and Jesuthasan, 2007).

The most widely used inducible element, the heat shock (*hsp70*) promoter, is a powerful tool for the induction of a transgene of interest at any time in development. A global heat shock, typically for 1 hr at 37°C (compared to the standard 28.5°C raising temperature), can be used to induce expression of transgenes throughout the embryo (Halloran et al., 2000; Yeo et al., 2001). However, this method is not suitable for experiments that require expression in only part of the embryo. Laser activation of the *hsp70*

The Supplementary Material referred to in this article can be viewed at [www.interscience.wiley.com/jpages/1058-8388/suppmat](http://www.interscience.wiley.com/jpages/1058-8388/suppmat)

<sup>1</sup>Department of Neurobiology and Anatomy, University of Utah, Salt Lake City, Utah

<sup>2</sup>Brain Institute, University of Utah, Salt Lake City, Utah

Grant sponsor: NIH; Grant numbers: 5T32 HD007491, R01 EY 12873.

\*Correspondence to: Chi-Bin Chien, Department of Neurobiology and Anatomy, 401 MREB, University of Utah Medical Center, 20 North 1900 East, Salt Lake City, UT 84132-3401. E-mail: [chi-bin.chien@neuro.utah.edu](mailto:chi-bin.chien@neuro.utah.edu)

DOI 10.1002/dvdy.21318

Published online 28 September 2007 in Wiley InterScience (www.interscience.wiley.com).

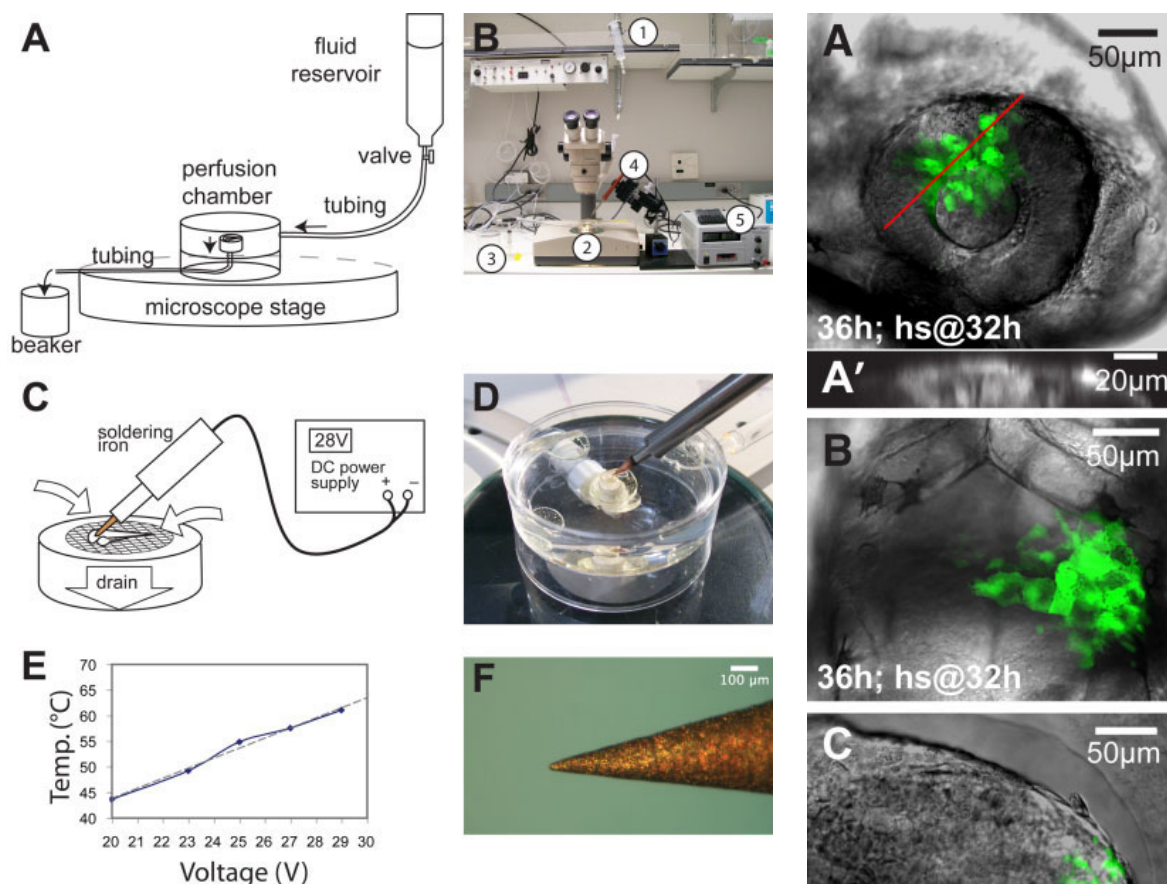


**Fig. 1.** Apparatus for local heat shock. The perfusion apparatus, schematized in **A** and shown in **B**, keeps fluid flowing over the embryo during heat shock. This prevents heating of the fluid around the embryo and keeps the area of activation small. **B** shows (1) fluid reservoir, (2) perfusion chamber, (3) outflow tubing and beaker, (4) soldering iron, (5) DC power supply. The soldering iron, powered by a DC power supply (**B**, **C**), is used to generate heat. The tip (**F**) is ground down to  $\sim 15$   $\mu\text{m}$  and touched to the embryo (**C**, **D**) to induce a heat shock response. The temperature at the tip is  $\sim 60^\circ\text{C}$  at 28.5V when measured in air (**E**).

promoter can induce expression in single cells (Halloran et al., 2000), but as the induction of the transgene is probably a response to stress rather than heat, careful titration of laser exposure is necessary to avoid killing cells. Moreover, success with the laser method varies greatly between different transgenic lines (J. Bonner and R. Dorsky, personal communication).

Here we introduce an alternate method for locally activating the heat shock response in transgenic animals by directly heating a small area of the embryo with a modified soldering iron. This method is fast, inexpensive, and technically simple, making it a useful addition to the zebrafish gain-of-function toolbox.

## RESULTS

### Principle

The idea of focally heating living tissue is not new. Nicklas (1973) used wire microheaters, 2  $\mu\text{m}$  in diameter, to locally heat a subcellular domain of grasshopper spermatocyte cells and observe focal changes in the mitotic spindle. Monsma et al. (1988) used a heated needle to induce gene expression under the control of the heat shock promoter in *Drosophila*. A limitation of both approaches is that the temperature at the heater tip is difficult to control. We took a different approach, reasoning that using a large thermal mass with good thermal conductivity (a copper

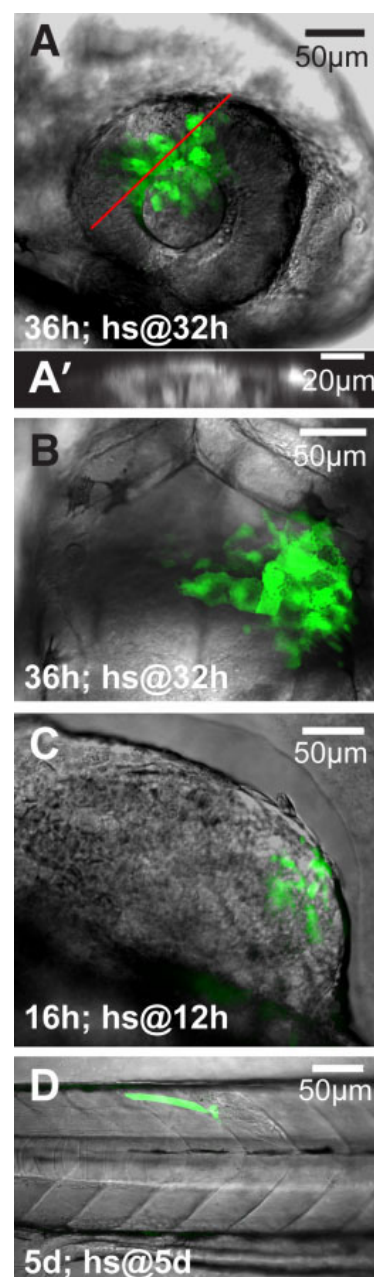


**Fig. 2.** Local heat shock induces GFP expression in multiple tissues and at multiple stages in the *hs:gfp* line. GFP can be induced in eye (**A**), hindbrain (**B**), forebrain (**C**), and somite (**D**). Local heat shock is effective from at least 12 hpf (**C**) until 5 dpf (**D**). GFP is activated to a depth of at least 20  $\mu\text{m}$ , as shown in **A'**, which is resliced across the red line shown in **A**. **A**, **C**, **D**: Lateral views, anterior to right; **B**: dorsal view, anterior is up; **A'**: surface up.

soldering iron tip, ground down to a tip diameter of  $\sim 15$   $\mu\text{m}$ ) as our local heat source would allow us to reli-

ably set its temperature without too much cooling when the tip was placed in water. By placing the tip in direct contact with an embryo, and flushing away heated media with a perfusion apparatus, we can effectively “temperature-clamp” a small region of tissue.

### Optimization

We first used a thermocouple to measure the tip temperature in air with voltage settings from 20–29V (Fig. 1E). We then tried to induce local heat shock using voltage settings from 26–29V (see Fig. 1E), and found that the most reliable local heat shock induction was obtained at 28.5V, which gave 60°C when measured in air. The tip presumably cools slightly when placed in water, but we have not measured the exact temperature decrease. We tried heating embryos for 2, 3, or 5 min. Touching the soldering iron to the embryo for 3 min gave more reliable results than 2 min, while 5 min of heating did not significantly improve the rate of induction, but did increase mortality slightly. We therefore used 3 min for the rest of the experiments.

An initial experiment, in which we applied the heated tip to the head of several *hsp70:gfp* embryos and assayed GFP several hours later, demonstrated the feasibility of the local heat shock method. However, the area of GFP expression covered a much greater area than expected, given the small tip diameter. We hypothesized that this was due to heating of the medium around the embryo, which in turn heated the embryo and induced expression in a large area. To prevent this indirect heating, we built a perfusion apparatus to flow fluid over the embryo (Fig. 1A,B). This allowed us to induce a much smaller domain of expression. We measured the spot size in the X and Y dimensions, using confocal projections from 39 embryos carrying three different transgenes (see below), and found an average spot size of  $74 \times 69 \mu\text{m}$ . While this is still larger than the size of the tip, using perfusion clearly yields much smaller spots. Indeed, our later experiments show a trend toward a smaller area of induction. For instance, the experiment using *hs: $\Delta$ Tcf-gfp* gave an aver-

age spot size of  $57 \times 41 \mu\text{m}$  ( $n = 7$ ; see below).

We also measured the depth of transgene induction along the Z axis. Using ImageJ to reslice the confocal stack of the *hsp70:gfp* embryo of Figure 2A showed that GFP was expressed to a depth of 20  $\mu\text{m}$  from the surface (Fig. 2A'). We also resliced a confocal stack from a locally heat shocked *hs: $\Delta$ Tcf-gfp* embryo (Fig. 3E and E'). GFP is visible to a depth of 40  $\mu\text{m}$ .

### Lines, Stages, and Tissues Tested

Once we optimized the voltage and time parameters, we tested if we could reliably induce local heat shock in different tissues and at different developmental stages. Using the *hs:gfp* line, local heat shock induced GFP at 12 hpf, 30–32 hpf, and 5 dpf, resulting in detectable GFP expression approximately 4 hr after local heat shock (Fig. 2). At 12 hpf, we did not use the perfusion apparatus because the round embryos roll freely on the netting. Instead, we held embryos in agarose grooves without perfusion. The size of the spots was, therefore, variable; however, local heat shock clearly works at this age (Fig. 2C). At 30–32 hpf, we induced GFP expression in multiple targeted tissues, including eye, hindbrain, and somites (Figs. 2A,B, 3D).

To quantitate our success rate using the *hs:gfp* line, we raised locally heat-shocked embryos to 48 hpf and scored for GFP expression in the lens, where *hsp70* is expressed independent of heat shock in transgenic carriers. To exclude earlier experiments before optimization of the method, we counted only experiments in which at least one embryo expressed GFP 4 hr after local heat shock. Using 28.5V (60°C in air), we locally heat-shocked 74 carriers (identified at 48 hpf by GFP expressed in the lens) in 9 experiments, of which 48 were GFP+, for a success rate of 65%.

We next repeated the 30 hpf local heat-shock in two other transgenic lines. We used the *hs:slit2-gfp* line to express Slit2-GFP in the eye and brain (Figs. 3C). Although we observe GFP by 4 hr after heat-shock, the GFP only persists for a few hours, presum-

ably because the Slit2-GFP protein is secreted and then degraded. This also explains the punctate expression pattern (Fig. 3C). In 6 experiments, we found 24 GFP+ fish out of 74 heat-shocked. As these experiments used outcrosses from *hs:slit2-gfp* heterozygotes, 37 embryos were expected to be carriers, for a success rate of 64%.

We also heat-shocked *hs: $\Delta$ Tcf-gfp* transgenic embryos (Lewis et al., 2004) at 30 hpf, imaging at 36 hpf. We successfully induced expression in both the eye and somites (Fig. 3B,E). As expected for a transcription factor fusion, GFP was expressed in cell nuclei. In a single experiment, 7 of 15 heat-shocked embryos expressed GFP. In this outcross, 50% carriers (7.5) were expected, for a success rate of close to 100%. This success rate was probably higher for two reasons. First, by the time we performed this experiment, we had optimized many details of the technique. Second, the *hs: $\Delta$ Tcf-gfp* line is more easily induced than the other two lines we used (R. Dorsky and J. Bonner, personal communication).

In successful experiments, we did not observe significant tissue damage or subsequent necrosis. Occasionally, if the level of medium in the Petri dish was too low, embryos would sustain significant tissue damage (presumably from overheating), but this was rare. In these cases, the embryos usually did not survive long enough to express GFP.

Finally, to determine if local heat shock itself affects a particular developmental event, we assayed axon guidance in the optic tract after local heat shock in the brain. At 36 hpf, the first axons have just crossed the optic chiasm and entered the optic tract, while at 50 hpf, the first axons have reached their final target, the optic tectum. We heat shocked *hs:gfp* embryos at 32 hpf and assayed them at 50 hpf. Axons in heat-shocked embryos ( $N = 4$ ) followed their normal path from the optic chiasm to the optic tectum (Fig. 4A,B); these projections were very similar to those in mock-treated embryos without heat shock (Fig. 4C).

In summary, local heat shock using a modified soldering iron works reliably in different tissues, in three different transgenic lines, and at embry-

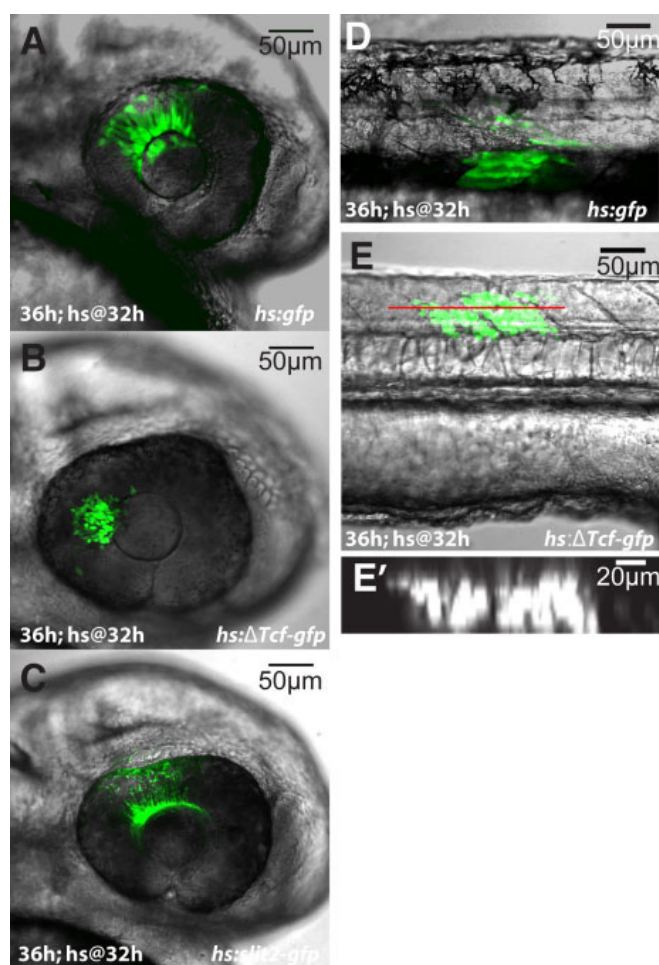


Fig. 3.

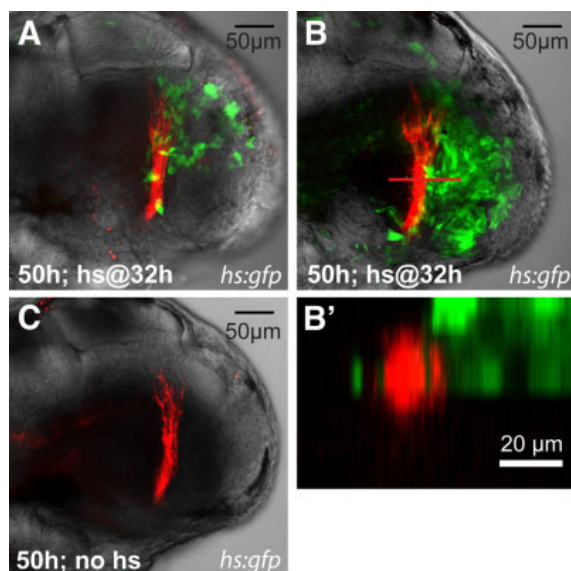


Fig. 4.

onic stages from 12 hpf to 5 dpf, with a success rate of between 65–100% of transgenic carriers. Tissue damage is minimal, and axons seem to grow normally through the region of heat shock.

## DISCUSSION

We have described a new method to spatially and temporally induce gene expression in zebrafish by locally heat shocking embryos using a modified soldering iron. This method should be generally useful for inducing small groups of cells to express a transgene under the control of the heat shock promoter. It is quick, easy, and inexpensive (less than \$200 for equipment), and works in a variety of tissues and stages. Moreover, use of the perfusion apparatus eliminates the need to mount embryos, at least for some tissues and stages. We routinely process 15 embryos/hr. We have so far only used the method in stable transgenic lines; however, local heat shock could be performed on transient transgenic embryos injected with a DNA construct that uses the heat shock promoter to drive expression, especially if mosaicism is low.

The most significant limitation of this method is that only relatively superficial cell types can be successfully targeted; deeper tissues can only be targeted if the overlying structures can be removed. Attempts to locally heat shock at gastrulation (6 hpf) were unsuccessful due to mechanical damage to embryos; better mounting and a modified perfusion apparatus would be required at this age. Potential nonspecific effects can be ruled out

**Fig. 3.** Local heat shock induction in three transgenic zebrafish lines. The method works reliably in *hs:gfp* (A,D), *hs:ΔTcf-gfp* (B,E), and *hs:slit2-gfp* (C). In *hs:ΔTcf-gfp*, GFP is present 40 μm from the surface, as shown in E', a reslice of E across the red line. Lateral views, anterior to right; E': surface up.

**Fig. 4.** Local heat shock does not affect axon pathfinding in the optic tract. Dil-labeled axons from heat-shocked embryos (A,B) pathfind normally through areas of the brain expressing GFP after local heat shock, as compared to control axons without heat shock (C). Lateral views, anterior to right; B': Surface up.

by using *hs:gfp* embryos as a negative control.

Our local heat shock method is a new tool for misexpression of transgenes, which may be more useful than existing methods for some biological questions. Electroporation, in which an applied voltage creates holes in cell membranes allowing molecules to enter, can be used for introducing DNA, RNA, and morpholinos into a small, targeted area of the embryo (Cerdeira et al., 2006; Hendricks and Jesuthasan, 2007). Local heat shock allows for a higher throughput of embryos, at least if the perfusion system is used instead of mounting in agarose. Precise targeting may also be easier, since targeted electroporation requires precise placement of electrodes. The necessary equipment for local heat shock is also less expensive.

Another tool for misexpression is DNA injection at the one-cell stage, which results in embryos with mosaic expression. By screening through a large number of embryos, it is possible to select embryos with construct expression in the correct location. Blastula transplants between embryos of different genotypes provide rough spatial control with use of the zebrafish fate map (Kimmel et al., 1990); however, the number and location of transplanted cells is still variable. Unlike local heat shock, both of these methods lack temporal control.

Inducible systems, on the other hand, can provide excellent temporal control. However, although the powerful Tet repressor and Cre/LoxP systems work in the zebrafish, spatial control of misexpression is dependent on tissue-specific promoters (Huang et al., 2005; Langenau et al., 2005). A new inducible Gal4 system using the ecdysone receptor is also promising (Esengil et al., 2007). Until more tissue-specific promoters are identified, however, the utility of such methods will be limited.

Here we have focused on misexpressing transgenes for gain-of-function analysis. In principle, local heat shock could also be used for loss-of-function applications, such as induction of dominant negative constructs. Finally, this method may also be useful in other organisms, such as medaka, *Xenopus*, or cultured chick or mouse embryos.

## EXPERIMENTAL PROCEDURES

### Fish Lines

Three different stable transgenic zebrafish lines were used to test the local heat shock method: Tg(*hsp70:gfp*)<sup>mik6</sup>, Tg(*hsp70:slit2-gfp*)<sup>rw015d</sup>, and Tg(*hs:ΔTcf:gfp*)<sup>w26</sup> (Halloran et al., 2000; Yeo et al., 2001; Lewis et al., 2004). Fish were raised at 28.5°C using standard methods and staged by time and morphology (Kimmel et al., 1995). Embryos were locally heat-shocked between 12–14 hr post-fertilization (hpf), 30–32 hpf, or at 5 dpf.

### Local Heat Shock

To locally heat shock zebrafish embryos, we used a 12W soldering iron (Weller, catalog number SP12) driven by a DC power supply (Tenma, catalog number 72-6628) in voltage-regulation mode (Fig. 1A,B). Copper soldering iron tips (Weller, catalog number MT70) were ground down using a Dremel tool to ~15-μm tip diameter. To induce local heat shock, we first adjusted the power supply voltage and allowed the soldering iron to equilibrate for at least 30 min, then touched the tip to each embryo for 1, 2, 3, or 5 min. The embryo was bathed in 1× E2 embryo medium with 10 μg/mL gentamycin and 0.4% tricaine (Hutson et al., 2004). We used a perfusion apparatus (described below) for most experiments (for details of construction, see Supplemental Fig. 1, which can be viewed at [www.interscience.wiley.com/jpages/1058-8388/suppmat](http://www.interscience.wiley.com/jpages/1058-8388/suppmat)). For 12-hpf embryos, we did not use the perfusion apparatus, but instead placed the embryos in the grooves of a standard agarose embryo-injection mold and applied the soldering iron tip for 1 min.

The perfusion apparatus consists of a fluid reservoir (60-mL syringe), connected by an intravenous drip regulator and Tygon tubing to a perfusion chamber constructed from two 60-mm Petri dishes. The centers of the plastic Petri dishes are drilled out and fitted with a drain, which consists of a pipette tip cut to size and covered with 150-μm nylon mesh (Aquatic Eco-Systems M150). The drain is connected to an outflow tube, whose height can be adjusted to adjust the fluid level cov-

ering the embryo. Embryo medium from the syringe travels to the perfusion chamber, down the drain, through the outflow tube, and is collected in a beaker (for complete specifications, see Supplemental Fig. 1). Fluid from the beaker is periodically poured back into the fluid reservoir to replenish levels. Zebrafish embryos are positioned on the mesh, where they are held in place by the gentle suction created by fluid flowing down the drain. For embryos older than 18 hpf, this eliminates the need to mount the embryos in agarose, although mounting might be necessary for earlier stages or particular embryo orientations. The strength of the suction is controlled by using the inflow valve to adjust the rate of flow. We generally set the flow rate to 10–20 mL/min.

### Imaging

Embryos were initially screened using a fluorescence dissecting scope (Olympus SZX-12). Live embryos were anesthetized in 0.4% tricaine and mounted in 1% low melt agarose in E2/gentamycin/tricaine. Other embryos were fixed in 4% PFA in PBS overnight at 4°C, then washed in PBS and mounted in 1% low-melt agarose for imaging. GFP+ embryos were imaged using an Olympus Fluoview 300 scanning laser confocal microscope using a 488-nm excitation laser. Images were captured with either a 20× air objective or 40× water objective. Images were processed in ImageJ (Rasband, 1997–2007; <http://rsb.info.nih.gov/ij>; NIH, Bethesda, MD) and Adobe Photoshop CS2.

For the axon guidance assay, we used *hs:gfp* fish, dissected off one eye at 28 hpf, locally heat shocked an area near the optic tract at 32 hpf in some embryos, screened for GFP at 36 hpf, then fixed at 50 hpf and labeled the optic tract with an intraocular DiI injection (Hutson et al., 2004). Dye was allowed to diffuse for 5 hr at 28.5°C, then embryos were mounted and imaged using 488- and 543-nm excitation.

### ACKNOWLEDGMENTS

We thank John Kuwada, Hitoshi Okamoto, and Richard Dorsky for generously sharing transgenic fish. Thanks

are extended to the Chien lab for helpful comments and support. M. E. H. is supported by an NIH institutional Developmental Biology Training Grant (5T32 HD007491). This work was supported by a grant from the NIH (R01 EY 12873) to C.-B. C.

## REFERENCES

- Amsterdam A, Hopkins N. 2006. Mutagenesis strategies in zebrafish for identifying genes involved in development and disease. *Trends Genet* 22:473–478.
- Cerda GA, Thomas JE, Allende ML, Karlstrom RO, Palma V. 2006. Electroporation of DNA, RNA, and morpholinos into zebrafish embryos. *Methods* 39:207.
- Esengil H, Chang V, Mich JK, Chen JK. 2007. Small-molecule regulation of zebrafish gene expression. *Nat Chem Biol* 3:154.
- Halloran M, Sato-Maeda M, Warren J, Su F, Lele Z, Krone P, Kuwada J, A Shoji W. 2000. Laser-induced gene expression in specific cells of transgenic zebrafish. *Development* 127:1953–1960.
- Hendricks M, Jesuthasan S. 2007. Electroporation-based methods for in vivo, whole mount and primary culture analysis of zebrafish brain development. *Neural Dev* 2:6.
- Huang C-J, Jou T-S, Ho Y-L, Lee W-H, Jeng Y-T, Hsieh F-J, Tsai H-J. 2005. Conditional expression of a myocardium-specific transgene in zebrafish transgenic lines. *Dev Dyn* 233:1294–1303.
- Hutson LD, Campbell DS, Chien, C-B. 2004. Analyzing axon guidance in the zebrafish retinotectal system. In: Detrich HW, Westerfield M, Zon LI, editors. *Methods in cell biology, the zebrafish: cellular and developmental biology*. San Diego: Elsevier Press. p. 13–35.
- Kimmel CB, Warga RM, Shilling TF. 1990. Origin and organization of the zebrafish fate map. *Development* 108:581–594.
- Kimmel CB, Ballard WW, Kimmel SR, Ullmann B, Schilling TF. 1995. Stages of embryonic development of the zebrafish. *Dev Dyn* 203:253–310.
- Langenau D, Feng H, Berghmans S, Kanki J, Kutok J, Look A. 2005. Cre/lox-regulated transgenic zebrafish model with conditional myc-induced T cell acute lymphoblastic leukemia. *Proc Natl Acad Sci USA* 102:6068–6073.
- Lewis JL, Bonner J, Modrell M, Ragland JW, Moon RT, Dorsky RI, Raible DW. 2004. Reiterated Wnt signaling during zebrafish neural crest development. *Development* 131:1299–1308.
- Liu Y, Halloran MC. 2005. Central and peripheral axon branches from one neuron are guided differentially by Semaphorin3D and transient axonal glycoprotein-1. *J Neurosci* 25:10556–10563.
- Monsma SA, Ard R, Lis JT, Wolfner MF. 1988. Localized heat-shock induction in *Drosophila melanogaster*. *J Exp Zool* 247:279–284.
- Nasevicius A, Ekker SC. 2000. Effective targeted gene “knockdown” in zebrafish. *Nat Genet* 26:129–130.
- Nicklas RB. 1973. Methods for gentle, differential heating of part of a single living cell. *J Cell Biol* 59:595–600.
- Rasband WS. 1997–2007. ImageJ. Bethesda, MD: U. S. National Institutes of Health: <http://rsb.info.nih.gov/ij/>
- Teh C, Chong SW, Korzh V. 2003. DNA delivery into anterior neural tube of zebrafish embryos by electroporation. *Bio-techniques* 35:950–954.
- Ungar AR, Kelly GM, Moon RT. 1995. Wnt4 affects morphogenesis when misexpressed in the zebrafish embryo. *Mech Dev* 52:153–164.
- Wienholds E, van Eeden F, Kosters M, Mudde J, Plasterk RH, Cuppen E. 2003. Efficient target-selected mutagenesis in zebrafish. *Genome Res* 13:2700–2707.
- Yeo SY, Little MH, Yamada T, Miyashita T, Halloran MC, Kuwada JY, Huh TL, Okamoto H. 2001. Overexpression of a slit homologue impairs convergent extension of the mesoderm and causes cyclopia in embryonic zebrafish. *Dev Biol* 230:1–17.

## CHAPTER 3

### THE ROLE OF SLIT1A AND SLIT2 IN AXON GUIDANCE IN THE ZEBRAFISH RETINOTECTAL SYSTEM

## Introduction

The formation of a nervous system requires cells to extend axons over long distances to form a precise wiring pattern. Although vertebrate nervous systems consist of billions of neurons, a limited number of axon guidance molecules have been identified. One strategy that allows such a small number of molecules to guide the great number of axons correctly is for guidance cues to perform different functions depending on the presence of other intracellular or extracellular cues. Many axon guidance cues have been shown to be bifunctional depending on other molecules expressed intracellularly or extracellularly. For instance, Netrin attracts growth cones that express DCC and repels growth cones that express DCC and Unc-5 (Leung-Hagesteijn et al., 1992; Keino-Masu et al., 1996; Guthrie, 1997; Hamelin et al., 1993; Hedgecock et al., 1990). Levels of intracellular cyclic nucleotides can switch a ligand from having an attractive effect to a repulsive one or *vice versa* (Song et al., 1997, 1998; Ming et al., 1997). Here, I examine Slit-Robo signaling *in vivo* to determine whether Slit can act nonrepulsively to Robo-expressing axons, using a retinal axon model in zebrafish.

Robo and Slit were first identified in *Drosophila*, where they were found to control midline crossing by axons of the ventral nerve cord. Commissural axons express low levels of Robo receptors as they cross the midline, but upregulate Robo after crossing the midline, which secretes the Slit ligand (Kidd et al., 1998, 1999). Robo-expressing axons are repelled by Slit, preventing recrossing of the midline. Longitudinal axons, which never cross the midline, always express Robo and are therefore repelled by the Slit-expressing midline. Robos and Slits have since been found to act in vertebrate axon guidance, including in the retinotectal system (Fricke et al., 2001; Plump et al., 2002; Inatani et al., 2003). As in *Drosophila*, Slits are generally thought to repel Robo-expressing axons. Co-culture

experiment using mouse spinal cord explants or chick retinal explants cultured in the presence of hSlit2-transfected cells show little or no outgrowth of axons on the side facing the Slit2-expressing cells (Brose et al., 1999; Niclou et al., 2000). Additionally, *Xenopus* RGC axons turn away from a pipette containing hSlit2 conditioned medium (Piper et al., 2006). However, Slits' effects may not always be negative, since Slits have also been shown to stimulate axon branching (Wang et al., 1999; Yeo et al., 2001; Miyashita et al., 2004; Ma et al., 2007). Intriguingly, Slit may function to attract Robo-expressing cells during muscle and trachea morphogenesis in *Drosophila* (Kramer et al., 2001; Englund et al., 2002). In this chapter, I present evidence for Slits functioning as attractive/permissive factors, instead of their commonly assumed roles as repulsive factors, during zebrafish retinotectal axon guidance.

The zebrafish retinotectal system is ideal for studying axon guidance, due to the organism's external fertilization, optical transparency, and amenability to genetic manipulation. Retinal ganglion cells, which produce the only retinal axons that leave the eye, are born beginning at 28 hours postfertilization (hpf). They then leave the eye at 32 hpf, cross the midline at the optic chiasm at 34 hpf, and enter the optic tract at 36 hpf (Burrill and Easter, 1995). They then pathfind dorsally along the pial surface of the brain toward the optic tectum, where they eventually form synapses. While there are also pretectal targets, the majority of the RGC axons synapse on the tectum. The Chien laboratory has previously shown that the *astray* mutant is deficient for Robo2 and displays a variety of pathfinding errors in the retinotectal pathway, including recrossing of the midline (Fricke et al., 2001; Hutson et al., 2002).

Previous work suggested that Slit2 and Slit3 might be providing guidance signals at the chiasm for Robo2-expressing RGC axons. *In situ* hybridization for both mRNA species

showed that Slit2 is expressed anterior to the chiasm at 36 hpf, and Slit3 is expressed both anterior and posterior to the chiasm (Hutson et al., 2002). This expression pattern of Slit2 and Slit3 at the optic chiasm suggested that Slit2/Slit3 provided surround repulsion, keeping Robo2-expressing axons confined to a single channel as they crossed the midline. Hutson et al. (2002) further showed that both wild-type and Robo2-deficient axons made errors as they crossed the midline; however, only Robo2-positive (wild-type) axons were able to correct these mistakes. It was assumed that as axons grew up a Slit gradient, the Robo2 receptors mediated a repulsive response, causing retraction of the growth cones that were extending in the wrong direction.

However, preliminary evidence suggested that Slit1a might act differently to affect RGC axons. *slit1a* is broadly expressed in the zebrafish embryonic brain at the stages when the retinotectal pathway is being established, including at the optic chiasm and in the cells underlying the optic tract. This pattern suggested a nonrepulsive role for Slit1a (Hutson et al., 2003). In addition, *slit1a* seems to have a nonrepulsive role at the ventral midline to guide axons of the postoptic commissure (POC; Barresi et al., 2005). These authors found that commissural axons of the POC grew over *slit1a*-expressing cells, and that knocking down *slit1a* reduced POC midline crossing. In addition, experiments in mouse suggest that mouse Slit1 and Slit2 may have different roles. Full-length mouse Slit1 is repellent to cortical axons in culture and induces dendrite branching and outgrowth. An N-terminal truncated form of the protein retains branching function but is no longer repellent to cortical axons (Whitford et al., 2002). However, the Slit1 N-terminal form was produced by truncating the protein between the fifth and sixth EGF repeats, which is where the Slit2 cleavage site is located. The sequence of *slit1* diverges from *slit2* at the cleavage site, but Slit1 is cleaved at an as-yet unmapped site (Brose et al., 1999; Whitford et al., 2002).

Therefore, the N-terminal Slit1 may not reflect an endogenous protein product. It is worth noting, however, that the N-terminal fragment of Slit2 has both branching and repulsive functions (Nguyen Ba-Charvet et al., 2001). These results suggest that Slit1 and Slit2 may function differently in mouse. Zebrafish Slit1a is 61.9% similar to zebrafish Slit2. As in mouse, *slit1a* does not appear to have the cleavage site present in *slit2* (Hutson et al., 2003; Brose et al., 1999). I therefore wanted to further investigate the function of *slit1a* in the optic tract.

Although Slits have been shown to act in *Drosophila* as an attractant for migrating muscle and cardiac cells, and to stimulate branching in vertebrate axons, they have not been previously shown to act as permissive/attractive cues for pathfinding axons. In this chapter, I show that zebrafish RGC axons indeed grow over cells expressing *slit1a* and that knocking down *slit1a* results in axon guidance defects in the optic tract. I further show that misexpressing either Slit1a or Slit2 anterior to the optic tract results in axon turning toward the misexpressed Slit protein. Surprisingly, I also find that RGC axons turn toward misexpressed Slit2 at the optic chiasm.

## Experimental Procedures

### Fish

All embryos were raised at 28.5°C unless otherwise noted. Wild-type embryos were from either the TL or Tübingen strain. Mutant and transgenic strains used were *ast<sup>te284</sup>*, *Tg(isl2b:GFP)<sup>zc7</sup>*, *Tg(isl2b:tagRFP)*, *Tg(hsp70l:mcherry)*, *Tg(hsp70l:slit1a-mcherry)*, and *Tg(hsp70l:slit2-egfp)<sup>rw015d</sup>* (Yeo et al., 2001). *astray* mutants were from either the *te284* allele, which encodes a Gly<sup>882</sup> to Asp change in the transmembrane domain of *robo2*, or from the *ti272* allele, which encodes a nonsense mutation before the transmembrane domain and is

therefore a presumptive null (Fricke et al., 2001). *astray* mutants are viable and fertile, so *astray* embryos were generated by incrossing known homozygotes. *Tg(hsp70l:mcherry)* and *Tg(hsp70l:slit1a-mcherry)* fish were generated by making Gateway constructs in a Tol2 *cmlc2:gfp* vector, pDestTol2CG2, then injecting DNA plus transposase RNA into 1-cell wild-type embryos (Kwan et al., 2007). Injected fish were raised to adulthood, then screened by assaying for GFP expression in the heart. Transgenic founders were outcrossed to wild-type fish to establish the lines. The *Tg(hsp70l:mcherry)* line seems to still bear multiple insertions, while the *Tg(hsp70l:slit1a-mcherry)* line bears a single expressing insertion. Experimental procedures followed NIH guidelines and were approved by the University of Utah Institutional Animal Care and Use Committee.

#### In situ hybridization and immunohistochemistry

In situ antisense probes were synthesized using a digoxigenin-UTP kit (Roche 11175025910) using previously published constructs and conditions (Yeo et al., 2001; Hutson et al., 2003). In situ hybridization was performed on *isl2b:gfp* or *isl2b:gfp;astray<sup>ti272</sup>* embryos using standard methods (Thisse and Thisse, 2008) with the following modifications: embryos were first permeabilized with 1% H<sub>2</sub>O<sub>2</sub> for 30 minutes, and polyclonal anti-GFP ( was added with anti-DIG antibody at 1:500 dilution. After the *in situ* was developed, embryos were washed in PBST several times, incubated overnight in 1:200 goat anti-rabbit Alexa-488 (Invitrogen A-11008) in NCST, washed several times in PBST, and then sectioned. For sectioning, embryos were dehydrated in methanol, infiltrated at 4°C in 1:1 Immuno-Bed:methanol for 30 minutes then 100% Immuno-Bed overnight, oriented and embedded in 20:1 Immuno-Bed:Immuno-Bed Solution B (EMS 14260-04), and sectioned at 15 µm on a Reichert-Jung 2050 Supercut microtome with a glass knife. Sections were then imaged on an Olympus compound microscope.

### Morpholino Injection

Wild-type embryos were injected with 1 nl morpholino stock at the one-cell stage using either a Picospritzer or ASI pressure injector. Morpholino was diluted in 0.1% phenol red and the size of the bolus was measured using an eyepiece micrometer. Morpholinos used were Slit1aMO1 (5'-GACAACATCCTCCTCTCGCAGGCAT-3'), Slit1aMO2 (5'-TTCCTAAGACTCCCCGAGAAAACTA-3'), Slit1aSDMO (5'-GAAATAAACTCACAGCCTCTCGGTG-3'), and standard control MO (5'-CCTCTTACCTCAGTTACAATTTATA-3') (Gene Tools). Slit1aMO1 targets nucleotides +1 to +25 of Slit1a and was injected at 2 ng/nl. Slit1aMO2 targets nucleotides -29 to -5 in the 5' UTR of Slit1a and was injected at 2 ng/nl. Slit1aSDMO targets the exon 1-intron 1 junction and was injected at 4 ng/nl. Control MO was injected at 4 ng/nl.

### Reverse transcription polymerase chain reaction

Wild-type embryos were injected at the one-cell stage with 4 or 8 ng of Slit1aSDMO and collected at 48 hpf. Reverse transcription-PCR was performed with RNA from 20 pooled embryos. mRNA was amplified using primers binding to exon 1 and exon 2 (forward primer 5'-ATGCCTGCGAGAGGAGGATG-3' and reverse primer 5'-GAGGCCAGTGAAGTCGTTTCTG-3'). In control embryos, the expected band of 231 bp was found, while in morphants the same wild-type band and a smaller band were observed. The morphant bands were gel purified, TOPO-TA cloned, and sequenced. The upper band was found to be the normal 231 bp splice product, while the lower band was found to be an 88 bp alternative splice product. Blocking the exon 1- intron 1 junction with Slit1aSDMO apparently activates a cryptic splice site 34 bp after the AUG, which splices to the beginning of exon 2, causing a frameshift. Knockdown was incomplete even at 8 ng of Slit1aSDMO.

### Fixed analysis of morphants

Control and *slit1a* morphants and *astray*<sup>te284</sup> mutants were fixed at 48 hpf overnight in 4% paraformaldehyde in PBS at 4°C. Mounting dishes were prepared by filling 60 mm Petri plates with 1.5% agarose in PBS and cutting grooves in the agarose with a razor blade. Fixed embryos were mounted with their tails in the grooves and heads exposed, then covered with 1% low-melt agarose. One eye was then injected with DiI dissolved in chloroform, which was allowed to diffuse overnight. The unlabeled eye was removed using a tungsten needle, and embryos were remounted and imaged laterally on an Olympus Fluoview 300 confocal microscope using a 543 or 568 nm laser for excitation. A 20x air objective was used to capture a z-stack of the axon labeling and a DIC image of the embryo.

Optic tract width was measured with the aid of a “bullseye” macro in NIH Image. A reference line was drawn from the optic chiasm to the corner of the tectal ventricle on z-projections of confocal stacks superimposed on a DIC image of the embryo. The bullseye macro then drew 10 concentric circles, centered on the optic chiasm. The radius of the smallest circle was 10% of the distance from the chiasm to the corner of the ventricle, and successive circles had radii of 20%, 30%, 40%, etc. For each circle, a chord was drawn between the most anterior and most posterior axon that intersected the circle and the chord length was measured. Significance was determined using Student’s t-test.

Each embryo was also scored for the presence or absence of axon guidance errors in both the anterior and posterior direction. An embryo was scored as having an axon guidance error if an axon or axon fascicle was observed 10  $\mu\text{m}$  or more from the main optic tract.

### Global heat shock

Embryos were heat shocked for 1 hour in a 38°C water bath at 24 or 32 hpf, allowed to recover at 28.5°C, then fixed at 48 hpf. Embryos were mounted as detailed above and the right eye was injected with either DiO or DiI. Embryos were imaged laterally using 488 and 568 nm lasers for excitation and a 20x air or 40x water objective to capture a z-stack of axon labeling and a DIC image of the embryo. Embryos were scored for optic tract width and axon guidance errors using the same criteria as for morphants. Significance was determined by using Student's t-test.

### Local heat shock

Embryos were raised to 24-28 hpf, then mounted in 3% methylcellulose in E2/GN. The right eye was removed using a glass needle. They were allowed to recover until 32 hpf, then locally heat shocked anterior or posterior to the presumptive optic tract using a modified soldering iron for 15-60s without perfusion or for 3 minutes with perfusion. Embryos were allowed to recover until 48 hpf, sorted for GFP or mCherry expression, then either imaged live or fixed with 4% paraformaldehyde in PBS for 4 hours at room temperature. Fixed embryos were prepared and imaged using the same protocol as for globally heat shocked embryos. Live embryos were anesthetized, mounted in 1.5% low-melt agarose in E2/GN in a glass bottom dish, and the left optic tract imaged with an Olympus Fluoview 300 confocal microscope. For local heat shock at the chiasm, embryos were processed as described above, except the left eye was not removed and local heat shock was performed anterior to the chiasm at 28 hpf. Embryos were blinded as to genotype and location of the misexpressed transgene and then scored for anterior or posterior axon guidance errors.

Time-lapse imaging was performed using *isl2b:gfp* embryos that were locally heat shocked at 32 hpf. Embryos were anesthetized, mounted in 1.5% low-melt agarose in E2/GN in a glass bottom dish, and imaged starting at 38-44 hpf using an Olympus Fluoview 300 confocal microscope. The microscope and sample were left at ambient room temperature. Z-stacks were collected every 10 minutes using a 20x air objective lens.

## Results

### Expression of *slits* near the optic tract

To determine which Slit proteins were likely to be expressed near the optic tract, I performed double labeling of *isl2b:gfp* embryos, which express GFP specifically in RGCs. RGC axons were labeled with anti-GFP antibody, while *slits* were labeled by *in situ* hybridization. Of the four *slits* found in zebrafish, only one, *slit1a*, was expressed near the optic tract (Figure 3.1). I therefore focused on *slit1a* for the rest of our analysis of optic tract axon guidance.

The previous analysis of *slit1a* showed that it was broadly expressed in the brain at 36 and 48 hpf, and was expressed in the region where RGC axons pathfind through the optic tract (Hutson et al., 2003). I therefore undertook more detailed expression studies to determine how close *slit1a* expression was located to the optic tract axons. I labeled *isl2b:gfp* and *isl2b:gfp;astray* embryos using anti-GFP and *in situ* hybridization for *slit1a*. For each embryo, I took 15  $\mu\text{m}$  sections in one of three planes (see cartoons in Figure 3.2). Parasagittal sections revealed that *slit1a* is expressed both anteriorly and posteriorly to the optic tract, along the whole dorsal-ventral axis, with a region of particularly high expression anterodorsal to the optic tract (Figure 3.2 A,D). Coronal sections showed *slit1a* expression at the optic chiasm, medial to the optic tract along the entire dorsal-ventral axis, and in the optic

Figure 3.1: *slit1a* is the only slit expressed near the optic tract. Parasagittal sections of 43 hpf *isl2b:gfp* embryos. mRNA detected by in situ hybridizations for each zebrafish *slit* is shown in purple. Anti-GFP antibody staining labels the RGC axons and is shown in green. The brown is pigment from the eye; the axons run just behind the retinal pigmented epithelium. (A) *slit1a* is expressed broadly at 43 hpf adjacent to the optic tract. Asterisk represents area of particularly high expression. (B-D) *slit1b*, *slit2*, and *slit3* are not expressed near the optic tract at this age. Orientations are dorsal up, anterior left. Arrowhead indicates optic chiasm. Scale bar represents 100  $\mu\text{m}$ .

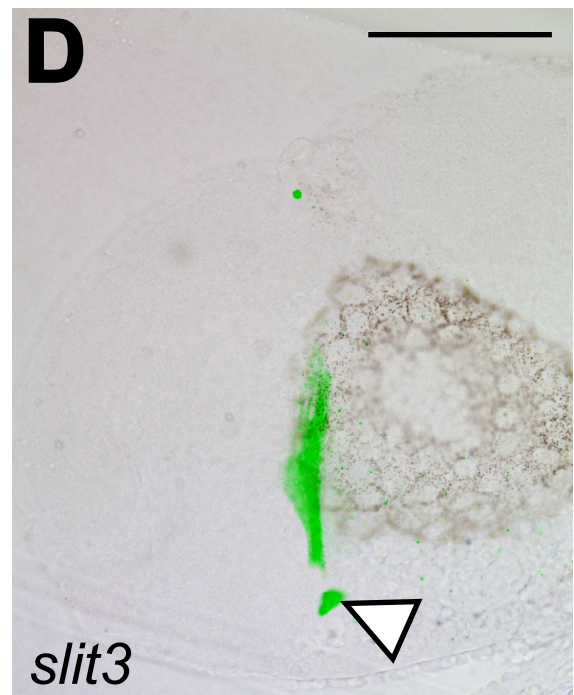
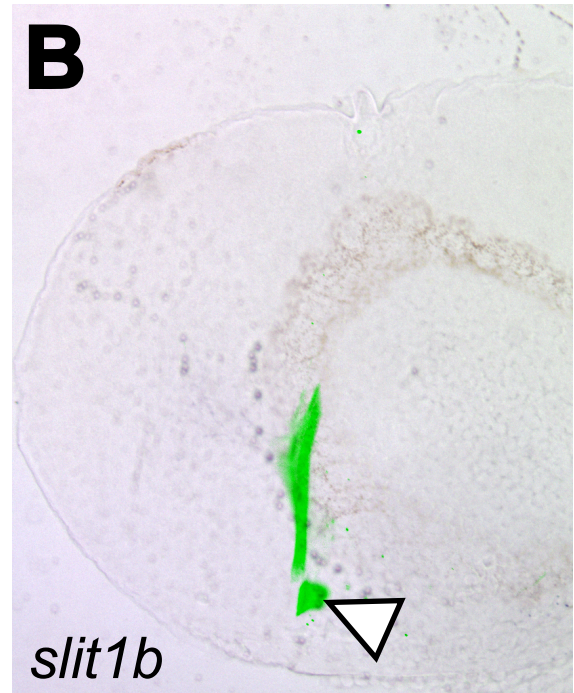
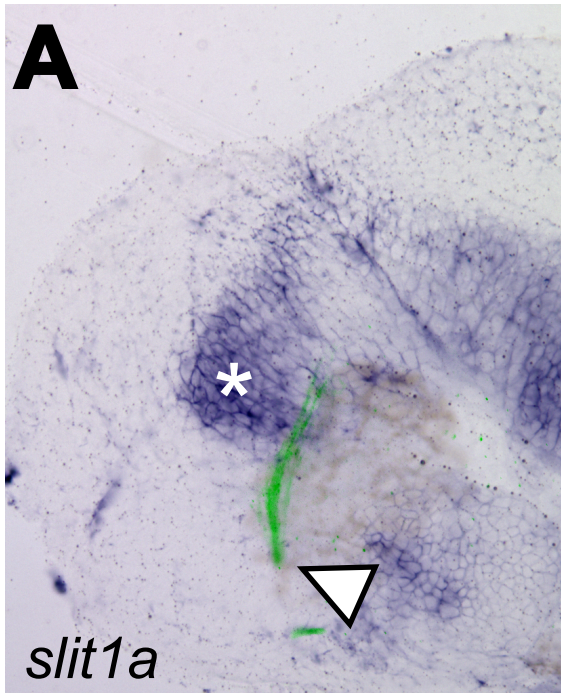
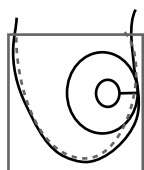
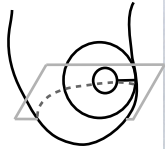
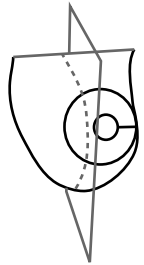
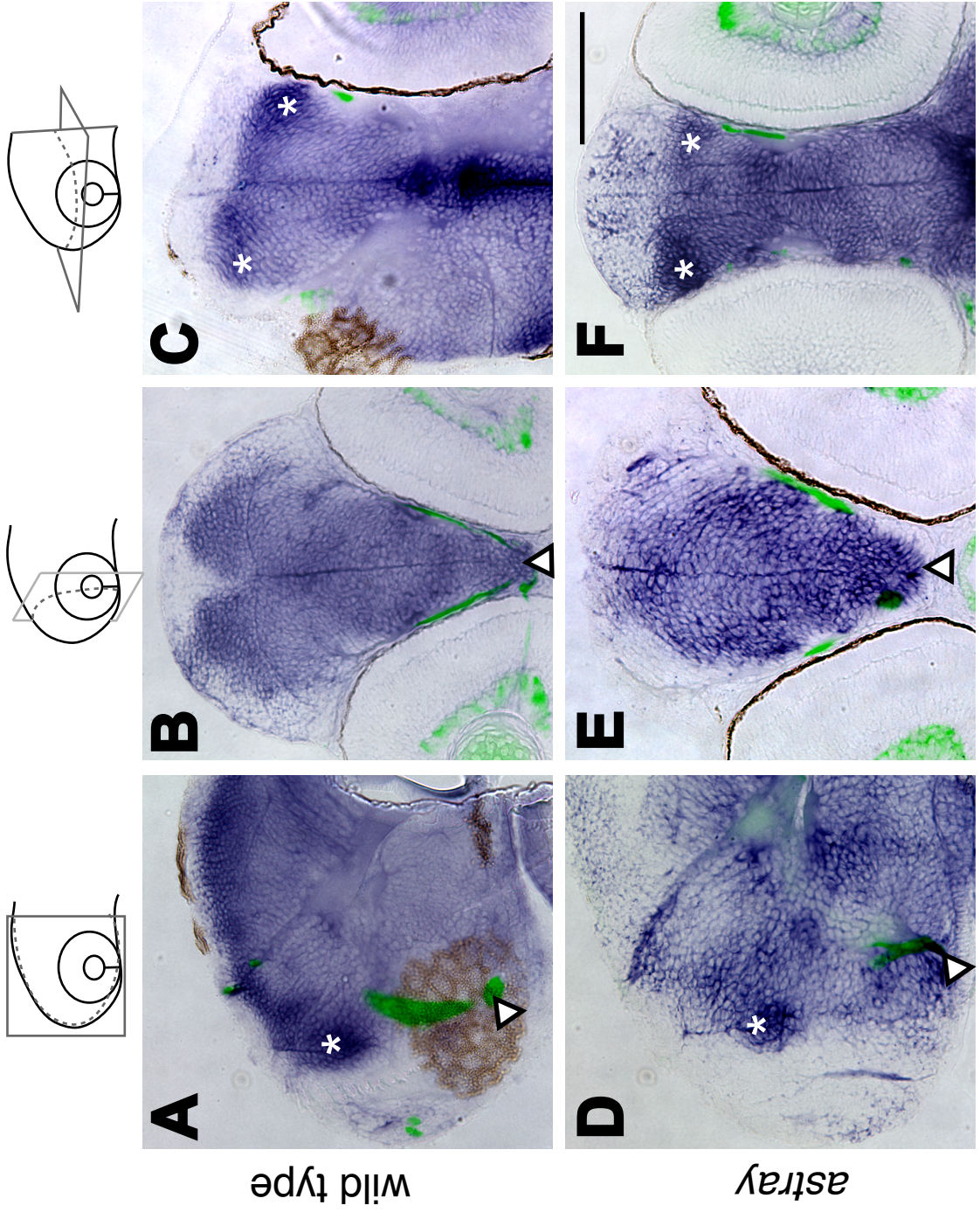


Figure 3.2: *slit1a* is expressed near RGC axons in wild-type and *astray* zebrafish. Sections of 48 hpf *isl2b:gfp* embryos. *slit1a* mRNA is shown in purple. RGC axons are shown in green. Cartoons above each set of panels show orientation with respect to the zebrafish head. (A, D) Parasagittal sections show *slit1a* expressed broadly both anteriorly and posteriorly to the optic tract, with a region of high expression near the anterodorsal part of the optic tract (asterisk). The expression pattern does not differ notably between wild-type and *astray* embryos. Arrowhead indicates the optic chiasm. (B, E) Coronal sections show *slit1a* expressed at the optic chiasm (arrowhead) and medial to the optic tract. (C, F) Horizontal sections show *slit1a* expressed medial to the optic tract, with the same region of high expression shown in A and D anterior to the tract (asterisk). Scale bar represents 100  $\mu\text{m}$ .



tectum, as previously described (Hutson et al., 2003; Barresi et al., 2005; Campbell et al., 2007) (Figure 3.2 B,E). Horizontal sections confirmed the presence of *slit1a* medial to the optic tract, as well as the high *slit1a*-expressing region anterior to the dorsal part of the optic tract (Figure 3.2 C,F). Double labeling in *isl2b:gfp;astray* embryos confirmed that *slit1a* expression is normal in *astray* embryos.

These results confirm that *slit1a* is expressed very near to the Robo2-expressing RGC axons. This finding is unexpected, given that the Robo-Slit interaction is generally repulsive. One might have expected that such a broad expression of Slit would simply cause retinal growth cones to collapse; instead, they grow through this region. To study how Slit1a interacts with the Robo2-expressing axons, I next designed loss-of-function and gain-of-function experiments.

### Morphant analysis

Although the expression pattern of *slit1a* was intriguing, I wanted to test functionally whether Slit1a had any role in axon guidance in the optic tract. Therefore, I used three antisense morpholinos against *slit1a*. I injected morpholinos at the 1-cell stage and assayed the optic tract for a phenotype at 48 hpf, when the first RGC axons have reached the optic tectum. Two of the morpholinos were translation-blocking morpholinos (Slit1aMO1 and Slit1aMO2) and one was a splice-blocking morpholino that targets the exon 1-intron 1 junction (Slit1aSDMO). Using a high dose of either translation-blocking morpholino (more than 2ng) resulted in embryos with convergent extension defects. I therefore injected these morpholinos at 2 ng, which resulted in embryos that were morphologically normal at 48 hpf. I was unable to assay the amount of translational knockdown because I could not generate an antibody that labeled Slit1a; however, given that I had to reduce the dose to avoid early

defects, knockdown of *slit1a* is probably not complete. I therefore used a splice-blocking morpholino to circumvent effects of the translation-blocking morpholinos on maternal *slit1a* mRNA. I was able to inject Slit1aSDMO at a higher dose without convergent extension defects; however, knockdown was still not complete at 48hpf. RT-PCR following injection of Slit1aSDMO gave two products, a normally spliced mRNA, whose abundance was much lower than in controls, and an alternatively spliced mRNA that used a cryptic splice site early in exon 1 and caused a frameshift (Figure 3.3).

Although each of the three morpholino injections probably represents a hypomorphic condition as compared to control morphants (Figure 3.4 A-B), I observed axon guidance phenotypes similar to those seen in *astray/robo2* embryos (Figure 3.4 C-J). Although a presumptive null allele of *astray* exists, I chose to use a weaker allele of *astray*, *te284*, because I could identify more embryos that did not have axon errors in the optic chiasm. I wanted to use embryos without errors in the chiasm in order to make a good comparison with the *slit1a* morphants, which do not seem to have errors at the optic chiasm. The first half of the optic tract was wider in both morphants and *astray* embryos as compared to control morphants (Table 3.1), and axon guidance errors occurred at a higher frequency (Figure 3.4L). In fact, embryos injected with Slit1aMO1 develop axon guidance errors at a similar frequency as in *astray<sup>te284</sup>*; 21 of 22 *astray* embryos have axon errors and 26 of 27 *slit1aMO1* morphants have axon errors. The other two morpholinos gave axon errors at lower frequencies: 15 of 20 for both Slit1aMO2 and Slit1aSDMO. The optic tract was widest in the *astray* embryos. Optic tract width was significantly wider than controls in all three morphant conditions. Axons left the main optic tract in both the anterior and posterior directions, sometimes as individual axons and sometimes in axon fascicles. Axon errors in the *slit1a* morphants were often in the same position as those seen in the *astray* embryos

Figure 3.3: *slit1aSDMO* results in an alternative splice product. (A,B) Schematic of splicing with or without *slit1aSDMO*. Lengths not to scale. Arrows indicate primer sites. (A) Embryos injected with control morpholino undergo normal splicing. (B) Embryos injected with *slit1aSDMO* use a cryptic splice site in exon 1, which results in an in-frame alternative splice product. (C) RT-PCR after injection of control morpholino results in a single band with the expected size of 231 bp. RT-PCR after injection of *slit1aSDMO* results in two bands, the wild-type splice product and an 88 bp splice product. Knockdown is not complete at 4 or 8 ng of morpholino. +/- indicates presence/absence of reverse transcriptase. CT, control MO.

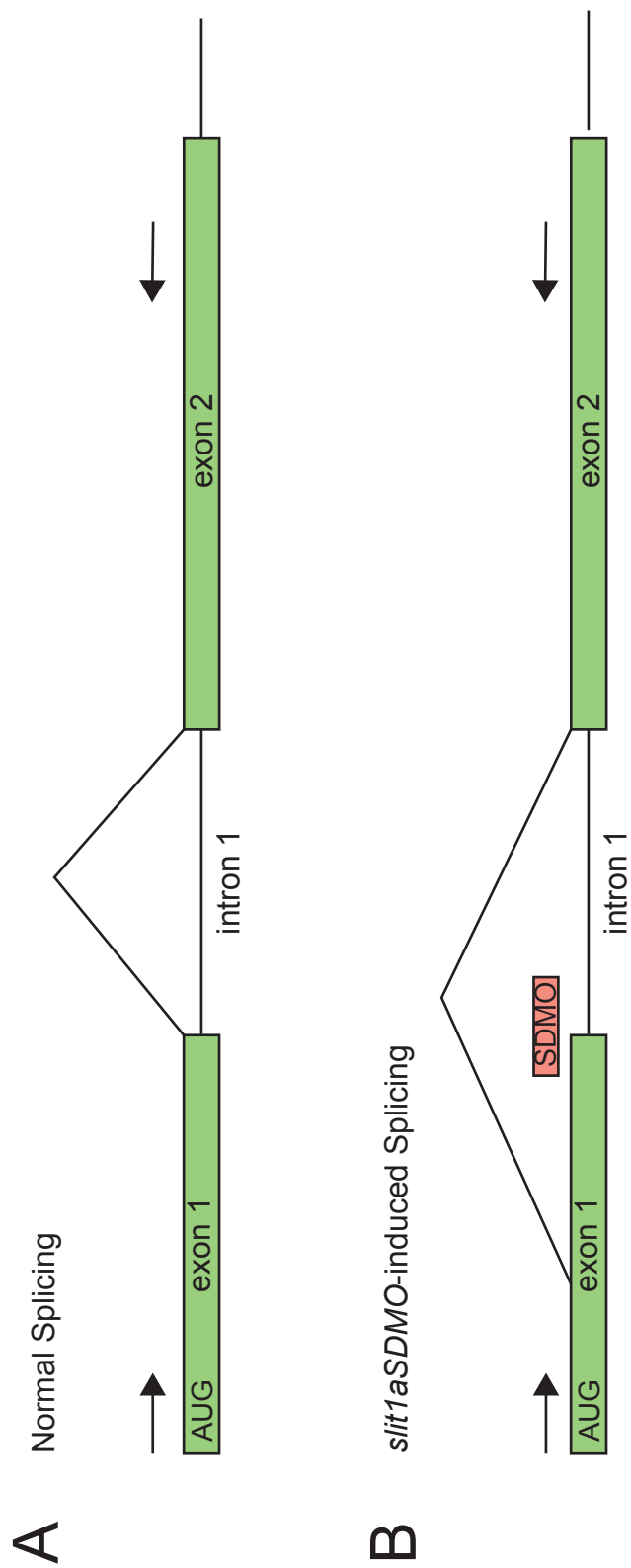


Figure 3.4: Three antisense morpholinos against *slit1a* result in axon errors similar to those seen in *astray/robo2*. (A-J) Maximum projections of confocal z-stacks at 48 hpf. DiI-labeled axons from the contralateral eye are shown in white. Asterisks denote the optic chiasm; arrowheads point to the approximate border of the optic tectum. Open arrows point to anterior axon errors; filled arrows point to posterior axon errors. Scale bar represents 50  $\mu\text{m}$ . Orientations are dorsal up, anterior left. (A,B) Embryos injected with control morpholino show normal optic tracts. (C,D) *astray* embryos show many axon errors both anteriorly and posteriorly. (E-J) Embryos injected with any of three morpholinos against *slit1a* show axon errors similar to those seen in the *astray* mutant. (K) Schematic of bullseye quantification scheme. (L) Quantification of optic tract width as seen in A-J. Error bars are S.E.M. (M) Frequency of embryos with axon errors.

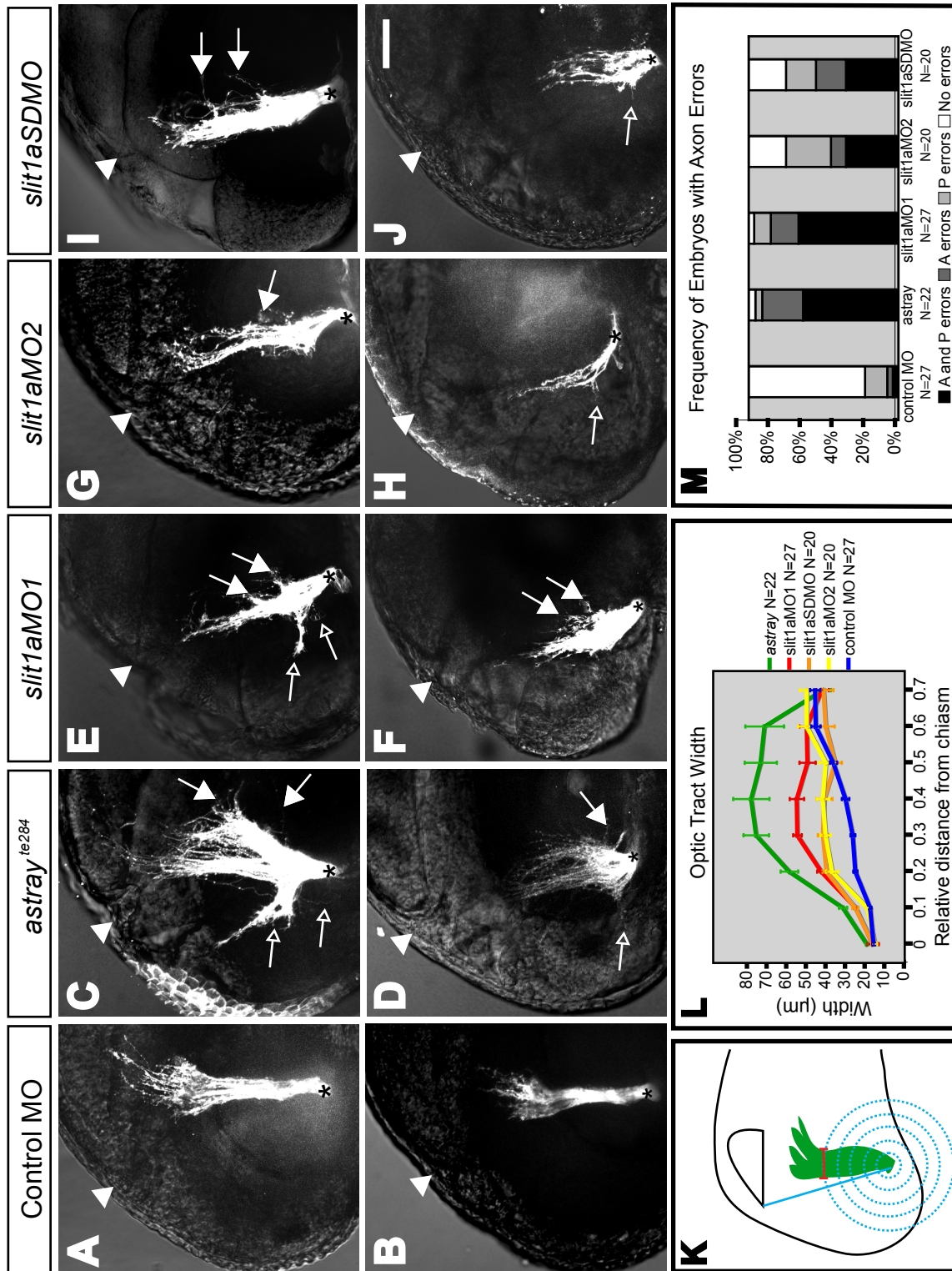


Table 3.1: Optic tract width for morphant analysis. Row headings are relative distance from the optic chiasm; data are mean width at each distance with standard deviation. Values which are significantly different ( $p < 0.1$ ) from the control morphant widths are shown in bold.

	<b>0</b>	<b>0.1</b>	<b>0.2</b>	<b>0.3</b>	<b>0.4</b>	<b>0.5</b>	<b>0.6</b>	<b>0.7</b>
Control MO	12.60 +/- 2.79	14.06 +/- 2.44	20.31 +/- 4.47	21.38 +/- 5.27	24.44 +/- 8.15	29.56 +/-7.70	36.98 +/-10.17	37.27 +/-11.07
<i>slit1aMO1</i>	12.96 +/- 2.76	<b>20.04</b> +/- <b>4.87</b>	<b>34.69</b> +/- <b>9.27</b>	<b>44.75</b> +/- <b>9.36</b>	<b>45.02</b> +/- <b>15.75</b>	<b>40.52</b> +/- <b>17.37</b>	40.78 +/-16.22	34.52 +/-14.77
<i>slit1aMO2</i>	12.00 +/-3.43	15.18 +/-3.46	<b>30.12</b> +/- <b>11.66</b>	<b>32.87</b> +/- <b>9.94</b>	<b>34.01</b> +/- <b>11.74</b>	32.78 +/-12.88	40.84 +/-16.20	40.81 +/-12.86
<i>slit1aSDMO</i>	12.84 +/-3.00	<b>20.34</b> +/- <b>5.77</b>	<b>32.43</b> +/- <b>7.87</b>	<b>33.94</b> +/- <b>9.81</b>	33.41 +/-15.14	28.81 +/-12.42	32.82 +/-16.46	33.71 +/-18.47
<i>astray<sup>te284</sup></i>	<b>15.44</b> +/- <b>2.69</b>	<b>25.52</b> +/- <b>7.98</b>	<b>48.17</b> +/- <b>17.29</b>	<b>62.15</b> +/- <b>25.20</b>	<b>64.23</b> +/- <b>35.77</b>	<b>60.25</b> +/- <b>31.90</b>	<b>58.59</b> +/- <b>38.27</b>	34.08 +/-16.25

(Figure 3.4 C-J). The fact that *slit1a* morpholino injections phenocopy *astray* suggests that Slit1a acts through Robo2.

These results indicate that Slit1a has a role in axon guidance of the RGC axons in the optic tract. However, they raise the question of how Slit1a is acting to guide axons: as a repellent, an attractant, or playing some other role. To answer this question, I turned to gain-of-function experiments to perturb axon guidance in the optic tract.

#### Global overexpression of Slits

I made stable transgenic lines that expressed either mCherry or Slit1a-mCherry under the control of the *hsp70l* promoter in order to test Slit1a function. I also obtained the *hsp70l:slit2-gfp* line to see if the two different Slits had different functions in the optic tract (Yeo et al., 2001). I predicted that Slit2 would be repulsive, based on previous studies in culture, as well as its expression pattern at the optic chiasm, where it is expressed in domains not usually entered by retinal axons. Moreover, zebrafish Slit2 collapses zebrafish RGC axons in culture (Rasband and Chien, personal communication).

I first performed global heat shock at 24 hpf to test the efficacy of my transgenic lines and to see if axon guidance at the optic chiasm was perturbed. Embryos were heat shocked for 1 hour at 38°C, resulting in robust GFP or mCherry expression as seen on a fluorescent dissecting microscope 4 hours later. At 48 hpf, I saw axon guidance defects at the chiasm in both *hsp70l:slit1a-mcherry* and *hsp70l:slit2-egfp* embryos, but not in the *hsp70l:mcherry* embryos (data not shown). In the *hsp70l:slit1a-mcherry* embryos, axon guidance errors (N=14/17) often included wandering from the main axon fascicle at the midline or ectopic midline crossing, and sometimes included ipsilateral projections. In the *hsp70l:slit2-egfp* embryos, errors were also very common (N=14/15), including defasciculation, axons

wandering from the main axon fascicle, and ectopic midline crossing. These results indicate that these transgenes are functional in the zebrafish retinotectal system and that overexpression of Slit1a or Slit2 results in axon guidance errors, suggesting that both act to guide axons through the optic chiasm.

I next performed global heat shock at 32 hpf to determine whether axon guidance in the optic tract was affected by overexpressing Slit1a or Slit2. I chose the 32 hpf timepoint because the transgenes are robustly expressed 3-4 hours after heat shock, which would be around the time the first axons are entering the optic tract at 36 hours. Surprisingly, I saw minor axon guidance errors in 12 of 13 of the *hsp70l:mcherry* controls, mostly in the posterior direction (Figure 3.5A). Because the errors were minor, and because they were not observed in the local heat shock experiments, I conclude that they are a side effect of the global heat shock. I also saw axon guidance errors in the *hsp70l:slit1a-mcherry* embryos (N=8/10; Figure 3.5B). The width of the optic tract and the frequency of embryos with errors was similar to controls, although *hsp70l:slit1a-mcherry* embryos were more likely to have anterior axon guidance errors. *hsp70l:slit2-egfp* embryos, on the other hand, showed profound axon guidance errors, at least as strong as those seen in *astray* embryos (Figure 3.5C, Table 3.2). The phenotype was completely penetrant, but absent from sibling nontransgenic controls.

Although these global overexpression experiments indicate that our transgenes are effective in perturbing axon guidance, they did not tell us how Slits act in the optic tract, as attractants or repellents. Also, the fact that *hsp70l:slit1a-mcherry* embryos do not show a phenotype stronger than controls is uninformative. One possible reason for this is there may be a high level of endogenous Slit1a protein surrounding the optic tract, as seen in the

Figure 3.5: Global heat shock at 32 hpf results in significant axon errors in *hsp70l:slit2-egfp* but not *hsp70l:slit1a-mcherry* transgenics. (A-C) Maximum projections of confocal z-stacks at 48 hpf after global heat shock at 32 hpf. Asterisks denote the optic chiasm; arrowheads point to the approximate border of the optic tectum. Open arrows point to anterior axon errors; filled arrows point to posterior axon errors. Scale bar represents 50  $\mu\text{m}$ . (A) Control embryos often have minor axon errors, especially posterior to the optic tract. (B) Similar to controls, most *hsp70l:slit1a-mcherry* embryos have minor axon errors. (C) Global heat shock causes profound disruption of optic tract axons in *hsp70l:slit2-egfp* embryos. (D) Quantification of optic tract width. Error bars represent S.E.M. (E) Frequency of embryos with axon errors.

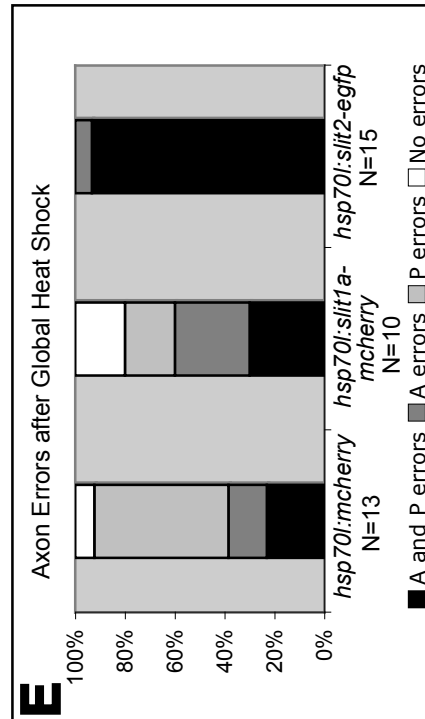
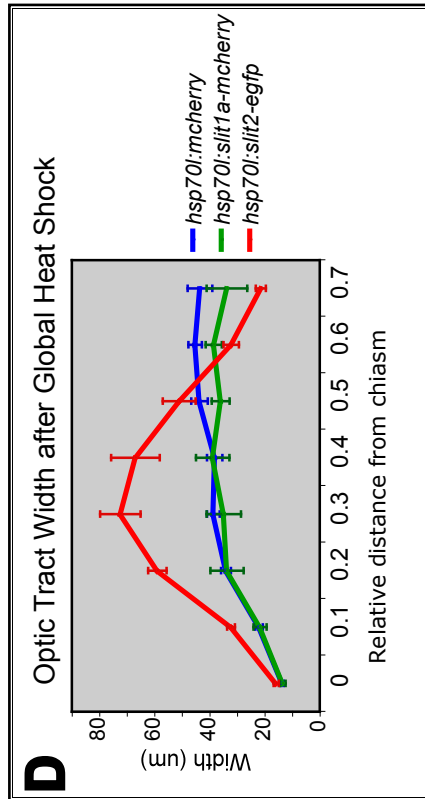
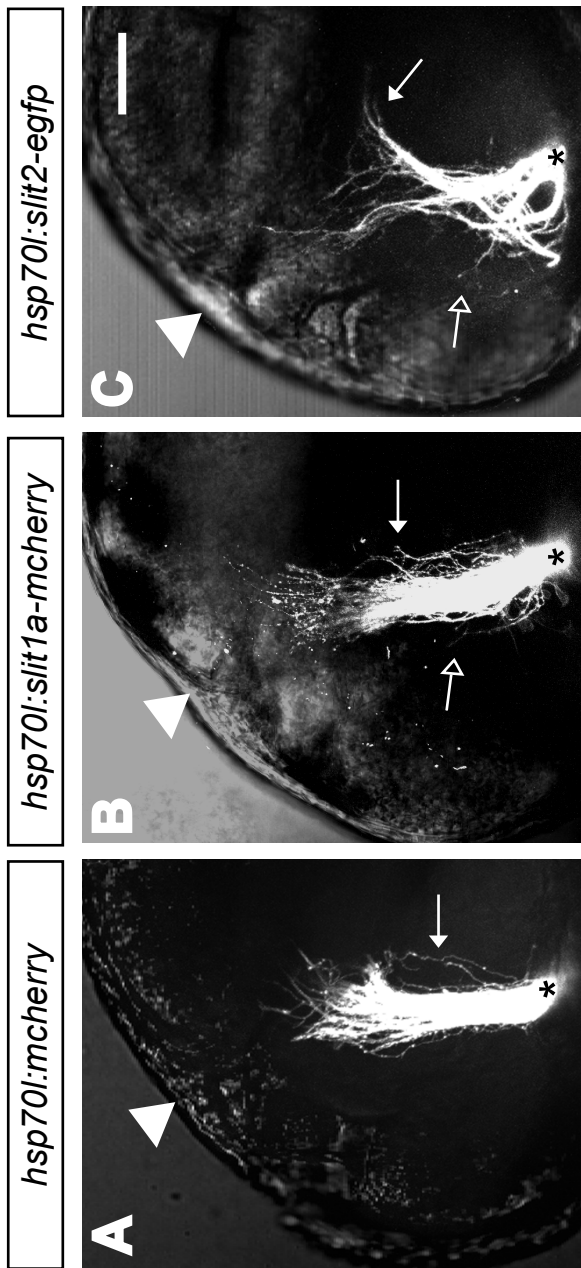


Table 3.2: Optic tract width for global heat shock analysis. Row headings are relative distance from the optic chiasm; data are mean width at each distance with standard deviation. Values which are significantly different ( $p < 0.1$ ) from the optic tract width of *hsp70l:mcherry* embryos are shown in bold.

	<b>0</b>	<b>0.1</b>	<b>0.2</b>	<b>0.3</b>	<b>0.4</b>	<b>0.5</b>	<b>0.6</b>	<b>0.7</b>
<i>hsp70l:mcherry</i>	13.61 +/-1.74	22.05 +/-4.99	34.05 +/-6.41	38.63 +/-8.32	38.13 +/-10.07	43.68 +/-10.81	45.23 +/-8.79	43.47 +/-16.10
<i>hsp70l:slit1a-mcherry</i>	13.43 +/-3.25	21.70 +/-7.50	33.67 +/-19.07	34.84 +/-19.78	38.87 +/-19.26	35.98 +/-10.24	38.49 +/-9.35	33.71 +/-23.34
<i>hsp70l:slit2-egfp</i>	15.83 +/-3.61	<b>32.20</b> <b>+/-5.43</b>	<b>58.95</b> <b>+/-12.86</b>	<b>72.38</b> <b>+/-28.38</b>	<b>66.92</b> <b>+/-34.12</b>	51.02 +/-23.07	<b>32.15</b> <b>+/-10.70</b>	<b>21.40</b> <b>+/-7.07</b>

expression studies. Adding more Slit1a everywhere may not change the pattern of Slit1a to which axons are exposed to as they pathfind through the tract. I therefore next expressed Slit1a on only one side of the tract to see if changing its pattern would elicit a different response in RGC axons.

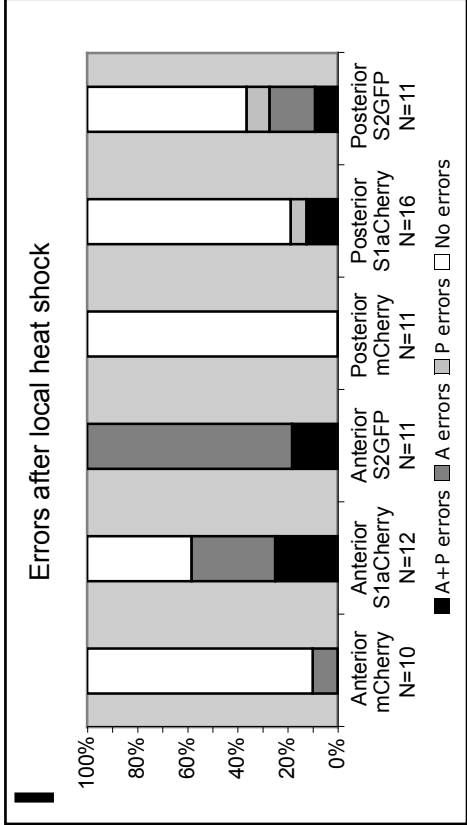
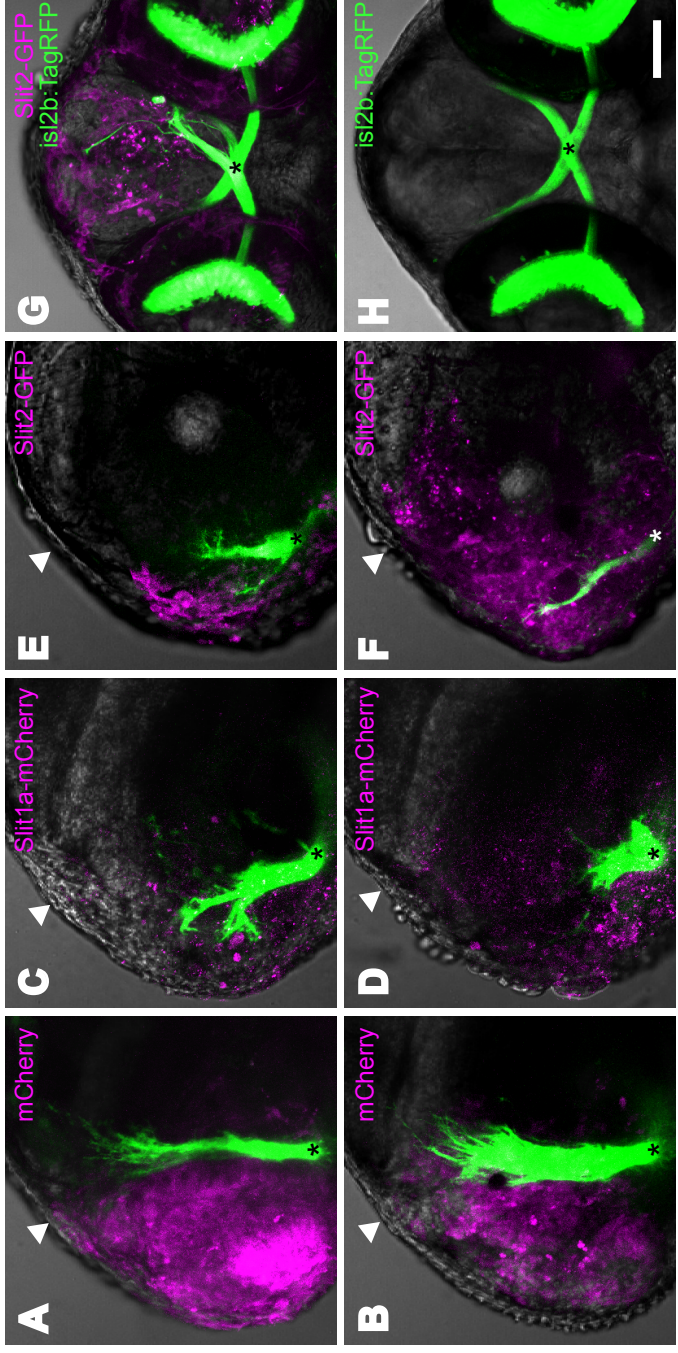
#### Local overexpression of Slits

I used the same transgenic lines to locally express mCherry, Slit1a, or Slit2 on either the anterior or posterior side of the optic tract. Our hope was to establish an “*in vivo* turning assay” to determine whether axons would turn from their normal path when exposed to a gradient of ectopic Slit1a or Slit2. I used a modified soldering iron to elicit a heat shock response in only a small region of the embryo, as described in Chapter 2. Robust expression of mCherry or EGFP was observed using a fluorescent dissecting microscope 3-4 hours after local heat shock. Embryos that were positive for fluorescence 4 hours after heat shock were raised to 48 hpf and assayed for axon guidance errors, or were imaged live to obtain time-lapse data.

I again used the *hsp70l:mcherry* embryos as a control. When I expressed mCherry either anterior or posterior to the optic tract, I saw no axon guidance errors (Figure 3.6 A,B). The optic tracts looked normal in 9/10 embryos in which mCherry was expressed anteriorly and 11/11 embryos in which it was expressed posteriorly. This is different than the minor errors seen with global heat shock, suggesting that whole embryo heat shock causes changes that result in minor axon errors, but that expression of the mCherry transgene does not attract or repel RGC axons.

Misexpressing Slit1a-mCherry on the anterior side of the optic tract caused axon errors in 7 of 12 embryos. Often, the entire optic tract pointed anterior to its normal

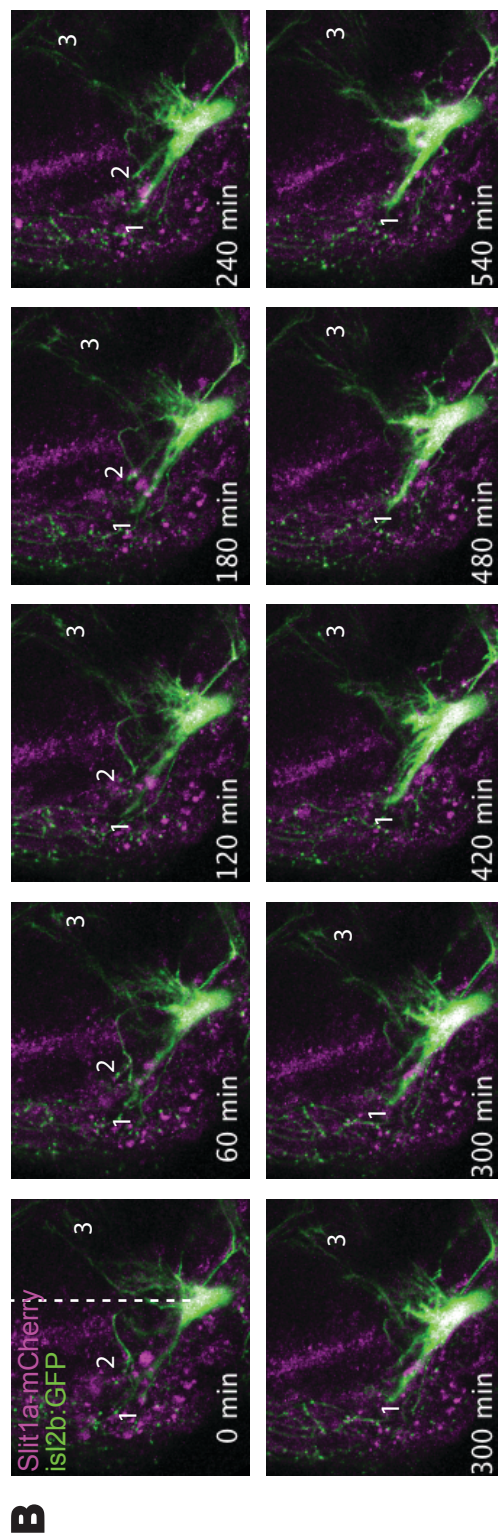
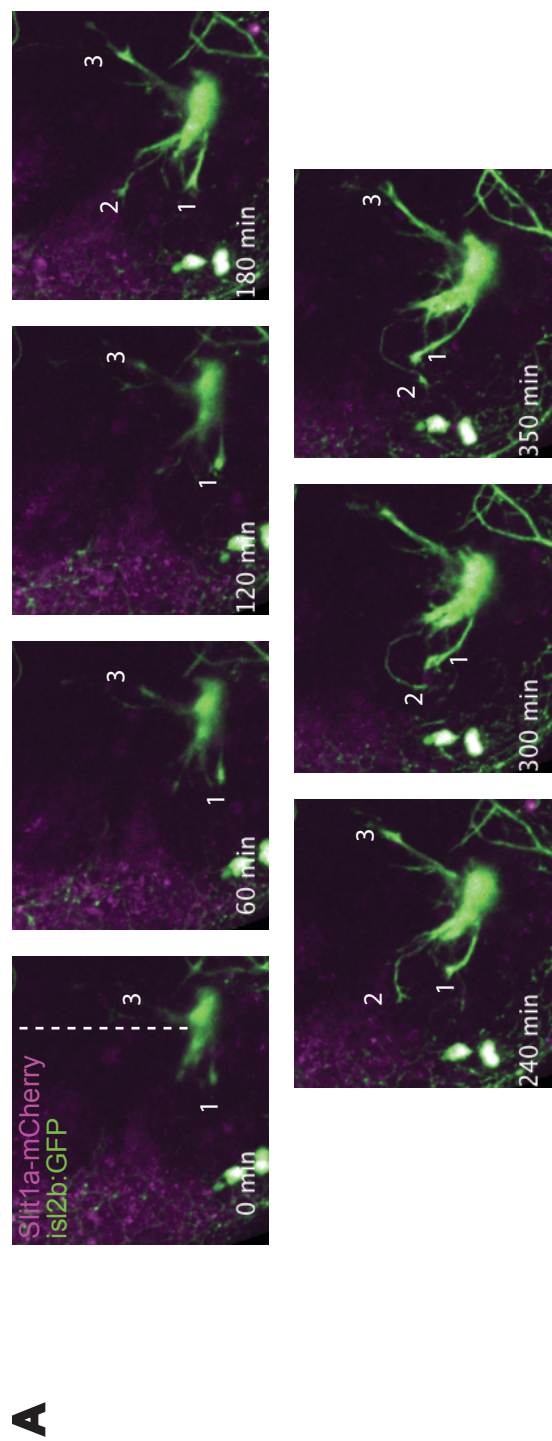
Figure 3.6: RGC axons turn toward ectopic Slit1a or Slit2 expressed anterior to the optic tract. (A-H) Maximum intensity projections of confocal z-stacks at 48 hpf after local heat shock at 32 hpf (A-F) or 28 hpf (G-H). Asterisks denote the optic chiasm; arrowheads point to the approximate border of the optic tectum. Scale bar represents 50  $\mu\text{m}$ . (A-B) Local misexpression of mCherry does not result in significant axon errors. (C-D) Local misexpression of Slit1a-mCherry often results in axon turning toward the ectopic Slit1a. (E-F) RGC axons turn toward ectopic Slit2-GFP. (G) Misexpressing Slit2-GFP anterior to the chiasm results in axon errors that turn anteriorly, toward the source of ectopic Slit2. (H) Nontransgenic sibling controls do not show anterior axon errors after local heat shock. (I) Frequency of embryos with axon errors. Misexpressing any of the transgenes posterior to the tract results in few or no axon errors.



pathway, and there were also individual axons or small fascicles that grew away from the main tract, usually in the anterior direction (Figure 3.6 C,D). The fact that axons tended to grow anteriorly, toward the ectopic Slit1a, suggests that Slit1a is attractive or permissive to RGC axons. Often, both anterior and posterior errors were observed, but the bulk of axons always grew anteriorly, toward the misexpressed Slit1a. On the other hand, only 3 of 16 embryos in which Slit1a-mCherry was expressed on the posterior side of the optic tract showed axon guidance errors. Two of these embryos had minor errors in both directions and one had a large fascicle growing posteriorly.

Time-lapse analysis of embryos with misexpressed anterior Slit1a-mCherry confirmed that axons were turning toward and growing into domains of high Slit1a-mCherry (Figure 3.7). For instance, in Figure 3.7A, most of the axons are growing toward the ectopic Slit1a-mCherry instead of toward the optic tectum, which is directly above them. The approximate normal trajectory is indicated with a dotted line. A single growth cone, labeled 1, grows anteriorly toward the ectopic Slit1a-mCherry. A second growth cone, labeled 2, grows into the Slit1a-mCherry and then curves ventrally. This curving behavior was seen in several time-lapse movies. A third growth cone is growing posteriorly, away from the Slit1a-mCherry. In Figure 3.7B, similar axon errors are observed. The main anterior fascicle, labeled 1, has grown into a region of high Slit1a-mCherry expression and remains there throughout the movie. Most of the axons in this tract grow toward the Slit1a-mCherry. The same axon curving behavior seen in Figure 3.7A is demonstrated by growth cone 2. As in Figure 3.7A, several axons are growing aberrantly in the posterior direction.

Figure 3.7: RGC axons turn toward and grow into areas of high ectopic Slit1a after local heat shock anterior to the tract at 32 hpf. Maximum projection images from time-lapse movies. *hsp70l:slit1a-mcherry* embryos are oriented anterior left, dorsal up. Slit1-mCherry is shown in magenta; EGFP in green. The white dotted line indicates the approximate normal trajectory of RGC axons. Growth cones and fascicles labeled 1 grow toward Slit1a-mCherry. 2 indicates growth cones that grow toward Slit1a-mCherry but also curve. 3 shows axons growing posteriorly. (A) Starting at 40 hpf, RGC axons grow aberrantly toward an ectopic source of Slit1a-mCherry. (B) Starting at 44 hpf, RGC axons send a fascicle into a region of high Slit1a-mCherry.



I next misexpressed Slit2-EGFP on the anterior side of the optic tract. Based on the expression pattern at the optic chiasm and previous studies in mouse, I had expected Slit2 to repel axons. Instead, I saw the opposite effect. Surprisingly, RGC axons turned anteriorly, toward the source of ectopic Slit2 (Figure 3.6 E,F). The phenotype was similar to that seen in *hsp70l:slit1a-mcherry* embryos, but was completely penetrant (N=11/11). I also tried expressing Slit2-EGFP on the posterior side of the optic tract and found that only 4 of 11 embryos had axon guidance errors. One of these had an aberrant posterior fascicle, one had an aberrant anterior fascicle, and two had errors in both directions. The remaining 7 embryos did not have guidance errors.

Given that misexpressed Slit2-EGFP seems to act as a permissive or attractive cue for RGC axons in the optic tract, I wanted to examine its effect at the optic chiasm. The data from the tract suggested two possibilities: either Slit2 is always attractive to RGC axons, or RGC axons switch their response to Slit2 from repulsive to attractive after crossing the midline. I therefore performed local heat shock on 28 hpf embryos, misexpressing Slit2-EGFP anterior to the optic chiasm. Robust Slit2-EGFP expression was seen 4 hours later, at the time when axons are crossing the midline at the chiasm. In all 15 embryos, I saw axon errors in the anterior direction, toward the misexpressed Slit2 (Figure 3.6 G). Non-transgenic sibling controls had normal optic chiasms (Figure 3.6 H). I only observed errors at or after the midline, but never in the optic nerve. These results indicate that RGC axons are attracted to ectopic Slit2, both in the optic tract and at the optic chiasm.

## **Discussion**

In this chapter, I investigated the function of Slit1a and Slit2 in the zebrafish retinotectal system. I found that RGC axons grow over a domain of high *slit1a* expression in the optic tract in both wild-type and *astray* embryos. This finding suggested that Slit1a does

not usually act in the optic tract to repel axons. I then investigated Slit1a function using both loss-of-function and gain-of-function manipulations.

Three independent morpholinos against *slit1a* mRNA each partially phenocopied a weak allele of *astray*. Although each condition is hypomorphic, the same types of axon errors were seen in the same positions as in the *astray* mutants. These results indicate that Slit1a has a role in guiding axons through the tract, and the phenocopy suggests that Slit1a is probably acting through Robo2. I did not perform true epistasis experiments (e.g. injecting morpholinos into *astray*) because the *astray* phenotype is so strong that even using a weaker allele than the presumptive null, an enhancement of the phenotype would have been impossible to quantitate.

Global heat shock experiments allowed me to confirm that both Slit1a and Slit2 transgenes were able to perturb axon guidance. Misexpression of Slit1a or Slit2 at 24 hpf, early enough to affect pioneer axon guidance at the chiasm, resulted in errors at the midline, similar to phenotypes seen in *slit1* and *slit2* knockout mice (Plump et al., 2002). Although culture experiments show that zebrafish Slit2 causes collapse in cultured RGCs (K. Rasband, Ph.D. thesis), I did not see evidence of large-scale axon retraction or failure to extend. Rather, axons seemed to enter the brain and pathfind normally to the chiasm, then make errors at the midline. This could be because high levels of Slit cause internalization of Robo2 receptors, making the growth cones insensitive to Slit, or it could be that masking of the Slit gradient allows axons to make errors due to a lack of directional guidance.

I also performed global heat shock at 32 hpf to observe the effect of overexpression on axons entering the optic tract. Interestingly, the *hsp70l:slit1a-mcherry* embryos had only minor axon guidance errors, while the *hsp70l:slit2-egfp* embryos had profound axon guidance errors. I speculate that the endogenous levels of Slit1a are so high that adding extra

Slit1a everywhere does not greatly affect axon guidance. On the other hand, axons do not normally encounter Slit2 once they leave the chiasm, so they may be more sensitive to this cue than to Slit1a, if we assume that growth cones can distinguish Slit1a from Slit2. The Slit2-overexpressing embryos look similar to strong *astray* mutants. It may be that such a high level of Slit2 overwhelms the Robo2 receptors, rendering them insensitive to the Slit1a protein as well, and resulting in major optic tract defects. A third possibility is that there is a difference in expression levels or efficacy between the two transgenes, a possibility supported by the fact that with global heat shock the Slit2 gain-of-function phenotypes were completely penetrant while the Slit1a gain-of-function phenotypes were not. In any case, these experiments are difficult to interpret in terms of understanding Slit function. Their main role was to establish that the Slit transgenes were functional in the zebrafish embryo.

I was able to successfully misexpress mCherry, Slit1a-mCherry, or Slit2-GFP on either side of the optic tract using the local heat shock method described in Chapter 2. I did not observe a strong effect of misexpressing any of these transgenes on the posterior side of the optic tract. However, misexpressing Slit1a or Slit2 on the anterior side of the tract resulted in a dramatic phenotype, with axons misprojecting toward the ectopic protein expression. Time-lapse microscopy also showed defasciculation of the axons and confirmed that they were indeed growing toward the misexpressed Slit1 or Slit2.

These data potentially reveal a new role for Slits in axon guidance. They strongly suggest that Slits act to attract Robo2-expressing RGC axons. The major caveat to these results is that the nature of the misexpression system likely dictates a high level of expression, as seen by the high fluorescence intensity. Without antibodies against Slit1a or Slit2, however, I am unable to test how this concentration compares to endogenous concentration of the Slits. Unfortunately, it has proved difficult to make antibodies against

the vertebrate Slits that work for immunohistochemistry (Lynda Erskine, personal communication). One could imagine that a very high concentration of Slit1a or Slit2 results in growth cone receptors being overwhelmed and becoming nonfunctional. However, although axons turned anteriorly in response to anteriorly expressed Slit1a or Slit2, there was little effect when I misexpressed them posteriorly. The fact that axons had a different response to Slits on the anterior side of the tract argues strongly against the possibility that Slit is overexpressed to the level that it causes the receptors on the growth cones to become nonfunctional, either through internalization or complete occupancy. Had that been the case, the results from expressing Slits anteriorly and posteriorly should have been the same, because if receptor functionality were abolished, the axons would have responded similarly in both cases to other cues in the environment. This raises the question: if Slits are attractive, why do RGC axons fail to turn posteriorly when Slits are expressed caudal to the optic tract? First, there may be a technical explanation. Local heat shock on the posterior side of the tract was more difficult to perform than on the anterior side and surviving embryos often had ectopic expression at a more dorsal level on the posterior side. Perhaps a lack of a co-ligand or a repulsive axon guidance cue on the posterior side of the tract prevents the axons of the optic tract from entering this area, or the extracellular matrix in this region may have different properties leading to a different diffusion pattern than on the anterior side.

Another caveat is that in some experiments, there were errors both anteriorly and posteriorly when Slit1a was expressed anteriorly, although many fewer posterior errors were observed. One possible explanation is that RGCs from different quadrants of the retina may have different levels of Robo2. *robo2* mRNA is expressed in the zebrafish RGC layer; however it is unclear if it is evenly distributed throughout (Lee et al., 2001).

Are Slit1a and Slit2 truly attractive to axons? RGC growth cones clearly turn toward both ectopic Slit1a and Slit2 *in vivo*. These results are promising; however, the Slit2 results are surprising enough that additional confirmation is desirable. One question that needs to be resolved is why Slit2 causes growth cone collapse in culture, but causes growth cone turning toward Slit2 *in vivo*. Adding media conditioned with zebrafish Slit2 to cultured RGCs induces collapse (K. Rasband, Ph.D. thesis); however, the Slit2 concentration in these experiments is unknown and it is unclear how it compares to the endogenous levels or to the levels of ectopic Slit2-EGFP in my local heat shock system.

The most surprising result from these experiments is the fact that axons at the optic chiasm turned anteriorly when exposed to an anterior source of Slit2. Because Slit1a was predicted to be attractive or at least permissive, given its expression pattern, I had originally hypothesized that axons were switching their responsiveness to Slits after crossing the chiasm. Response switching over time has been previously demonstrated in axons of the mouse mesoprefrontal pathway, explants of which are repelled by Sema3F at E12.5 and attracted to Sema3F at E14.5 (Kolk et al., 2009b). However, misexpressed Slit2 at the chiasm also proved to be attractive to RGC axons. Although it may seem farfetched that Slit2 is attractive to Robo2-expressing axons, recent evidence from *Drosophila* suggests that the Slit-Robo interaction may be positive to midline crossing axons. Although dRobo1 is targeted for degradation by Comm to allow axons to cross the Slit-expressing midline, and upregulated after crossing to prevent subsequent midline crossing, dRobo2 acts to promote midline crossing (Spitzweck et al., 2010). dRobo2 and zRobo2 are not orthologs; however these data suggest that Robos can act to promote crossing over a zone of Slit expression.

Previously, Slit2 and Slit3 were proposed to repel axons at the optic chiasm in order to channel them across the midline to the contralateral optic tract (Hutson et al., 2002).

However, my results suggest that perhaps Slit2 attracts RGC axons to the midline.

Interestingly, Hutson and Chien (2002) showed that axons in *astray* embryos sometimes make errors even before the chiasm. In these embryos, axons appear to have wandered away from the optic nerve before reaching the chiasm, although it is also possible that they grew to the midline before retracting and projecting ipsilaterally. These data are consistent with the loss of an attractive cue as well as the loss of a repulsive cue.

Hutson and Chien (2002) also found that *slit2* is expressed at the rostral margin of the optic recess and *slit3* is expressed at the rostral and caudal margins of the optic recess. Unfortunately, without antibodies to the Slits, it is not possible to know if this mRNA expression pattern is recapitulated by the protein expression pattern. Depending on how far Slit2 and Slit3 diffuse, RGC axons may encounter Slit protein on their normal pathway. A closer view of the ventral diencephalon shows that *slit2* and *slit3* are expressed anteriorly and posteriorly to the postoptic commissure, which is just caudal to the optic chiasm, while *slit1a* is expressed in a broad band directly adjacent to the postoptic commissure (Barresi et al., 2005).

Given the relatively small number of axon guidance cues relative to the number of synapses that must be made in an embryo, it makes sense that cues could be used in different ways to modulate the response of axons toward their environment. Since Slits are possibly attractive to some migrating cells (Kramer et al., 2001; Englund et al., 2002), it is plausible that they can also act in some contexts to attract axons. Moreover, other canonical axon guidance cues are clearly able to act as either attractants or repellents (reviewed in Chapter 1), so it is quite likely that Slit is bifunctional in some contexts as well.

## Acknowledgements

Lara Hutson designed the *slit1a* morpholinos and performed preliminary morpholino experiments. The *isl2b:gfp<sup>zc7</sup>* line was originally made by Andrew Pittman. The *hsp70l:slit2-egfp<sup>rw015d</sup>* was a gift from the Okomoto lab. I would like to thank Nicholas Dambrauskas, Michael Brems, and Brooke Gaynes for excellent technical assistance, Kristen Kwan for advice and reagents, and members of the Chien Lab for helpful discussions.

## References

- Barresi, M. J. F., Hutson, L. D., Chien, C., and Karlstrom, R. O. (2005). Hedgehog regulated Slit expression determines commissure and glial cell position in the zebrafish forebrain. *Development* 132, 3643-3656.
- Brose, K., Bland, K. S., Wang, K. H., Arnott, D., Henzel, W., Goodman, C. S., Tessier-Lavigne, M., and Kidd, T. (1999). Slit proteins bind Robo receptors and have an evolutionarily conserved role in repulsive axon guidance. *Cell* 96, 795-806.
- Burrill, J. D., and Easter, S. S. (1995). The first retinal axons and their microenvironment in zebrafish: cryptic pioneers and the pretract. *J. Neurosci* 15, 2935-2947.
- Campbell, D. S., Stringham, S. A., Timm, A., Xiao, T., Law, M., Baier, H., Nonet, M. L., and Chien, C. (2007). Slit1a inhibits retinal ganglion cell arborization and synaptogenesis via Robo2-dependent and -independent pathways. *Neuron* 55, 231-245.
- Englund, C., Steneberg, P., Falileeva, L., Xylourgidis, N., and Samakovlis, C. (2002). Attractive and repulsive functions of Slit are mediated by different receptors in the *Drosophila* trachea. *Development* 129, 4941-4951.
- Fricke, C., Lee, J. S., Geiger-Rudolph, S., Bonhoeffer, F., and Chien, C. B. (2001). *astray*, a zebrafish roundabout homolog required for retinal axon guidance. *Science* 292, 507-510.
- Hutson, L. D., and Chien, C. B. (2002). Pathfinding and error correction by retinal axons: the role of *astray/robo2*. *Neuron* 33, 205-217.
- Hutson, L. D., Juryec, M. J., Yeo, S., Okamoto, H., and Chien, C. (2003). Two divergent *slit1* genes in zebrafish. *Dev. Dyn* 228, 358-369.
- Inatani, M., Irie, F., Plump, A. S., Tessier-Lavigne, M., and Yamaguchi, Y. (2003). Mammalian brain morphogenesis and midline axon guidance require heparan sulfate. *Science* 302, 1044-1046.
- Kidd, T., Bland, K. S., and Goodman, C. S. (1999). Slit is the midline repellent for the robo receptor in *Drosophila*. *Cell* 96, 785-794.
- Kidd, T., Brose, K., Mitchell, K. J., Fetter, R. D., Tessier-Lavigne, M., Goodman, C. S., and Tear, G. (1998). Roundabout controls axon crossing of the CNS midline and defines a novel subfamily of evolutionarily conserved guidance receptors. *Cell* 92, 205-215.
- Kolk, S. M., Gunput, R. F., Tran, T. S., van den Heuvel, D. M. A., Prasad, A. A., Hellemons, A. J. C. G. M., Adolfs, Y., Ginty, D. D., Kolodkin, A. L., Burbach, J. P. H., et al. (2009). Semaphorin 3F is a bifunctional guidance cue for dopaminergic axons and controls Their fasciculation, channeling, rostral growth, and intracortical targeting. *J. Neurosci.* 29, 12542-12557.

- Kramer, S. G., Kidd, T., Simpson, J. H., and Goodman, C. S. (2001). Switching repulsion to attraction: changing responses to slit during transition in mesoderm migration. *Science* 292, 737-740.
- Kwan, K. M., Fujimoto, E., Grabher, C., Mangum, B. D., Hardy, M. E., Campbell, D. S., Parant, J. M., Yost, H. J., Kanki, J. P., and Chien, C. (2007). The Tol2kit: a multisite gateway-based construction kit for Tol2 transposon transgenesis constructs. *Dev. Dyn* 236, 3088-3099.
- Lee, J., Ray, R., and Chien, C. (2001). Cloning and expression of three zebrafish roundabout homologs suggest roles in axon guidance and cell migration. *Dev. Dyn.* 221, 216-230.
- Ma, L., and Tessier-Lavigne, M. (2007). Dual branch-promoting and branch-repelling actions of Slit/Robo signaling on peripheral and central branches of developing sensory axons. *J. Neurosci* 27, 6843-6851.
- Ming, G. L., Song, H. J., Berninger, B., Holt, C. E., Tessier-Lavigne, M., and Poo, M. M. (1997). cAMP-dependent growth cone guidance by netrin-1. *Neuron* 19, 1225-1235.
- Miyashita, T., Yeo, S., Hirate, Y., Segawa, H., Wada, H., Little, M. H., Yamada, T., Takahashi, N., and Okamoto, H. (2004). PlexinA4 is necessary as a downstream target of Islet2 to mediate Slit signaling for promotion of sensory axon branching. *Development* 131, 3705-3715.
- Nguyen Ba-Charvet, K. T., Brose, K., Ma, L., Wang, K. H., Marillat, V., Sotelo, C., Tessier-Lavigne, M., and Chédotal, A. (2001). Diversity and specificity of actions of Slit2 proteolytic fragments in axon guidance. *J. Neurosci* 21, 4281-4289.
- Niclou, S. P., Jia, L., and Raper, J. A. (2000). Slit2 is a repellent for retinal ganglion cell axons. *J. Neurosci* 20, 4962-4974.
- Piper, M., Anderson, R., Dwivedy, A., Weinl, C., van Horck, F., Leung, K. M., Cogill, E., and Holt, C. (2006). Signaling mechanisms underlying Slit2-induced collapse of *Xenopus* retinal growth cones. *Neuron* 49, 215-228.
- Plump, A. S., Erskine, L., Sabatier, C., Brose, K., Epstein, C. J., Goodman, C. S., Mason, C. A., and Tessier-Lavigne, M. (2002). Slit1 and Slit2 cooperate to prevent premature midline crossing of retinal axons in the mouse visual system. *Neuron* 33, 219-232.
- Song, H., Ming, G., He, Z., Lehmann, M., McKerracher, L., Tessier-Lavigne, M., and Poo, M. (1998). Conversion of neuronal growth cone responses from repulsion to attraction by cyclic nucleotides. *Science* 281, 1515-1518.
- Song, H., Ming, G., and Poo, M. (1997). cAMP-induced switching in turning direction of nerve growth cones. *Nature* 388, 275-279.
- Spitzweck, B., Brankatschk, M., and Dickson, B. J. (2010). Distinct protein domains and

- expression patterns confer divergent axon guidance functions for *Drosophila* Robo receptors. *Cell* *140*, 409-420.
- Thisse, C., and Thisse, B. (2008). High-resolution in situ hybridization to whole-mount zebrafish embryos. *Nat Protoc* *3*, 59-69.
- Wang, K. H., Brose, K., Arnott, D., Kidd, T., Goodman, C. S., Henzel, W., and Tessier-Lavigne, M. (1999). Biochemical purification of a mammalian slit protein as a positive regulator of sensory axon elongation and branching. *Cell* *96*, 771-784.
- Whitford, K. L., Marillat, V., Stein, E., Goodman, C. S., Tessier-Lavigne, M., Chédotal, A., and Ghosh, A. (2002). Regulation of cortical dendrite development by Slit-Robo interactions. *Neuron* *33*, 47-61.
- Yeo, S. Y., Little, M. H., Yamada, T., Miyashita, T., Halloran, M. C., Kuwada, J. Y., Huh, T. L., and Okamoto, H. (2001). Overexpression of a slit homologue impairs convergent extension of the mesoderm and causes cyclopia in embryonic zebrafish. *Dev. Biol* *230*, 1-17.

CHAPTER 4

AXON TRACKING IN SERIAL BLOCK-FACE

SCANNING ELECTRON MICROSCOPY

ELIZABETH JURRUS, MELISSA HARDY, TOLGA TASDIZEN,  
P. THOMAS FLETCHER, PAVEL KOSHEVOY, CHI-BIN CHIEN,  
WINFRIED DENK, ROSS WHITAKER

MEDICAL IMAGE ANALYSIS 13:180-188, 2009.

## Introduction

Mapping the neural connections within the brain is a Herculean task. The only nervous system that has been completely mapped is that of *C. elegans* (White et al., 1986b). The authors painstakingly reconstructed the nematode's connectivity using serial transmission electron micrographs. Even with a nervous system consisting of only 302 neurons, they found over 7000 synapses (approximately 5000 chemical synapses, 2000 neuromuscular junctions, and 600 gap junctions). Considering that the human brain is estimated to have around 100 billion neurons, the prospect of mapping it completely requires the development of new imaging, computational, and data management methods (Azevedo et al., 2009).

One method that has been recently developed to obtain large serial datasets is Scanning Blockface Serial Electron Microscopy (SBFSEM). This method involves preparing samples with methods used for transmission electron microscopy (TEM) and then performing automated serial sectioning within the chamber of a scanning electron microscope (Denk and Horstmann, 2004). The automation of serial sectioning makes it theoretically possible to obtain large datasets quickly, since the need for manually handling slices is obviated. This makes it a good candidate for collecting data for reconstructing neural circuits. Another major advantage is that registration between slices is not needed; since the image is taken in reflection mode from the blockface, which does not undergo deformation like individual sections, the serial images are already registered. The main disadvantage of this method is that the resolution and contrast are not as good as in images taken using TEM.

I wanted to take advantage of this new method to study axon sorting within the optic tract. Axon sorting takes place in the retinotectal pathway, presumably to prepare axons to

find their correct synaptic partners on the topographically organized optic tectum. When RGC axons leave the eye, they are sorted according to their circumferential position in the retina; however, they reorganize after the optic chiasm such that axons from the dorsal eye grow in a ventral branch of the optic tract and enter the ventral tectum and axons from the ventral eye enter the dorsal tectum via a dorsal branch of the optic tract (Stuermer, 1988). Zebrafish mutant for *ext2* (*dackel*) or *extl3* (*boxer*) have sorting defects in which axons from the dorsal eye missort to the dorsal branch of the optic tract. Double mutants have strong pathfinding defects in addition to missorting (Lee et al., 2004).

Ideally, I wished to know how axon sorting differs in wild-type and mutant embryos. The axon missorting phenotype is strong in mutants at 5 dpf and absent in wild-type embryos. However, at 48 hpf, the ventral and dorsal branches of the optic tract have not yet formed. At 3 dpf, weak missorting is present in both wild-type and *boxer* mutants and *dackel* mutants have strong missorting phenotypes (Lee et al., 2004). This suggests that proper sorting of axons is a dynamic process that takes place after the pioneer axons have reached the tectum at 48 hpf. My strategy was to take SBFSEM datasets of wild-type and *dackel* embryos at 3 dpf and compare axon sorting between the two. Ideally, we would have also taken 5 dpf datasets to compare how axon sorting changed over time. This would have allowed us to determine how the optic tract in *dackel* compares to the wild-type tract.

Unfortunately, due to technical difficulties with SBFSEM sample preparation and obtaining time on the equipment, we were only able to obtain one dataset of a 3 dpf wild-type embryo. This dataset was also somewhat dorsal from the region of sorting. However, the dataset was useful for developing computational methods for reconstructing axon tracts from SBFSEM datasets. Our collaborators were able to use their method to successfully track axons automatically through many serial slices and validated their results by comparing them

with my hand tracking. This is described in the published paper in Part 2 of Chapter 4, which was published in *Medical Image Analysis* and is used with permission.

Future directions for this project include obtaining high-resolution serial sections through the ventral part of the optic tract. We are already collaborating with Robert Marc and Bryan Jones in the Department of Ophthalmology to obtain datasets. They have developed new ways to handle and process serial conventional TEM sections through large volumes, which will allow higher resolution and therefore easier automated tracking. In addition, they have developed new computational tools to help solve mosaicking and registration problems with TEM images (Anderson et al., 2009).

If we are able to obtain datasets, we should be able to see in great detail how axon sorting takes place in the zebrafish optic tract and how it is defective in *dackel* mutants. This descriptive work will inform hypotheses about how heparan sulfate proteoglycans act to sort axons.

## References

- Anderson, J. R., Jones, B. W., Yang, J., Shaw, M. V., Watt, C. B., Koshevoy, P., Spaltenstein, J., Jurrus, E., U V, K., Whitaker, R. T., et al. (2009). A computational framework for ultrastructural mapping of neural circuitry. *PLoS Biol* 7, e1000074.
- Azevedo, F. A., Carvalho, L. R., Grinberg, L. T., Farfel, J. M., Ferretti, R. E., Leite, R. E., Filho, W. J., Lent, R., and Herculano-Houzel, S. (2009). Equal numbers of neuronal and nonneuronal cells make the human brain an isometrically scaled-up primate brain. *The Journal of Comparative Neurology* 513, 532-541.
- Denk, W., and Horstmann, H. (2004). Serial Block-Face scanning electron microscopy to reconstruct three-dimensional tissue nanostructure. *PLoS Biol* 2, e329.
- Lee, J., von der Hardt, S., Rusch, M. A., Stringer, S. E., Stickney, H. L., Talbot, W. S., Geisler, R., Nüsslein-Volhard, C., Selleck, S. B., Chien, C., et al. (2004). Axon sorting in the optic tract requires HSPG synthesis by ext2 (dackel) and extl3 (boxer). *Neuron* 44, 947-960.
- Stuermer, C. (1988). Retinotopic organization of the developing retinotectal projection in the zebrafish embryo. *Journal of Neuroscience* 8, 4513-4530.
- White, J. G., Southgate, E., Thomson, J. N., and Brenner, S. (1986). The structure of the nervous system of the nematode *Caenorhabditis elegans*. *Philosophical Transactions of the Royal Society of London. B, Biological Sciences* 314, 1-340.



Contents lists available at ScienceDirect

## Medical Image Analysis

journal homepage: [www.elsevier.com/locate/media](http://www.elsevier.com/locate/media)

### Axon tracking in serial block-face scanning electron microscopy

Elizabeth Jurrus<sup>a,\*</sup>, Melissa Hardy<sup>b</sup>, Tolga Tasdizen<sup>a</sup>, P. Thomas Fletcher<sup>a</sup>, Pavel Koshevoy<sup>a</sup>,  
Chi-Bin Chien<sup>b</sup>, Winfried Denk<sup>c</sup>, Ross Whitaker<sup>a</sup>

<sup>a</sup>Scientific Computing and Imaging Institute, University of Utah, Salt Lake City, UT, United States

<sup>b</sup>Department of Neurobiology and Anatomy, University of Utah, Salt Lake City, UT, United States

<sup>c</sup>Max Planck Institute for Medical Research, Heidelberg, Germany

#### ARTICLE INFO

##### Article history:

Received 16 April 2007

Received in revised form 24 April 2008

Accepted 19 May 2008

Available online 5 June 2008

##### Keywords:

Image processing

Tracking

Kalman filtering

Active contours

Scanning electron microscopy

Neurobiology

#### ABSTRACT

Electron microscopy is an important modality for the analysis of neuronal structures in neurobiology. We address the problem of tracking axons across large distances in volumes acquired by serial block-face scanning electron microscopy (SBFSEM). Tracking, for this application, is defined as the segmentation of an axon that spans a volume using similar features between slices. This is a challenging problem due to the small cross-sectional size of axons and the low signal-to-noise ratio in our SBFSEM images. A carefully engineered algorithm using Kalman-snakes and optical flow computation is presented. Axon tracking is initialized with user clicks or automatically using the watershed segmentation algorithm, which identifies axon centers. Multiple axons are tracked from slice to slice through a volume, updating the positions and velocities in the model and providing constraints to maintain smoothness between slices. Validation results indicate that this algorithm can significantly speed up the task of manual axon tracking.

© 2008 Elsevier B.V. All rights reserved.

#### 1. Introduction

The answers to many biological questions depend on a better understanding of cellular ultrastructure, and microscopic imaging is providing new possibilities for exploring these questions. For instance, an important problem in neurobiology is deciphering the patterns of neuronal connections that govern neural computation and ultimately behavior. However, relatively little is known about the physical organization and connectivities of neurons at the cellular level.

Medical imaging modalities such as MRI provide three-dimensional (3D) measurements of the brain with resolutions on the order of 1 mm (Xiao et al., 2003). This resolution provides macroscopic information about brain organization, but does not allow analysis of individual neurons. Scanning confocal (Minsky, 1961) and two-photon (Denk et al., 1990) light microscopy have several advantages, including the ability to visualize live specimens, but are limited to 200 nm lateral resolution and 500 nm z resolution, which are insufficient to reconstruct connections of individual neurons. Newer light microscopic methods such as 4Pi, STORM, and PALM (Egner and Hell, 2005; Rust et al., 2006; Betzig et al., 2006) promise higher resolution, but 4Pi still cannot resolve closely-bundled axons, while STORM and PALM, at present,

are 2D methods requiring very long imaging times. Thus, electron microscopy remains the primary tool for resolving the 3D structure and connectivity of neurons. A number of researchers have undertaken extensive imaging projects in order to create detailed maps of neuronal structure (Fiala et al., 2002) and connectivity (Dacheux et al., 2003; White et al., 1986). At 20 nm resolution, the number of voxels needed to cover a volume sufficient to contain complete dendritic trees is about  $10^{12}$  (Denk and Horstmann, 2004), which is beyond any prospect of manual reconstruction. *The reconstruction of neural connectivity thus requires better tools for the automated analysis of such large data sets.*

A new and promising technique for imaging large arrays of cells at nanometer resolution is *serial block-face scanning electron microscopy* (SBFSEM) (Denk and Horstmann, 2004), shown in Fig. 1a. In SBFSEM, successive slices are cut away and discarded, and the electron beam is scanned over the remaining block face to produce electron backscattering images. An example image is shown in Fig. 2b. SBFSEM imaging has several advantages over other electron microscopic methods for the analysis of long axonal processes. For instance, because the dimensions of the solid block remain stable after slicing, SBFSEM images have smaller deformations than serial-section transmission electron microscopy (TEM). The resolution and signal-to-noise properties of SBFSEM are generally not as good as those of TEM, but they are sufficient for manual tracking of individual axon paths. Furthermore, unlike TEM, SBFSEM images do not require registration. While 3D data sets can

\* Corresponding author.

E-mail address: [liz@sci.utah.edu](mailto:liz@sci.utah.edu) (E. Jurrus).

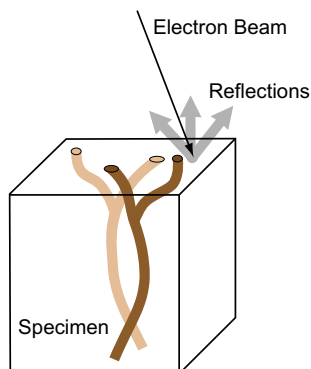


Fig. 1. Serial block-face scanning electron microscopy.

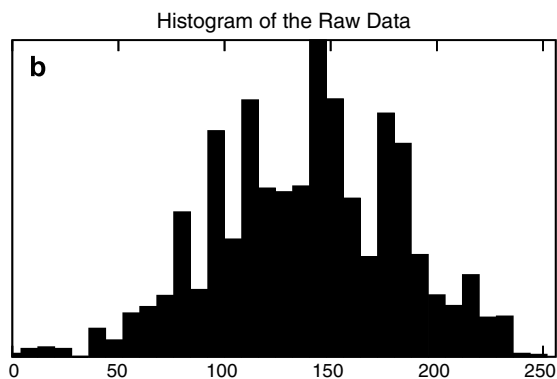
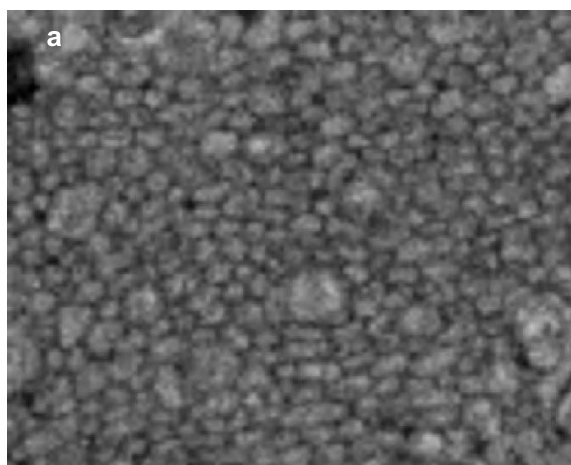


Fig. 2. (a) Sample image from SBFSEM and (b) its corresponding histogram for a  $24 \times 36$  image subset. If the axons contrasted clearly with their membranes, there would be a bimodal distribution of intensities. However, this histogram shows that the distribution is not bimodal, making membrane detection a difficult task when based on intensities alone.

also be obtained by electron microscope tomography (EMT) which has a resolution similar to TEM, EMT typically introduces reconstruction artifacts and does not provide the field of view (particularly in the  $z$  direction) needed to track neural processes across large distances.

This paper addresses the problem of automatically tracking individual axons in SBFSEM data sets, specifically for the analysis of the optic tract in the embryonic zebrafish. Tracking individual axons is an essential step in analyzing the different organizations of the optic tract in wildtype and mutants (Lee et al., 2004). While, more generally, neurons are composed of dendrites, a cell body, synapses and an axon, here we focus on tracking axons, which are generally more difficult to track than dendrites because of their greater length and smaller diameter.

SBFSEM data presents several challenges for segmentation. Mainly, the axonal cross-sections (see Fig. 2a) are barely discernible by eye, and yet a large number of axons are tightly packed in the optic tract. In addition, the actual axon membranes are difficult to identify by intensity alone as evident in the histogram in Fig. 2b of 20 axons, a very small subset of the data. Also challenging is that the data acquired with SBFSEM does not have isotropic resolution: the out-of-plane resolution is significantly less (50 nm) than the lateral resolution of the slices (26 nm) making segmentation in three dimensions difficult. However, the block is oriented so that the imaged surface is nearly perpendicular to the axon axis so that cross-sections are cut through elongated processes. A single axon will traverse thousands of slices, slowly winding its way around other axons. Axons will rarely branch or terminate, which aids in segmentation.

These SBFSEM data sets of the optic tract present, in some sense, a *two-and-a-half-dimensional* data processing problem. Thus, the proposed method approaches the problem of segmenting axons from electron microscopy images as a 2D segmentation problem combined with a tracking problem in the third dimension. This avoids the much more difficult full 3D problem of finding thin processes in noisy data amidst a dense packing of similar processes. This also allows an effective interface for user input. When the algorithm fails, the user can, in principle, correct the segmentation and continue tracking on a slice by slice basis. Completed axon pathways can also be viewed in two- and three-dimensional plots.

There is some related work in the literature that applies computer vision and object tracking to medical data. For instance, Vazquez et al. introduced a semi-automatic, differential geometric method for segmenting neurons in two-dimensional EM images (Vazquez et al., 1998). In their method, a user initializes points on the boundary of the neuron, then a minimal length geodesic criterion is used to complete the boundary. Bertalmio et al. propose a slice-to-slice tracking/segmentation approach for electron microscopy images that uses two-dimensional deformable curve models (Bertalmio et al., 1998). This method is similar to ours; however, tracking is not explicit, but is achieved indirectly with coupled partial differential equations. Furthermore, the tracked structures span a much smaller number of slices than axons. Researchers have also proposed segmentation methods for confocal microscopy images (Holmes et al., 2002; Dima et al., 2002; De Solzano et al., 1999; Wang et al., 2003). Curvilinear structure detection has been studied in various applications, such as detection of blood vessels in magnetic resonance angiography data (Sato et al., 2000; Lorigo et al., 2000). Three-dimensional deformable models for segmentation of tubular objects have also been proven to be effective (Pinho et al., 2007; Behrens et al., 2003; Feng et al., 2004). These methods are tailored to the resolution and specific properties of their application domains and do not readily extend to tracking axons in electron microscopy images.

## 2. Methods

The field of computer vision provides numerous methods for tracking features through a set of images. By treating the 3D volume as a sequence of 2D images in time, feature tracking meth-

ods can be applied to the volume. This tracking application is built on the Kalman-snakes framework (Terzopoulos and Szeliski, 1992; Peterfreund, 1999). The processing pipeline begins with a denoising of the input volume. Next, using an active contour model, initial contours are computed in the first 2D slice at user defined or automatically detected locations using a watershed filter (Beucher and Meyer, 1992; Ibanez et al., 2003). A simple smoothing constraint is used in the fitting of the contour to the axon, maintaining the shape for each slice. Each successive contour is then tracked through the 3D volume using a Kalman filter that predicts axon locations in upcoming slices. Each contour contains a series of points with a position in the image, and a velocity, which is the direction a point moves between slices. These points are weighted according to the strength of the underlying data to produce a new axon location at each slice. When tracking is completed, users can scroll through slices in the volume, inspecting the tracking for errors and re-initializing the tracking if necessary.

### 2.1. Image preprocessing

The SBFSEM data set used in the experiments has resolution  $26 \times 26 \times 50$  nm per voxel and has a relatively poor signal-to-noise ratio, partly due to nonoptimized specimen preparation. Given this resolution, and orienting the block such that the main axon bundles are roughly perpendicular to the imaging plane, axons range from four to six pixels in width in each 2D slice. Tracking such small features through a large number of slices is a challenging problem.

Denoising the data to obtain a cleaner representation of the axons is necessary as a preprocessing step. For this work, the UINTA algorithm (Awate and Whitaker, 2005) is applied to the data, denoising images by reducing the entropy of the density function associated with image neighborhoods. Fig. 3 shows images before and after denoising. A  $7 \times 7$  pixel neighborhood is used, representing roughly the size of the structures of interest, and 5 iterations of the filter are applied to each 2D slice of the SBFSEM volume. This algorithm relies on nonparametric representation of the neighborhood statistics which it develops from samples from the image itself. Thus, UINTA learns the statistics of the image and reduces noise and enhances structure by reducing randomness. In this sense UINTA is particularly well suited for the highly repetitive (texture-like) structure of the block-face images of the optic tract. There are faster image denoising methods that can be used as alternatives to UINTA. These include patch based denoising methods (Mahmoudi and Sapiro, 2005; Buades et al., 2005) and algorithms that take into account information from previous images in a sequence of images, i.e. video, to more quickly denoise data (Antoni Buades et al., 2008; Jerome et al., 2007).

### 2.2. Kalman filter based axon tracking

Axons have a tendency to “drift” at a slowly changing velocity through the image stack. They also change shape between sections despite the near perpendicular arrangement of the cells to the cutting plane. For this reason, we implement a tracking algorithm that takes into account the slowly varying velocity and change in shape to predict the location of the axon in each slice. The framework in the Kalman filter allows us to follow an axon through several slices, with simple updates to position and velocity estimates.

#### 2.2.1. Kalman filter

Kalman filtering (Blake et al., 1995) provides a feedback control loop for predicting the location of the axon at each slice, sampling the image, and correcting the estimate. Each axon is represented by a series of contours which consist of a set of points. Each point is associated with its own Kalman Filter that updates the state,

$$w_k = [x_k, y_k, u_k, v_k]^T, \quad (1)$$

where  $[u_k, v_k]$  is the velocity at contour position  $[x_k, y_k]$ . Every iteration of the Kalman filter consists of three computations: a prediction,  $\hat{w}_k$ , measurement,  $z_k$ , and correction,  $w_k$ . A linear update using the previous state estimate,  $w_{k-1}$ , gives the prediction state,

$$\hat{w}_k = Aw_{k-1}, \quad (2)$$

where

$$A = \begin{bmatrix} 1 & 0 & 1 & 0 \\ 0 & 1 & 0 & 1 \\ 0 & 0 & 1 & 0 \\ 0 & 0 & 0 & 1 \end{bmatrix}. \quad (3)$$

This prediction assumes constant velocity and adds the current velocity to the current position to predict the next position. The measurement state,  $z_k$ , is a combination of positions from active contour measurements (see Section 2.2.2) and velocities from optical flow (see Section 2.2.3). The filter combines the predicted and measured state to produce the corrected state estimate,

$$w_k = \hat{w}_k + K_k(z_k - H\hat{w}_k), \quad (4)$$

where  $K_k$  is the Kalman gain matrix, given by

$$K_k = \hat{P}_k H^T (H \hat{P}_k H^T + R)^{-1}, \quad (5)$$

and  $\hat{P}_k$  is the a posteriori error covariance of the current state estimate, given by

$$\hat{P}_k = AP_{k-1}A^T Q. \quad (6)$$

The Kalman gain matrix blends the measurement and predicted states so as to minimize  $P_k$ . After each estimate,  $P_k$  is updated by

$$P_k = (I - K_k H) \hat{P}_k. \quad (7)$$

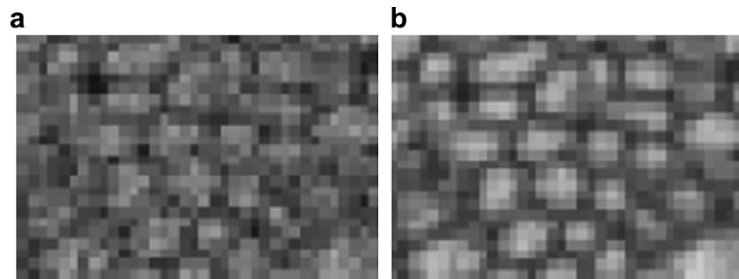


Fig. 3. (a) A portion of an SBFSEM image and (b) after denoising.

$H$  defines the relationship between the measurement and the model. For this model,  $H$  is the identity, while  $Q$  and  $R$  are  $4 \times 4$  diagonal matrices defining the process and measurement noise covariance. We assume the covariance process noise, represented by  $Q$ , is constant. However, we can model the measurement noise at a contour point using a membrane strength metric. The strength of a membrane can be defined as the second derivative in the direction perpendicular to the membrane:

$$\mu = \frac{d^2}{d\vec{n}^2} I', \quad (8)$$

where

$$I' = I * B_{\vec{d}}. \quad (9)$$

$I'$  is the intensity along the vector  $\vec{n}$ , normal to the contour point.  $B$  is a box filter used to smooth any remaining noise and is oriented along the vector  $\vec{d}$ , perpendicular to  $\vec{n}$ . As the membrane strength approaches zero, the Kalman gain matrix will favor the input from  $z_k$  more strongly in calculating  $w_k$ . If the membrane strength is large (closer to one), the Kalman gain will favor  $\hat{w}_k$  more. To scale  $\mu$  to a range between zero and one, we calculate,

$$\mu' = \exp\left(-\frac{\mu^2}{c}\right), \quad (10)$$

where  $c$  is a constant representing the value of a strong edge weight. In order to maintain continuity between the weights of neighboring contour points, preventing jagged contours, we smooth the weights across the sequence of points using a 1D Gaussian filter. This maintains a smooth transition between points on the contour.

This system, with input from the positional and velocity measurements, provides a set of steps for predicting and finding the location of axons at each slice in the volume.

### 2.2.2. Positional measurement – active contour models

Active contour models (Kass et al., 1988), or snakes, are often used in image segmentation and feature tracking (Terzopoulos and Szeliski, 1992; Peterfreund, 1999). Provided some user input or initialization, active contour models can lock onto and identify local features in an image. The Kalman filter uses the contour control points,  $[x_k, y_k]$ , as part of its state model (described in Section 2.2.1).

There are two main energies,  $E_{\text{int}}$  and  $E_{\text{image}}$ , that control the placement of the snake,

$$E_{\text{snake}} = \int_{s=0}^1 w(s)(E_{\text{int}}(v(s)) + E_{\text{image}}(v(s))) ds. \quad (11)$$

The internal snake energy,

$$E_{\text{int}} = \alpha |v_s(s)|^2 + \beta |v_{ss}(s)|^2, \quad (12)$$

serves as a smoothness constraint.  $v(s)$ ,  $v_s(s)$ , and  $v_{ss}(s)$  are the parameterized contour model and its first and second derivatives with respect to arclength, respectively.  $E_{\text{int}}$  uses  $\alpha$  and  $\beta$  to control how elastic and stiff the final snake will be with respect to the surrounding data points. This maintains the circular shape of the axon as it may change in size between slices.

$E_{\text{image}}$  is computed by sub-sampling the image along a ray  $\vec{R}$ , as shown in Fig. 4a. An axon edge is defined to be along

$$\vec{R} = P_i + t\vec{v}. \quad (13)$$

$C$  is the center of the axon and  $t$  is the sampling interval along  $\vec{v}$ , the normalized vector from  $C$  to  $P_i$ . An edge is defined to be at the maximum of  $\frac{d}{dt} I_R$  on the interval  $[-m, m]$ , where  $m$  is the size of the axon membrane and

$$I_R(t) = I(R(t)) * B_{\vec{v}}. \quad (14)$$

$B$  is a box filter operating over the vector perpendicular to  $\vec{v}$ . This allows for contribution from neighboring pixels and smoothing of any remaining noise. The external image energy,

$$E_{\text{image}} = -\left|\frac{d}{dt} I_R\right|^2 \quad (15)$$

represents the edge information needed to fit the snake to the axon membranes. Finally, the strength of the edge,  $w(s)$ , is used as a weight to constrain the contour more tightly to points with strong edges.

The set of contours used to define the axon through the volume is found using an iterative sampling process driven, in part, by the Kalman filter. The Kalman filter provides an initial set of predicted contour points, as in Fig. 4b. The contour location constraints provided by the Kalman filter enables contours to maintain their shape and location even when the data in a particular slice is not sufficient for axon detection.

This sampling method prevents self-intersecting contours through the use of non overlapping rays. The algorithm settles on a fit that minimizes the energy function  $E_{\text{snake}}$ . The Kalman filter uses the positions on the contour and the strength of the edge at those points to compute the final contour.

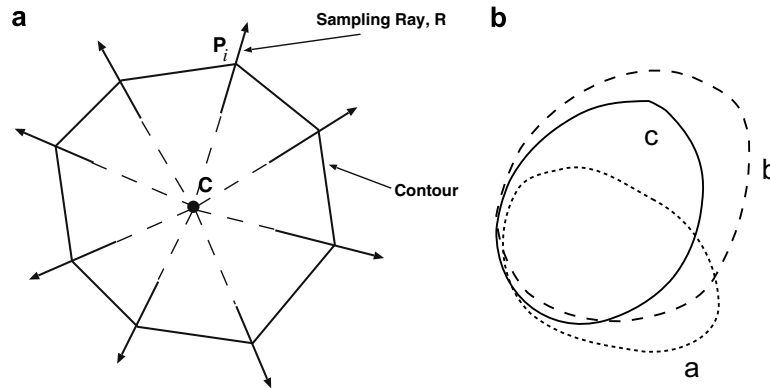


**Fig. 4.** (a) The contour is refined by iteratively sampling along the rays and recomputing the new edge location.  $C$  is the center of the axon. (b) The final location of the contour is dependent on a weighted combination of the predicted contour,  $a$ , and measured contour,  $b$ . The corrected estimate is the final contour  $c$ . New control points for each slice are repeatedly sampled, computing new contours until they converge.

Axon tracking is initialized with a user defined point at the approximate center of the axon. The area immediately around this point is sampled for edges and the Kalman filter is initialized. The algorithm continues to track the axon in each slice, iteratively sampling the image data and updating the state estimate in the Kalman filter.

### 2.2.3. Velocity measurement – optical flow

The shape and size of axonal cross-sections remain relatively constant as we move from one slice to the next, but the contour positions in the image will change unless an axon runs exactly perpendicular to the imaging plane. The change in position is proportional to the angle between the axonal axis and the imaging plane normal. This is used as the velocity component,  $[u_k, v_k]$ , of the measurement state,  $z_k$ , in Eq. (4) of Section 2.2.1. The Kalman filter uses this estimate to help determine the location of the axon in each slice.

Optical flow is the traditional method of estimating motion vectors from consecutive images. Common techniques used to compute optical flow include differential methods (Bruce et al., 1981) and cross correlation algorithms (Sun, 1999). In the SBFSEM data, the velocity field varies smoothly because nearby axons have similar orientations. Therefore, the structure tensor can be computed using Gaussian convolutions, which is computationally more efficient than the nonlinear diffusion model. For this reason we do not need to compute optical flow using the eigenvectors of the piecewise-smooth structure tensor (Liu et al., 2002; Brox and Weickert, 2002). Let  $I$  and  $G_\sigma$  denote an input 3D intensity image and a 3D Gaussian kernel with standard deviation  $\sigma$ , respectively. The input image is smoothed by convolution with  $G_\sigma$ :  $J = I * G_\sigma$ . Then the structure tensor is defined as

$$\mathcal{S} = G_\rho * (\nabla J \otimes \nabla J), \quad (16)$$

where  $G_\rho$  is another Gaussian kernel with standard deviation  $\rho$  and  $\otimes$  is the vector outer product operation. Typically,  $\sigma$  is 1 pixel or less, whereas  $\rho$  is chosen to define the size of structures of interest (Schar and Weickert, 2002). For best results, we choose to fix  $\sigma = 0.6$  and  $\rho = 5$  pixels (the approximate axon diameter). This tensor summarizes the first-order neighborhood structure of axons: it has two large eigenvalues and one small eigenvalue. The eigenvector,  $e_1$ , associated with the smallest eigenvalue is oriented along the long axis of the axon. Since consecutive slices in a 3D volume represent fixed increments in the  $z$  position,  $\Delta z$ , the change in the position of points from slice to slice along the axon boundaries can easily be computed as

$$\Delta x = \frac{e_{1,x}}{e_{1,z}} \Delta z \quad (17)$$

$$\Delta y = \frac{e_{1,y}}{e_{1,z}} \Delta z \quad (18)$$

where  $e_{1,x}$ ,  $e_{1,y}$  and  $e_{1,z}$  represent the  $x$ ,  $y$  and  $z$  components of the eigenvector  $e_1$  computed at the point of interest, respectively. Due to the alignment of the imaging plane perpendicular to the main running direction of the optic tract, individual axons are never parallel to the imaging plane; hence, the division by  $e_{1,z}$  does not pose a practical problem.

### 2.3. Multiple axon initialization

For tracking initialization, users select individual axons with a single click, marking the center of the axon they want to track. Selecting multiple axons with this method can be time consuming. For this reason, we use a watershed filter to automatically segment and select axons. The user selects a point in the data and all axons within an  $n \times n$  area of the click will be identified for tracking.

The watershed algorithm treats the image intensities as a height function, so that high intensities correspond to boundaries. The boundaries form regions in the image; water poured from above would tend to pool in those regions, creating segmentations. Each image is thresholded as a percentage of the maximum depth to remove shallow regions and help prevent over-segmentation. Then, using a top-down steepest descent algorithm, regions are segmented by following each maximum pixel to its local minimum. The top-down approach makes access to different levels of the segmentation straightforward, allowing users to customize their segmentation.

For this axon tracking application, we invert the region image so the high intensities represent axon boundaries and apply an edge preserving anisotropic diffusion filter to smooth out any remaining noise. The watershed filter threshold is set to 20% and the user is allowed to choose the depth of the segmentation, allowing for an optimal distribution of axon initialization points.

## 3. Results

Manual tracking of axons through a volume is tedious, requiring hours of careful labeling and correction, while automatic tracking allows for much faster annotation of axon locations. To demonstrate, results on the reliability and expected tracking distance of a series of axons tracked through a  $900 \times 500 \times 500$  voxel volume are presented. Fig. 5 shows three different slices through the volume. The closed curves are automatically detected contours and the points are tracking annotations by an expert. In this section, we also demonstrate how large selections of axons can be tracked using a watershed initialization approach. Finally, a three-dimensional rendering using the contours generated in the volume (Fig. 11) is examined.

Detecting membranes automatically requires parameters tuned for small distances and changes in the data. For this reason, the

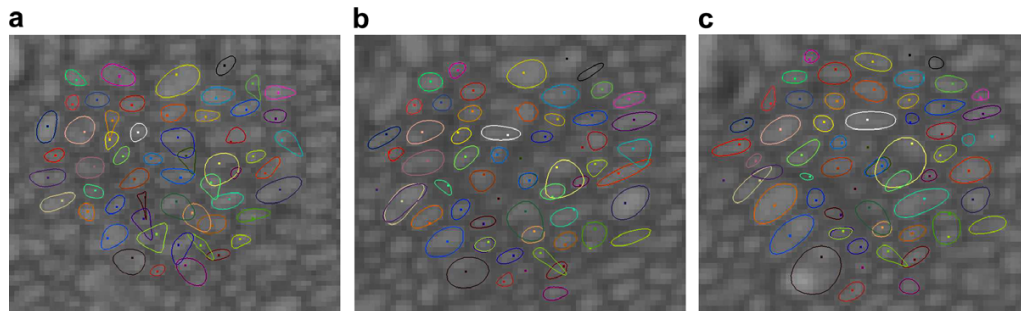


**Fig. 5.** Sequence of 56 axons tracked through 21 slices in a volume. Images are at slice 1, 11, and 21. Points inside the contour mark axons that are tracking correctly. Points not inside an axon contour are those for which tracking failed.

length of  $\vec{n}$  in Eq. (8) is 4.0 and  $\vec{d}$  in Eq. (9) is 2.5. This represents the number of pixels the algorithm will use to compute the best location of the membrane. In addition,  $c$ , in Eq. (8) equals 4.0. The noise model,  $Q$ , in Eq. (5) is set to 0.4. The active contour model uses  $\alpha$  and  $\beta$  parameters which are set to 0.4 and 2.0, respectively. Finally, when we sample the ray  $\vec{R}$  in Eq. (13),  $t$  equals 0.1 and  $m$  equals 2.5.

The computational costs of axon tracking are relatively low. Image denoising takes approximately 20 minutes per slice and the computation of structure tensors takes 1 minute per slice on a standard desktop PC. These steps are the computational bottlenecks; however, both can be computed offline. Tracking 56 axons takes about 10 seconds per slice. Alternatively, the tensor calculation can be performed locally while tracking, taking up to 5 seconds more per slice, depending on the size of the image buffer used. In comparison, the time it took for an expert to track the same 56 axons over 500 slices is approximately 14 hours, averaging 1.7 minutes per slice. The automated method is 10 times faster if the tensors are recomputed and 7 times faster if the tensor calculation is buffered.

We performed several validation experiments using human expert segmentations as ground truth. Fifty six axons were tracked through 500 slices by a human expert to provide ground truth; additionally, another three axons were tracked through 700 slices. The human expert placed markers at the pixel locations closest to the centers of the 56 tracked axons in each of the 500 slices and the centers of the three axons in the 700 slices. The expert was provided with a graphical user interface which allowed her to place colored markers and scroll through the slices. She was asked to use a unique color for each axon; hence, the markers are uniquely identifiable with these axons. To quantitatively assess the performance of the algorithm several metrics are defined. Let  $\mathbf{m}_i(k)$  denote the position of the marker for the  $i$ th axon at the  $k$ th slice.

**Definition 1.** The segmentation for axon  $i$  at slice  $k$  is defined as correct if  $\mathbf{m}_i(k)$  falls inside the region defined by the final contour for axon  $i$  at slice  $k$  given by the segmentation algorithm; otherwise, it is defined as incorrect.

In the 700 slice volume, the human expert selected axons that were visually easy to track. Our algorithm tracked one axon through 608 slices, and the other two through 657 slices. In the 500 slice/56 axon volume, a more diverse population of axons was used, including many that were visually more challenging to track. Fig. 6 plots the number of correct axon segmentations, according to the above definition, as a function of the slice number.

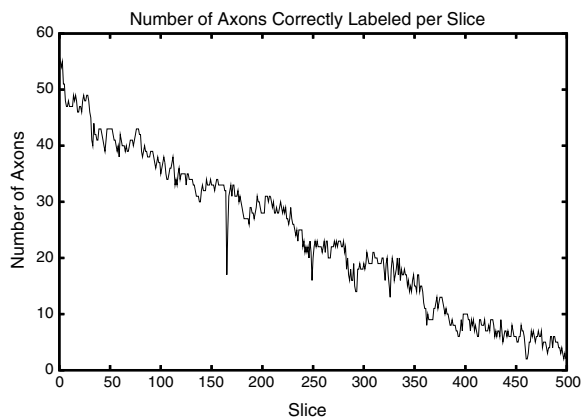


Fig. 6. Number of contours at each slice correctly identifying the axons they were initialized to track.

As expected, the number of correct segmentations starts at 56, and declines as the slice number grows. A less intuitive observation is that this number does not decrease monotonically but can also increase. However, this observation fits well with the expectations of the algorithm. It is expected that segmentations that miss the axons they are tracking due to bad data slices will recover to the correct segmentation, due to the correction by the Kalman filter, as long as the number of consecutive bad slices is not too large. Due to this robustness, it can be more meaningful to ignore intermediate errors from which the segmentation recovers in assessing the performance of the algorithm. The following definition addresses this property.

**Metric A:** The segmentation for axon  $i$  is defined to have failed at slice  $n$  if, for all slice numbers larger than or equal to  $n$ , the segmentation for axon  $i$  according to Definition 1 is incorrect.

It can be argued that *Metric A* is overly optimistic: if an axon segmentation recovers after a large number of consecutive failed slices, is the recovery due to the Kalman filter, or due to chance? To address this question another definition of “last correctly tracked slice number” can be made.

**Metric B:** The segmentation for axon  $i$  is defined to have failed at slice  $n$  if, for all slices in the range  $[n, n + k - 1]$ , the segmentation for axon  $i$  according to Definition 1 is incorrect.

We chose  $k = 10$  for the above definition in this paper. Fig. 7 compares the two metrics by plotting the number of correctly tracked axons as a function of the slice number. Notice that the performance reflected by *Metric B* is lower than *Metric A*, as expected. The curve for *Metric A* demonstrates an approximately linear decline whereas the curve for *Metric B* appears roughly exponential. Using these curves, the expected number of slices after which a certain fraction of axons will be mistracked can be computed. For instance, according to *Metric A* approximately 90% and 50% of the axons will still be correctly tracked after 30 and 250 slices, respectively.

Most failures occur when an axon disappears from view for too many slices. Fig. 8 shows how the tracking fails when an edge appears in the middle of a feature separating the tracked axon from its actual path. It is also not unusual for a tracked axon to “latch onto” a neighboring axon and then find its way back to the correct axon within 3 or 4 slices. Parameters affecting the tracking include

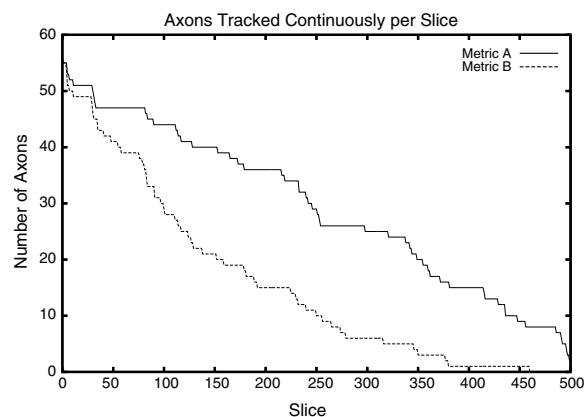
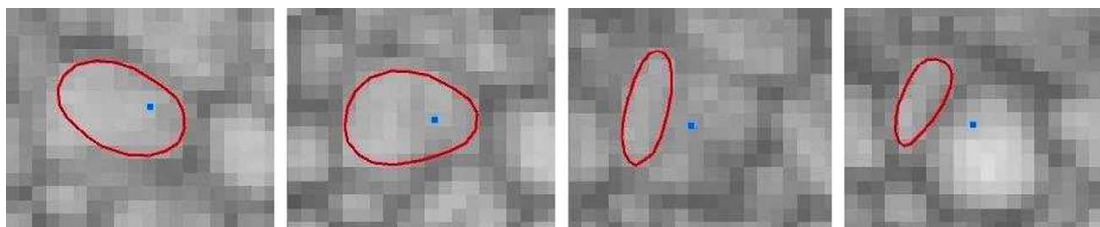


Fig. 7. Comparison of the number of axons tracking correctly at each slice, for both *Metric A* and *B*,  $k = 10$ .



**Fig. 8.** Common mode of failure over a sequence of slices. The tracked axon is shown with a red contour and the expert tracked axon with a blue point. The axon appears to split in the third image when the tracking picks up an edge (which first appears in the second image). (For interpretation of the references in colour in this figure legend, the reader is referred to the web version of the article.)

the  $\alpha$  and  $\beta$  terms of the active contour and the measurement and noise covariance values in the  $Q$  and  $R$  matrices of the Kalman filter. Small changes to the Gaussian standard deviations in the structure tensor computation do not have an effect. Computing membrane weights for the positional measurement, however, provides a better fit for the data.

Fig. 9 is a close-up view of the axon contours with their respective predicted and measured contours. Images (a) and (b) are examples of how a weighted noise covariance in the Kalman filter helps the contour stay on track of the correct axon when the measured axon has a weak membrane. The Kalman filter used on the points of the contour in image (a) is weighting the measured (red) and predicted (yellow) contour more evenly to produce the corrected (blue) contour. In doing this, the contour misses the actual location of the contour, as indicated by the blue point just outside of the corrected contour in image (a). In contrast, the corrected contour in image (b) conforms more to the predicted contour, maintaining the correct position. Images (c) and (d) have similar outcomes except the membranes are much stronger causing the filter to fit more closely to the measured contour. In this case, the edge strength of the measured (red) contour is very strong, forcing the final corrected (blue) contours to fit the measured data.

In order to speed up the initialization process, a watershed filter is used to automatically find axon centers, allowing many axons to be initialized at once. Fig. 10 shows the results of this initialization compared to the axon centers identified by the expert. In some

cases the axon initialization is very close to the expert's initialization, while in other cases, the watershed segmentation places a boundary where an axon center should lie. Poorly initialized axons can be easily identified by the algorithm during tracking and removed. The user can adjust the level of the watershed to find the best fit and reinitialize axons when the watershed initialization fails.

Examining the complex 3D nature of the data is possible with 3D renderings of the tracked axons. A 3D representation is formed by connecting contours from each traced axon. Fig. 11 shows a three-dimensional rendering of axons from the  $900 \times 500 \times 500$  volume and Fig. 12 shows similar tracking results for two different sets of axons in the same volume. All axons were compared against expert tracking, including Fig. 11a, which required manual reinitialization.

#### 4. Conclusions

The described system can successfully track axons through a series of slices in a volume. Given the noisy nature of the data and the small axon sizes, denoising provides a cleaner view of the data in which to perform tracking. Tracking from slice to slice is made possible with the Kalman filter, which predicts and corrects the placement of the axon in each slice using optical flow and active contours as velocity and position estimates. Initialization and correction of the algorithm is performed with user

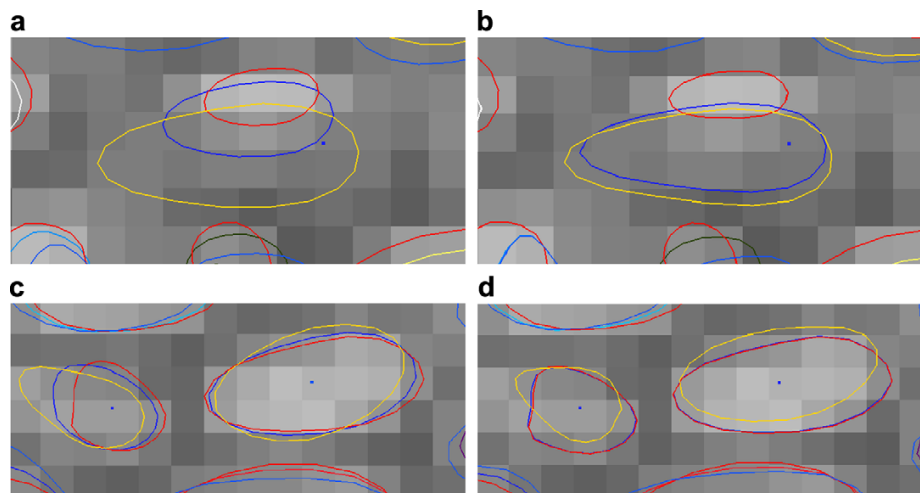


**Fig. 9.** Examples of how the Kalman filter maintains axon continuity between slices. Yellow contours are predicted axon contours, red contours are measured contours, and blue contours are corrected contours. Corrected contours in images (a) and (c) are computed using a constant measurement noise covariance and corrected contours in (b) and (d) are computed with a weighted measurement noise covariance. (For interpretation of the references in colour in this figure legend, the reader is referred to the web version of the article.)

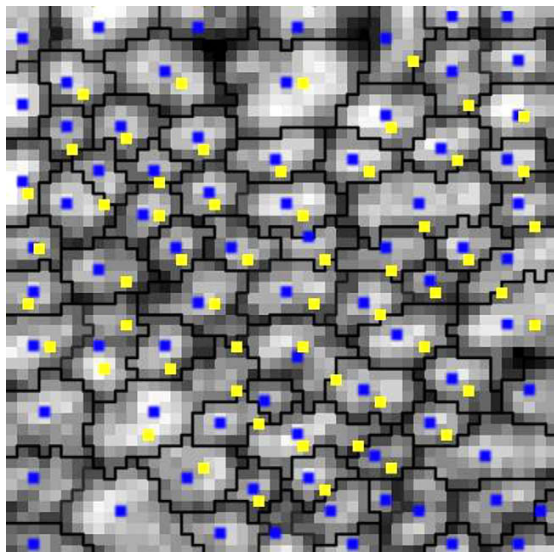


**Fig. 10.** Result of a watershed segmentation used to initialize axon tracking. Yellow points are expert labeled axons and blue points are watershed labeled axons. (For interpretation of the references in colour in this figure legend, the reader is referred to the web version of the article.)

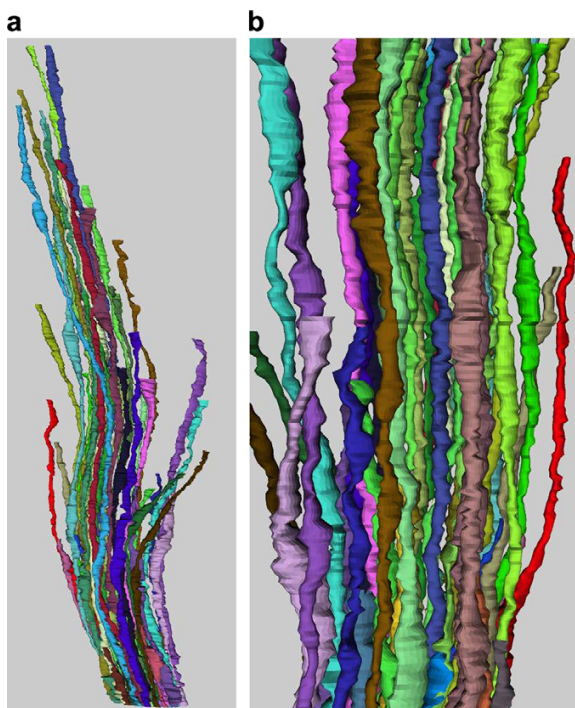


**Fig. 11.** 3D renderings of 56 axons tracked through 500 slices and validated using Metric B: (a) entire volume and (b) close-up.

interaction. We have also presented a validation study that effectively tracked multiple axons through slices of an SBFSEM volume.

Future work will include using the entire set of contour points as a single state vector in the Kalman Filter, accounting for the entire contour rather than individual points on the contour. It is

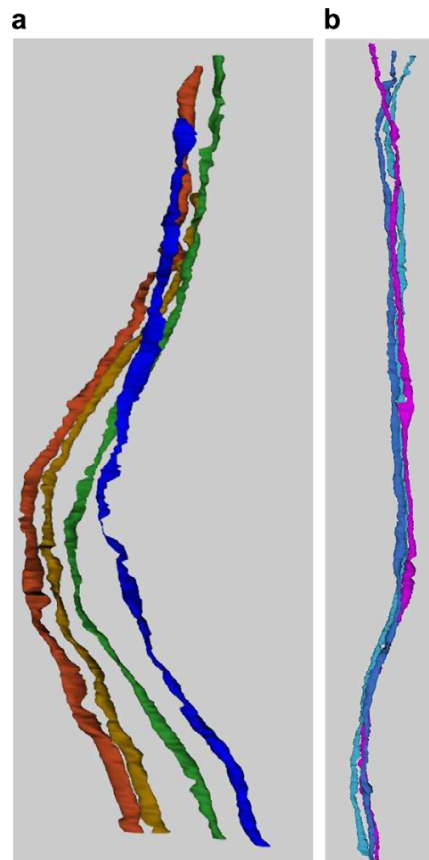


**Fig. 12.** (a) A 3D rendering of 4 axons tracked through approximately 300 slices with some manual reinitialization. This demonstrates the movement and twisting nature typical of features in these data; (b) 3 axons tracked through 600 slices. All tracking was validated by an expert.

worth exploring other methods, such as particle filters (Smal et al., 2007), which track multiple axons with similar displacements and have the potential of more accurately estimating axons' locations in larger volumes. We also want to validate our tracking with more axons through larger volumes (of at least 1000 slices), and compare the axon organization of wildtypes with mutants. In addition, more advanced volume visualization methods are being developed to more easily examine the contours within the data, helping to detect errors in tracking and restart tracking at those locations.

The software to aid in the image processing was written using the Insight Segmentation and Registration Toolkit (ITK) (ITK, XXX). The 3D axon renderings were created using the Visualization Toolkit (VTK) (VTK, XXX).

#### Acknowledgements

This work was supported in part by NIH RO1 EB005832, NIH RO1 EY12873, and the Max-Planck Society.

#### References

- Awate, Suyash P., Whitaker, Ross T., 2005. Higher-order image statistics for unsupervised, information-theoretic, adaptive, image filtering. CVPR 2, 44–51.

- Behrens, T., Rohr, K., Stiehl, H.S., 2003. Robust segmentation of tubular structures in 3-d medical images by parametric object detection and tracking. *IEEE Trans. Syst. Man Cybern. Part B* 33 (4), 554–561.
- Bertalmio, M., Sapiro, G., Randall, G., 1998. Morphing active contours: a geometric approach to topology-independent image segmentation and tracking. *Proc. ICIP*, 318–322.
- Betzig, E., Patterson, G.H., Sougrat, R., Lindwasser, O.W., Olenych, S., Bonifacio, J.S., Davidson, M.W., Lippincott-Schwartz, J., Hess, H.F., 2006. Imaging intracellular fluorescent proteins at nanometer resolution. *Science* 313 (5793), 1642–1645.
- Beucher, S., Meyer, F., 1992. The morphological approach of segmentation: the watershed transform. *Math. Morphol. Image Process.*
- Blake, Andrew, Curwen, Rupert, Zisserman, Andrew, 1995. A framework for spatio-temporal control in the tracking of visual contours. *Real-time Comp. Vis.*, 3–33.
- Boulanger, Jerome, Kervrann, Charles, Bouthemy, Patrick, 2007. Space-time adaptation for patch-based image sequence restoration. *IEEE Trans. on Pattern Anal. Mach. Intell.* 29 (6), 1096–1102.
- Brox, T., Weickert, J., 2002. "Nonlinear matrix diffusion for optic flow estimation. DAGM. Springer-Verlag, pp. 446–453.
- Bruce D. Lucas, Takeo Kanade. An iterative image registration technique with an application to stereo vision. In: Proceedings of the 7th International Joint Conference on Artificial Intelligence (IJCAI'81), April 1981, pp. 674–679.
- Buades, A., Coll, B., Morel, J.M., 2005. A review of image denoising algorithms, with a new one. *Multiscale Model. Simulat.* 4 (2), 490–530.
- Buades, Antoni, Coll, Bartomeu, Morel, Jean-Michel, 2008. Nonlocal image and movie denoising. *Int. J. Comput. Vis.* 76 (2), 123–139.
- Dacheux, R.F., Chimento, M.F., Amthor, F.R., 2003. Synaptic input to the on-off directionally selective ganglion cell in the rabbit retina. *J. Comp. Neurol.* 456 (3), 267–278.
- Denk, W., Horstmann, H., 2004. Serial block-face scanning electron microscopy to reconstruct three-dimensional tissue nanostructure. *PLoS Biol.* 2 (11).
- Denk, W., Strickler, J.H., Webb, W.W., 1990. Two-photon laser scanning microscopy. *Science* 248, 73–76.
- De Solrzano, C.O., Rodriguez, E.G., Jones, A., Pinkel, D., Gray, J.W., 1999. Segmentation of confocal microscopy images of cell nuclei in thick tissue sections. *J. Microsc.* 193 (3), 212–226.
- Dima, A., Scholz, M., Obermayer, K., 2002. Automatic segmentation and skeletonization of neurons from confocal microscopy images based on the 3-d wavelet transform. *IEEE Trans. Image Process.* 11 (7), 790–801.
- Egner, A., Hell, S.W., 2005. Fluorescence microscopy with super-resolved optical sections". *Trends Cell Biol.* 15 (4), 207–215.
- Feng, J., Ip, H.H.S., Cheng, S.H., 2004. A 3d geometric deformable model for tubular structure segmentation. In: Proceedings of the 10th International Multimedia Modelling Conference, 5–7 January, pp. 174–180.
- Fiala, J.C., Allwardt, B., Harris, K.M., 2002. Dendritic spines do not split during hippocampal ltp or maturation. *Nature Neurosci.* 5 (4), 297–298.
- Holmes, D.R., Moore, M.J., Mantilla, C.B., Sieck, G.C., Robb, R.A., 2002. Rapid semi-automated segment. and analysis of neuronal morphology and function from confocal image data. In: Proceedings of IEEE International Symposium on Biomedical Imaging, pp. 233–236.
- <http://www.itk.org>. NLM Insight Segmentation and Registration Toolkit.
- <http://www.vtk.org>. The visualization toolkit.
- Ibanez, L., Schroeder, W., Ng, L., Cates, J., 2003. The ITK Software Guide, Kitware, Inc., ISBN 1-930934-10-6. <<http://www.itk.org/ItkSoftwareGuide.pdf>>, first edition.
- Ihor Smal, Katharina Draegestein, Niels Galjart, Wiro J. Niessen, Erik H.W., 2007. Meijering, Rao-blackwellized marginal particle filtering for multiple object tracking in molecular bioimaging. In: IPMI, 2007, pp. 110–121.
- Kass, M., Witkin, A., Terzopoulos, D., 1988. Snakes: active contour models. *Int. J. Comp. Vis.* 1 (4), 321–331.
- Lee, J.S., von der Hardt, S., Rusch, M.A., Stringer, S.E., Stickney, H.L., Talbot, W.S., Geisler, R., Nsslein-Volhard, C., Selleck, S.B., Chien, C.B., Roehl, H., 2004. Axon sorting in the optic tract requires hspg synthesis by ext2 (dackel) and extl3 (boxer). *Neuron* 44 (6), 947–960.
- Liu, H., Chellappa, R., Rozenfeld, A., 2002. Accurate dense optical flow estimation using adaptive structure tensors and a parametric model. In: Proceedings of the International Conference on Pattern Recognition.
- Lorigo, L.M., Faugeras, O., Grimson, W.E.L., Keriven, R., Kikinis, R., Nabavi, A., Westin, C.-F., 2000. Codimension-two geodesic active contours for the segmentation of tubular structures. *Proc. IEEE CVPR*, 444–451.
- Mahmoudi, M., Sapiro, G., 2005. Fast image and video denoising via nonlocal means of similar neighborhoods. *IEEE Signal Process. Lett.* 12 (12), 839–842.
- Minsky, M., 1961. Microscopy apparatus. U.S. Patent Number 3013467.
- Peterfreund, N., 1999. Robust tracking of position and velocity with kalman snakes. *IEEE Trans. Pattern Anal. Mach. Intell.* 21 (6), 564–569.
- Pinho, R., Sijbers, J., Huysmans, T., 2007. Segmentation of the human trachea using deformable statistical models of tubular shapes. In: ACIVS07, pp. 531–542.
- Rust, Michael J., Bates, Mark, Zhuang, Xiaowei, 2006. Sub-diffraction-limit imaging by stochastic optical reconstruction microscopy (storm). *Nature Meth.* 3 (10), 793–796.
- Sato, Y., Westin, C.F., Bhalerao, A., Nakajima, S., Shiraga, N., Tamura, S., Kikinis, R., 2000. Tissue classification based on 3d local intensity structures for volume rendering. *IEEE Trans. Vis. Comp. Graph.* 6 (2), 160–180.
- Scharr, H., Weickert, J., 2002. A scheme for coherence-enhancing diffusion filtering with optimized rotation invariance. *J. Vis. Commun. Image Represent.* 13 (1/2), 103–118.
- Sun, C.M., 1999. Fast optical flow using cross correlation and shortest-path techniques. In: Proceedings of Digital Image Computing: Techniques and Applications, pp. 143–148.
- Terzopoulos, D., Szeliski, R., 1992. Tracking with Kalman snakes. In: Active Vision. MIT Press, Cambridge, MA, pp. 3–20.
- Vazquez, L., Sapiro, G., Randall, G., 1998. Segmenting neurons in electronic microscopy via geometric tracing. *Proc. ICIP*, 814–818.
- Wang, Juhui, Trubuil, A., Graffigne, C., Kaeffer, B., 2003. 3-d aggregated object detection and labeling from multivariate confocal microscopy images: a model validation approach. *IEEE Trans. Syst. Man Cybern. Part B* 33 (4), 572–581.
- White, J.G., Southgate, E., Thomson, J.N., Brenner, F.R.S., 1986. The structure of the nervous system of the nematode *Caenorhabditis elegans*. *Phil. Trans. Roy. Soc. Lond. Ser. B Biol. Sci.* 314, 1–340.
- Xiao, Y.P., Wang, Y., Felleman, D.J., 2003. A spatially organized representation of colour in macaque cortical area v2. *Nature* 421 (6922), 535–539.

## CHAPTER 5

## DISCUSSION

## **Summary**

Although Sperry's model of chemoaffinity was proposed in 1963 and axon guidance has been extensively studied in the half-century since, many questions about how guidance cues act to guide axons through the developing brain remain. One important question is how guidance cues can be bifunctional, acting in one context to attract axons and in another to repel them. Different intracellular cues, such as receptors and Rho GTPases, can modulate extracellular signals to mediate different responses, and extracellular molecules may also regulate growth cone response to axon guidance ligands. The zebrafish retinotectal system is an excellent model for studying axon guidance and sorting.

In this dissertation, I describe the development of a new method which allows misexpression of genes of interest in a temporally and spatially controlled manner in the zebrafish. I used this method to investigate the function of Slits in the zebrafish optic tract. Prior to this work, Slits were known to act repulsively and to stimulate branching in axon guidance, but had not been shown to act attractively. I showed that, at least in some contexts, axons turn toward a source of ectopic Slit1a or Slit2. I also undertook work to map axon sorting within the zebrafish optic tract using electron microscopy. With my collaborators, I helped to publish a new method of axon reconstruction and am currently collaborating to obtain more complete datasets. This work adds both to available methods and to our understanding of axon guidance.

### **Local heat shock as a method of misexpression**

There are several methods to misexpress genes in zebrafish, including electroporation, mRNA injection, DNA injection, and inducible gene expression systems (Ungar et al., 1995; Teh et al., 2003; Liu and Halloran, 2005; Huang et al., 2005; Langenau et al., 2005; Cerda et al., 2006; Hendricks and Jesuthasan, 2007; Esengil et al., 2007). In the

long term, the most promising methods for tissue-specific expression are inducible systems such as the Tet repressor, Cre/LoxP, and Gal4/ecdysone receptor systems (Esengil and Chen, 2008). However, these systems, while potentially quite powerful, are limited in utility until more tissue-specific promoters are identified or until large-scale gene trapping is performed. There are currently no published tissue-specific promoters for the brain regions in which I wished to misexpress genes. Therefore, I developed a new method of misexpression: local heat shock using a modified soldering iron.

This method is fast, technically simple, inexpensive, and results in robust misexpression 3-4 hours after local heat shock. Limitations of the method are that misexpression is confined to tissues close to the surface (40  $\mu\text{m}$  or less) and that it is difficult to induce a very small spot of misexpression. A recent paper describes a new method of activating the *hsp70l* promoter by using a laser pointer to power optical fibers (Placinta et al., 2009). This potentially offers great spatial control since the optical fibers can be pulled to small diameters. However, my method was sufficient to test the function of Slits in the optic tract because the RGC axons grow along the pial surface of the brain; therefore, misexpression of protein near the brain's surface is close enough to have effects on the axons. Although greater spatial control would have been helpful, the relatively high throughput nature of my system meant that I was able to collect enough informative embryos with three or four rounds of local heat shock experiments. This method allowed me to test the function of Slit1a in the optic tract and Slit2 in the optic tract and optic chiasm.

### **Slit function in the zebrafish retinotectal system**

Slit is known from experiments in invertebrates and *in vitro* cultures as an axon guidance molecule that functions to repel Robo-expressing axons or collapse growth cones.

Although many other axon guidance molecules are known to be bifunctional, there is little previous evidence that Slit can act to attract axons. However, Slit has been shown in *Drosophila* to be capable of attracting migrating cells, and in vertebrates to cause axon branching. Recent research in *Drosophila* suggests that dRobo2 may have a positive role in midline crossing, unlike dRobo1, which mediates repulsion by Slit (Spitzweck et al., 2010). In addition, experiments in zebrafish sonic hedgehog-pathway mutants suggested that Slit1a may not act to repel axons of the postoptic commissure but instead somehow facilitates midline crossing (Barresi et al., 2005). However, my results are the first demonstration that Slits may act *in vivo* as axon attractants. My results are summarized in Figure 5.1.

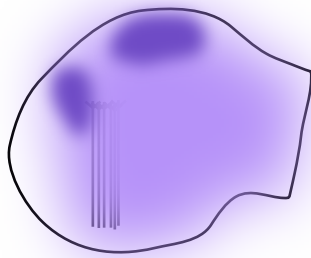
The expression pattern of *slit1a* was the first evidence that Slit1a might not act as a repellent for Robo2-expressing RGC axons. *slit1a* loss-of-function experiments resulted in axon guidance errors in the optic tract, indicating that Slit1a functioned to help guide axons from the optic chiasm to the tectum. *slit1a* morpholinos phenocopied *astray*, suggesting that Slit1a acts through the Robo2 receptor. Overexpression of Slit1a or Slit2 anterior to the optic tract resulted in RGC axon turning toward the ectopic Slit1a or Slit2, suggesting an attractive role for these two Slits. Ectopic Slit2 was also attractive to RGC axons at the optic chiasm.

These data raise several questions: what is the function of Slit1a and Slit2 in guiding RGC axons? Does Slit1a act differently than Slit2? Do growth cones change their responsiveness as they move through the retinotectal pathway?

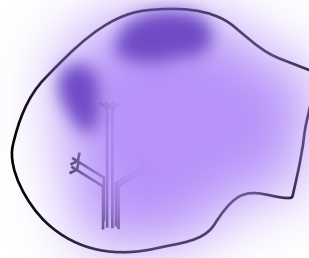
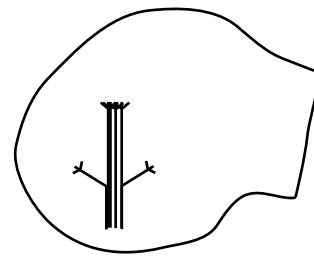
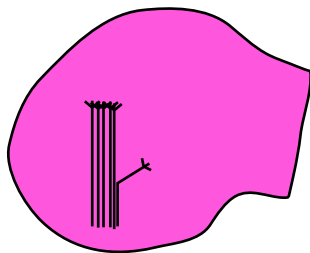
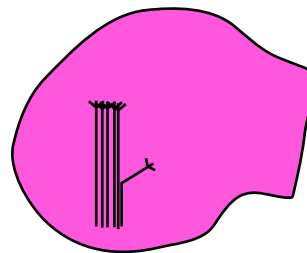
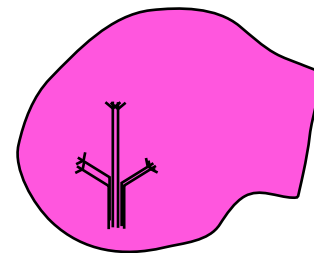
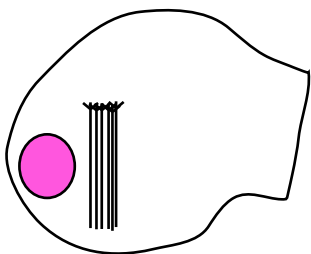
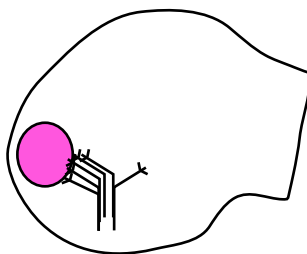
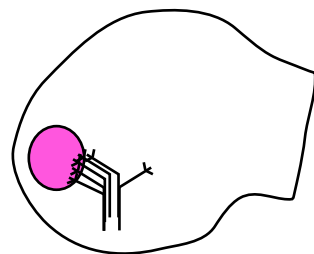
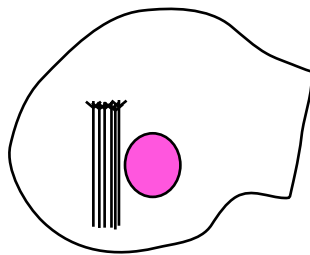
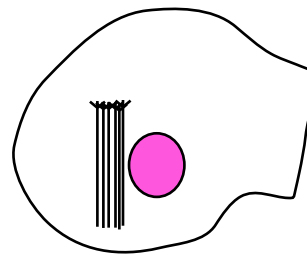
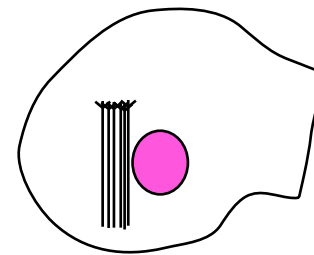
What is the endogenous function of Slit1a and Slit2?

These results suggest a novel role for Slits in guiding axons *in vivo*. Our loss-of-function data show that Slit1a has a role in guiding axons through the optic tract and, together with the expression data, suggest that this role may be nonrepulsive. The similarity

Figure 5.1: Cartoon of results of Slit-Robo manipulation in the optic tract. Purple represents endogenous *slit1a* expression, magenta represents ectopic mCherry, Slit1a-mCherry, or Slit2-EGFP. Stereotypical responses of RGC axons to each manipulation are schematized.



wild-type

*astray**slit1a*  
morphantmCherry  
global OESlit1a-mCherry  
global OESlit2-GFP  
global OEmCherry  
anteriorSlit1a-mCherry  
anteriorSlit2-GFP  
anteriormCherry  
posteriorSlit1a-mCherry  
posteriorSlit2-GFP  
posterior

between *slit1a* morphants and *astray* mutants suggests that this role is mediated by Robo2.

The local heat shock experiments show that, at least in the context of misexpressed Slit1a and Slit2 anterior to the tract, these proteins act to attract Robo2-expressing axons. I propose that endogenous Slit1a acts in the tract to attract axons to the dorsal diencephalon and then to the optic tectum, as growth cones grow up gradients emanating from domains of strong expression in these two locations.

One caveat to these results is that I do not know how the concentrations of misexpressed Slit1 and Slit2 compare to endogenous levels. It is possible that lower levels of Slit2 or Slit1a are repulsive, while higher levels are somehow attractive, and that axons have a different response to the levels of Slits expressed in our misexpression system than they do to endogenous Slits. Alternately, perhaps high levels of misexpressed protein result in an artifact due to insufficient levels of an *in vivo* modulator, such as heparan sulfate, which is required for Slit-Robo binding (Hu, 2001).

Any model incorporating a repulsive function for Slit1a is hard to reconcile with the normal trajectory of RGC axons as they pathfind through the optic tract toward the optic tectum. Since *slit1a* is expressed anterior, posterior, and medial to the RGC axons, as well as in their final target, the optic tectum, a repulsive role for Slit1a seems unlikely. It is possible that posttranscriptional regulation results in a different, more restricted expression pattern of active Slit1a protein, but since I was unable to generate a Slit1a antibody, this possibility remains untested. An attractive or permissive role is a more parsimonious explanation and, indeed, was already a plausible model based on the mRNA expression pattern and on previous work (Barresi et al., 2005).

The results of posterior misexpression of Slit1a and Slit2 are confusing. Although a few embryos showed posterior errors, most embryos did not. There are three possible

explanations that are consistent with the results of anterior misexpression. First, performing heat shock posterior to the tract was much more technically difficult than anterior heat shock because of the topography of the brain: this region lies in a concavity, so that targeting the posterior region at the same dorsal-ventral level as the anterior misexpression was difficult without damaging the yolk. As a result, the area of misexpression tended to fall in the dorsal half of the tract. RGCs may not respond in the same way here as they do more ventrally. The best way to test this would be to use a more precise method of heat shock activation (e.g., the optic fiber method of Karlstrom et al.) to misexpress Slits near the ventral half of the tract. Second, there could be a repulsive factor that is expressed posterior to the tract that keeps axons from misprojecting into this area dorsal to the tract. Although I see axons aberrantly misprojecting posteriorly in *astray* mutants and *slit1a* morphants, these errors tend to be in the ventral part of the optic tract. Third, extracellular diffusion of Slits could be different on the posterior side of the tract. Perhaps the extracellular matrix is somehow stickier. This could be tested by doing local heat shock anterior and posterior to the tract in embryos that are transgenic for both *hsp70l:gfp* and *hsp70l:slit1a-mcherry* or *hsp70l:mcherry* and *hsp70l:slit2-egfp*. Comparing the location of the Slit signal to the cells that express GFP or mCherry cytoplasmically would tell us whether there is a difference in diffusion between the two sides of the tract.

Could Slit1a be repulsive?

One possible interpretation of the broad *slit1a* expression pattern is that Slit1a acts at short range to repel axons, pushing them laterally to the pial surface of the brain. This does not explain why they continue to grow toward areas of even higher concentration of *slit1a*, but it is a formal possibility, especially if there is post-transcriptional regulation of Slit1a. The loss-of-function data are somewhat consistent with this model since the axons in *astray*

mutants and *slit1a* morphants misproject. However, I almost never saw axons projecting deeper into the brain; instead they splayed out over the pial surface. Moreover, the anterior misexpression results are difficult to reconcile with a repulsive role without invoking another factor such as a cofactor or modulator.

Could Slit1a and Slit2 be inducing branching?

Slit2 is generally repulsive to growth cones; however in some contexts it has been shown to induce branching (Wang et al., 1999), though Robo2 inhibits retinal axon branching in the tectum (Campbell et al., 2007). Anterior misexpression of Slit1a or Slit2 results in optic tracts that seem to turn anteriorly. Could this phenotype actually be due to collateral branching? I cannot rule out the possibility that axons are forming branches without doing single-cell labeling. However, random stimulation of branching does not explain the phenotype in the optic tract since most misrouted axons leave the normal trajectory of the optic tract and projecting anteriorly. Therefore, if branching is occurring, most branches are still directed toward the ectopic Slit. At the chiasm, the majority of RGC axons projected normally in embryos with misexpressed Slit2, with a minority of axons making errors at the midline. These misprojected axons could be collateral branches, but they always turn anteriorly, which still suggests attraction by Slit. The presence of branches could be tested by labeling single cells in these embryos by *in vivo* electroporation or by mosaic labeling of RGCs.

Could Slits be promoting fasciculation?

Another possible explanation is that Slit1a promotes fasciculation of RGC axons. The loss-of-function data is certainly consistent with this model, since axons in the tract spread out when either *robo2* or *slit1a* function is decreased. However, the gain-of-function

data do not support this model. RGC axons spread out when exposed to either Slit1a or Slit2 either globally or locally. If only defasciculation occurred, one could imagine that the Robo2 receptor was being overwhelmed with excess Slit and growth cones were effectively insensitive to Slits, thus giving a similar phenotype to Robo2 loss-of-function. However, the fact that axons also turn toward Slit1a or Slit2 expressed anterior to the tract makes this explanation unlikely. It is not clear that spreading out of axons reflects changes in direct axon-axon contacts, i.e., bona fide defasciculation. EM data at 3 dpf shows that axons of the optic tract are tightly packed, directly contacting one another. However, I do not have EM data for wild-type embryos at the time of optic tract formation, 36-48 hpf, nor for mutants or morphants.

Do Slit1a and Slit2 elicit different responses from RGC axons?

At the beginning of this project, I hypothesized that Slit1a would act as a permissive or attractive cue to RGC axons, while Slit2 would act as a repellent, based on the expression patterns of both molecules and the body of literature showing repellent effects of Slit2 on growth cones. *slit2* is expressed anterior to the optic chiasm, suggesting a role in keeping RGC growth cones from leaving the retinotectal pathway at the midline and misprojecting anteriorly, but I did not detect expression near the optic tract. *slit1a*, on the other hand, is expressed broadly throughout the brain, including cells near the optic chiasm and the optic tract. Global overexpression of Slit2 resulted in severe RGC axon guidance defects, while the errors in the Slit1a global overexpression embryos were mild at best. However, as previously discussed, global overexpression phenotypes are difficult to interpret in terms of endogenous function.

Local misexpression of either Slit1a or Slit2 anterior to the optic tract elicited the same response: axon turning toward the source of ectopic Slit. Therefore, at least in this

context, Slit1a and Slit2 seem to function in the same way, attracting Robo2-expressing RGC axons in the optic tract. Since anterior misexpression of Slit1a or Slit2 produces a strong phenotype that is different from that seen in *astray*, epistasis experiments can now be done to test whether Slit1a and Slit2 are acting through the Robo2 receptor. Anterior misexpression of Slit1a or Slit2 in an *astray* mutant would tell me whether these Slits signal through Robo2. An *astray* phenotype would indicate that they do, as expected. If RGC axons still turn toward ectopic Slit, that would suggest the presence of a different receptor that mediates the Slit signal.

How do Slit1a and Slit2 act at the chiasm?

*slit2* and *slit3* form a guardrail pattern at the zebrafish optic chiasm (Hutson and Chien, 2002), which led us to believe that they functioned repulsively at the chiasm to channel RGC axons across the midline to the contralateral optic tract. Although there was no direct evidence to support a repulsive role for Slit2, this was the logical conclusion given that Slits have been shown both genetically and biochemically in other systems to be repulsive ligands for Robo receptors. Moreover, unpublished results showed that zebrafish Slit2 can cause growth cone collapse in zebrafish RGC cultures (Rasband and Chien, personal communication). In addition, RGC axons in *astray* embryos, which lack functional Robo2, make mistakes at the chiasm, primarily anteriorly, and do not correct these mistakes through growth cone collapse and retraction, which fits the guardrail model of axon guidance at the chiasm. Local misexpression of Slit2 at the chiasm, however, results in axons leaving their normal path and growing toward the ectopic Slit2. This result suggests that Slit2 acts to attract axons at the chiasm, which is contrary to the model of Slit2/Slit3 function. Can these gain-of-function results be reconciled with the *astray* phenotype and the *slit2* and *slit3* expression pattern?

An experiment that would perhaps clarify these results is a co-culture of zebrafish retina and a piece of zebrafish tissue from an *hsp70l:slit2-egfp* embryo that has been heat shocked prior to culturing. Assaying whether the RGC axons grow toward the explanted tissue would add weight to either the culture results or the *in vivo* results. However, it could also be the case that the *in vivo* and culture systems are fundamentally different due to the lack of other factors in the explant cultures. HSPGs are a critical component of the Slit-Robo signaling complex (Hussain et al., 2006). Perhaps the lack of HSPGs in the RGC culture system makes RGC growth cones behave differently than they would *in vivo*.

One possible model to explain the attraction of RGC axons toward ectopic Slit2-GFP is that there is balanced attraction at the midline. In this model, axons are attracted to both Slit2 and Slit3, which diffuse from zones anterior and posterior to the midline. However, this model does not explain why wild-type axons that make errors subsequently correct them. One would predict that, if axons were experiencing balanced attraction, a growth cone that had made an error would continue to be attracted to higher concentrations of Slit2 or Slit3 and continue to misproject.

A second possibility is that there is another repellent expressed near the chiasm that keeps the RGC growth cones from making errors. Slit3 is a candidate. Slit3 is also expressed at the chiasm, both anterior and posterior to the RGC axons' normal pathway. Perhaps it functions as a repellent to keep axons from misprojecting anteriorly and posteriorly. However, this is speculation given that we do not have any data to address whether Slit2 and Slit3 have different functions.

Finally, it is possible that growth cones switch their response to Slits at the midline, initially being repelled by Slit2 but later becoming attracted to Slits to facilitate growth through the optic tract within a zone of high Slit1a expression.

Do RGC growth cones change their responsiveness over time?

The fact that Slit2 caused axons to turn toward it when expressed anterior to the optic tract led me to hypothesize that perhaps RGC axons change their response to Slits over time. I reasoned that perhaps Slits were repellent to axons as they crossed the midline, consistent with the published model of Slit2 function, but became attracted to Slits once they entered the optic tract. However, the experiment that I designed to test this hypothesis did not support it. RGC axons turned toward misexpressed Slit2 at the optic chiasm. I did not see errors prior to the midline, in the optic nerve. *astray* mutants occasionally have errors in the optic nerve prior to the midline, although errors at the midline are more common (Hutson et al., 2002). It is possible that RGC growth cones become responsive to Slit2 at the midline, or switch from being repelled to being attracted at the midline; however my data do not directly test this. To test this hypothesis directly, I propose two experimental strategies. The first is to test RGC growth cones in culture. Slit2 causes collapse of Robo2-expressing RGC growth cones. However, if there is a switch at the midline, these growth cones in culture probably would not have undergone the molecular change that would cause response switching because they have not been exposed to the midline environment. A coculture experiment using explanted retina and explanted ventral diencephalon could expose RGC growth cones to midline factors. Subsequent bath application of Slit2 would show whether these growth cones still undergo collapse. If they do not collapse, this would be evidence that RGCs do change their response to Slit at the midline. If they do collapse, it suggests that RGCs do not change their response; however, it would not be definitive proof since there could be contact-

dependent factors. A better test would be to misexpress Slit2 across the normal path of RGC axons before they reach the midline and observe whether growth cones collapse or turn to avoid the ectopic Slit2. Unfortunately, the soldering iron heat shock probably does not give precise enough spatial control to perform this experiment. Electroporation or perhaps a new method using optical fibers to activate the heat shock response would be necessary (Placinta et al., 2009).

How could RGC axons switch their response to Slits? There are several possibilities, including regulation of receptor levels, expression of different receptor isoforms, or expression of a coreceptor. In the *Drosophila* ventral nerve cord, Comm targets Robo for degradation prior to the midline (Myat et al., 2002; Keleman et al., 2002, 2005). In the mouse spinal cord, one isoform of Robo3 serves a similar function by antagonizing Robo and Robo2 before midline crossing, while another isoform is repelled by Slit (Sabatier et al., 2004; Chen et al., 2008). Although *robo3* has not been detected in zebrafish RGCs, perhaps another factor plays the same role. Alternately, expression of a coreceptor at or after the midline might switch growth cone response. In vertebrates, only Robos have been identified as Slit receptors, although EVA-1 in *C. elegans* is also a Slit receptor (Fujisawa et al., 2007). A BLAST search shows that proteins with a similar domain organization to EVA-1 are found in many vertebrate species, including human, mouse, and zebrafish. Moreover, Slit1a in the zebrafish optic tectum shows Robo-dependent and Robo-independent effects during synaptogenesis, suggesting that another Slit receptor may be present in RGC axons (Campbell et al., 2007).

To more thoroughly test Slit function in the zebrafish retinotectal system, several further experiments should be done. First, loss-of-function experiments are necessary to see which, if any, Slits act to guide axons across the midline. *slit1a* morpholinos do not seem to

result in errors at the optic chiasm. Preliminary experiments with *slit2* and *slit3* morpholinos resulted in normal midline crossing. However, higher doses of *slit1a*, *slit2*, and *slit3* morpholinos result in convergent extension defects. It is entirely possible that the *slit2* and *slit3* morpholinos were not injected at the correct dose to affect axon guidance without causing earlier defects in convergent extension. Splice-blocking morpholinos should be used to test for the necessity of Slit2 and Slit3 at the chiasm. If Slit2 is attractive but Slit3 repellent, knockdown of *slit3* should result in anterior errors as growth cones would be free to grow toward the endogenous anterior source of Slit2. If both are repellent, it is possible that both *slit2* and *slit3* need to be knocked down simultaneously to see axon errors. Few errors were seen in RGC axons at the chiasm in *slit1* and *slit2* mouse knockouts, but the double *slit1/slit2* knockout had many axon errors (Plump et al., 2002). Collapse assays in culture should be done for both Slit1a and Slit3 to test RGC growth cone response to these Slits. Local misexpression experiments similar to those described in Chapter 3 should determine whether the effect of Slit3 is the same as, or different than, Slit2 at the chiasm and in the optic tract. Finally, a critical experiment would be to make a stable *hsp70l:slit3-mCherry* line and perform local heat shock. This would determine whether Slit2 and Slit3 act differently in my assay or not. If so, this would lend support to the model that Slit3 is responsible for keeping axons on the correct trajectory at the optic chiasm. If Slit3 is also found in my assay to be attractive at the midline, further experiments would be helpful to test whether the RGC attraction to misexpressed Slit2 reflects its true biological function.

The isolation of *slit* mutants and characterization of the endogenous promoters for the *slit* genes would be extremely helpful for performing further experiments to confirm the attractive role of Slit1a and Slit2. To create the perfect *in vivo* turning assay, one would ideally like to remove all endogenous Slit1a and/or Slit2 and then reintroduce it only in a few

cells close to the optic tract or chiasm. This could also resolve the question of whether Slit1a has any function in RGCs, as it is very weakly expressed in the RGC layer. Unfortunately, strong doses of translation-blocking morpholino result in convergent extension defects. It is possible that a null allele of either Slit1a or Slit2 would not be viable, depending on whether maternal mRNA is sufficient to allow development past these stages. However, if a mutant were isolated, cell transplants from wild-type embryos into mutant embryos could yield patches of cells that expressed Slit in a Slit-negative background. Even better, if the *slit1a* or *slit2* promoters were isolated, a construct driving Slit1a or Slit2 under its endogenous promoter could be electroporated next to the retinotectal pathway in a Slit mutant embryo. If RGC axons turned toward these cells, that would be very convincing. If confirmed, my Slit results represent an important finding in the field of axon guidance.

### **Axon sorting in the zebrafish retinotectal system**

The SBFSEM dataset I obtained of the zebrafish optic tract allowed development and testing of a new method of automated axon tracking. I hand-validated the results of automated tracking. Although the biological importance of the data obtained so far is limited, it demonstrated the power of serial section electron microscopy combined with automated tracking methods.

Once datasets of wild-type and *dackel* embryos are obtained, it should be relatively easy to track all of the RGC axons through the tract. This will tell us whether axon sorting errors in wild-type and *dackel* are similar. Since even wild-type axons make sorting errors, perhaps *boxer* and *dackel* embryos make similar errors and lack the means to correct them. Alternately, the errors in *dackel* might be due to a fasciculation problem which is not visible using confocal microscopy. An important question is how HSPGs act to sort axons correctly. Since HSPGs can be expressed in both the ECM or on the cell surface, a high resolution

description of axon sorting could reveal whether sorting errors are due to axon-axon interactions or axon interaction with the ECM.

Preliminary data from our zebrafish dataset shows that neighboring axons tend to stay together throughout at least the dorsal part of the tract, suggesting that they are interacting through cell adhesion molecules. The EM shows that the axons are very tightly packed within the optic tract, making it less likely that they are interacting with the ECM. In mutants, these axon-axon interactions may be disrupted. Another possibility is that early axons are missorted through interactions with the surrounding tissue and subsequent axons follow them into an inappropriate region of the optic tract. This hypothesis is supported by the fact that the missorting phenotype worsens between 3 dpf and 5 dpf in *boxer* and *dackel* (Lee et al., 2004). However, there must also be a means of error correction that is missing in the mutants, since the wild-type phenotype improves over the same time period.

## **Conclusions**

The new methods reported in this dissertation add a new technique for gene misexpression in the embryonic zebrafish and a new computational technique for tracking axons through electron microscopy datasets. The finding that Slit1a and Slit2 are attractive to RGC axons in my misexpression assay is an important finding to the field of axon guidance. Previous work has shown that Netrins, Semaphorins, and Ephrins can act bifunctionally to guide axons, either attracting or repelling growth cones depending on extracellular and intracellular context. These data add Slits to the list of canonical guidance factors that can act both attractively and repulsively. Future studies will determine whether Slit1a and Slit3 also act attractively at the optic chiasm. Future directions for the axon sorting project will produce a high resolution description of axon sorting in wild-type and

*dackel* mutants. Altogether, my results add to our understanding of axon guidance in the zebrafish retinotectal system and have broader implications for axon guidance and sorting.

## References

- Cerda, G. A., Thomas, J. E., Allende, M. L., Karlstrom, R. O., and Palma, V. (2006). Electroporation of DNA, RNA, and morpholinos into zebrafish embryos. *Methods* 39, 207-211.
- Esengil, H., Chang, V., Mich, J. K., and Chen, J. K. (2007). Small-molecule regulation of zebrafish gene expression. *Nat. Chem. Biol* 3, 154-155.
- Esengil, H., and Chen, J. K. (2008). Gene regulation technologies in zebrafish. *Mol Biosyst* 4, 300-308.
- Hendricks, M., and Jesuthasan, S. (2007). Electroporation-based methods for in vivo, whole mount and primary culture analysis of zebrafish brain development. *Neural Dev* 2, 6.
- Huang, C., Jou, T., Ho, Y., Lee, W., Jeng, Y., Hsieh, F., and Tsai, H. (2005). Conditional expression of a myocardium-specific transgene in zebrafish transgenic lines. *Developmental Dynamics* 233, 1294-1303.
- Langenau, D. M., Feng, H., Berghmans, S., Kanki, J. P., Kutok, J. L., and Look, A. T. (2005). Cre/lox-regulated transgenic zebrafish model with conditional myc-induced T cell acute lymphoblastic leukemia. *Proceedings of the National Academy of Sciences of the United States of America* 102, 6068-6073.
- Lee, J., von der Hardt, S., Rusch, M. A., Stringer, S. E., Stickney, H. L., Talbot, W. S., Geisler, R., Nüsslein-Volhard, C., Selleck, S. B., Chien, C., et al. (2004). Axon sorting in the optic tract requires HSPG synthesis by ext2 (dackel) and extl3 (boxer). *Neuron* 44, 947-960.
- Liu, Y., and Halloran, M. C. (2005). Central and peripheral axon branches from one neuron are guided differentially by Semaphorin3D and transient axonal glycoprotein-1. *J. Neurosci* 25, 10556-10563.
- Placinta, M., Shen, M., Achermann, M., and Karlstrom, R. O. (2009). A laser pointer driven microheater for precise local heating and conditional gene regulation in vivo. *Microheater driven gene regulation in zebrafish. BMC Dev. Biol* 9, 73.
- Teh, C., Chong, S. W., and Korzh, V. (2003). DNA delivery into anterior neural tube of zebrafish embryos by electroporation. *BioTechniques* 35, 950-954.
- Ungar, A. R., Kelly, G. M., and Moon, R. T. (1995). Wnt4 affects morphogenesis when misexpressed in the zebrafish embryo. *Mech. Dev* 52, 153-164.